DISSOLUTION KINETICS OF LUNAR SIMULANTS AND THE SORPTION OF OXYANIONS AND NICKEL ON SECONDARY WEATHERING PRODUCTS

by

Matthew J. Eick

A dissertation submitted to the Faculty of the University of Delaware in partial fulfillment of the requirements for the degree of Doctor of Philosophy in Soil Science

May 1995

DISSOLUTION KINETICS OF LUNAR SIMULANTS AND THE SORPTION OF OXYANIONS AND NICKEL ON SECONDARY WEATHERING PRODUCTS

by

Matthew J. Eick

Approved: Donald L. Sparks

Donald L. Sparks, Ph.D.
Chair of the Department of Plant and Soil Sciences

Approved: John C Nye

John C. Nye, Ph.D.
Dean of the College of Agricultural Sciences

Approved: Carol E. Hoffecker

Carol E. Hoffecker, Ph.D.
Associate Provost for Graduate Studies

I certify that I have read this dissertation and that in my opinion it meets the academic and professional standard required by the University as a dissertation for the degree of Doctor of Philosophy.

Signed: _____

Donald L. Sparks, Ph.D.
Professor in charge of dissertation

I certify that I have read this dissertation and that in my opinion it meets the academic and professional standard required by the University as a dissertation for the degree of Doctor of Philosophy.

Signed: _____

J. Thomas Sims, Ph.D.
Member of dissertation committee

I certify that I have read this dissertation and that in my opinion it meets the academic and professional standard required by the University as a dissertation for the degree of Doctor of Philosophy.

Signed: _____

Douglas W. Ming, Ph.D.
Member of dissertation committee

I certify that I have read this dissertation and that in my opinion it meets the academic and professional standard required by the University as a dissertation for the degree of Doctor of Philosophy.

Signed: _____

Theodore H. Carski, Ph.D.
Member of dissertation committee

ACKNOWLEDGMENTS

There are many people whose help and support have made this endeavor possible. First and foremost is my advisor Dr. Donald Sparks. He provided me with the opportunity to pursue my Ph.D. by encouraging me to apply for the NASA graduate student fellowship. His friendship, guidance, and support have made my three years both challenging and enjoyable. Next, I would like to thank my dissertation committee, whose stimulating discussions helped guide and focus my research. Also, I would like to thank the people at the L.B.J. Space Center in Houston, Texas. The opportunity to conduct research and interact with these outstanding scientists broadened my learning experience. Special thanks are extended to my NASA advisor Doug Ming, and also to D.C. Golden and Charlie Galindo. I would like to especially acknowledge the financial support provided by the graduate student fellowship from NASA

The most rewarding aspect of my Ph.D. degree has been the opportunity to work, collaborate, and socialize with other graduate students, post-docs, and visiting professors. I would especially like to thank all my colleagues in the soil chemistry group, especially Dr. C.V. Toner, Jerry Hendricks, Mike Stapleton, John DiVincenzo, Dr. D.D. Stefens, and Amy Brennen. Their friendship, thought-provoking discussions, and practical jokes always brightened the day. I would like to extend a special thanks to Drs. Scott Fendorf and Paul Grossl. Their guidance, patience, helpful discussions, collaboration, and most of all their friendship were an invaluable part of my degree.

Finally, I would like to thank my family for their loving support during the difficult times. I would especially like to thank my wife, Katie, who made it all possible. Her constant support, encouragement, and love helped me overcome many obstacles. Although distance separated us, she was always there for me. I dedicate this dissertation to her.

TABLE OF CONTENTS

LIST OF TABLES

LIST OF FIGURES

ABSTRACT

As the 21st century approaches, the National Aeronautics and Space Administration (NASA) is considering extending permanent human presence beyond low Earth orbit. Among the missions being considered by NASA are human exploration of Mars and its satellites, establishment of a manned lunar outpost, and evolutionary expansion of humans into our inner solar system. A permanent human outpost on the moon will be a staging area for launching manned missions to other planets and is therefore a necessary first step to achieving NASA's goals. Due to the exorbitant costs of transporting food and resources to a lunar base, it will be essential to establish a regenerative life support system (RLSS). The RLSS will depend upon green plant photosynthesis to provide food, potable water, and oxygen and to remove wastes and carbon dioxide. Lunar soils will play an essential role in the development of lunar based agriculture. Therefore, the study of how lunar soils will react when exposed to a terrestrial environment is important to the success of a manned lunar outpost.

Lunar soils are similar to terrestrial analogs. However, they are devoid of water and are extremely reduced. Additionally, they contain potentially toxic concentrations of Cr and Ni. NASA has only a limited supply of lunar soils retrieved from the Apollo missions and these are considered a national treasure. Lunar simulants have been developed by NASA to be used as a first step in understanding the reactivity of lunar materials and establish research protocols that may be used with actual lunar soils. In this study we examined the long-term dissolution kinetics and

mechanisms of a basalt and glass simulant under conditions that may be encountered in a plant root rhizosphere. Mineral surfaces were examined with transmission and scanning electron microscopy and the microscopic analyses support mechanisms determined from dissolution data. Additionally, we investigated the sorption kinetics and mechanisms of chromate, arsenate, and Ni on potential lunar soil secondary weathering products employing an array of sophisticated atomic-resolution techniques and a pressure-jump relaxation kinetic technique for studying rapid kinetic reactions .

Long term dissolution studies were conducted, using both lunar simulants at pH values of 3, 5, and 7 and in the presence of citric and oxalic acid. At pH 3 and 5, dissolution of the lunar glass simulant followed a two stage process. The first stage involved the parabolic release of Ca, Mg, Al, and Fe and the linear release of Si. Dissolution was incongruent resulting in a leached layer rich in Si and Ti that was verified by transmission electron microscopy. During the second stage, the release of Ca, Mg, Al, and Fe was linear, which was attributed to the repolymerization of a Si-rich leached layer. The Si-rich leached layer scavenged Si from solution and created a porous network that was no longer a diffusional barrier to the release of cations. During this second stage, hydrolysis of the bulk glass, not diffusion through the leached layer, was the rate-limiting step. In the presence of the organic acids, the dissolution of the synthetic lunar glass proceeded by a one stage process. The release of Ca, Mg, Al, and Fe followed a parabolic relationship, while the release of Si was initially linear and eventually approached a steady state. The rate-limiting step was the diffusion of cations through the Si/Ti rich leached layer which was observed with transmission electron microscopic analysis. A two-step mechanism was proposed involving the initial surface adsorption of the organic ligand followed by hydrolysis of the surface and chelation of cations in solution.

For the basalt simulant, the rate of dissolution for all experiments followed a two-stage process. During the first stage, the rate of dissolution for all elements was rapid, followed by a slower, more linear rate during the second stage. The first stage was attributed to the dissolution of ultrafine particles created during the sample grinding process. During the second stage, dissolution proceeded on the larger mineral surfaces at higher energy sites such as dislocations, twinning planes, fluid inclusions, etc. The order of cation release was related to the stabilities of the minerals present in the MLS-1 basalt. For the pH experiments, it was proposed that H^+ ions dissolved the minerals present in the basalt through a combination of diffusion exchange with structural cations and protonation of the surface. In the organic acid experiments, a two step mechanism was proposed involving the initial surface adsorption of the organic ligand followed by hydrolysis of the surface and chelation of cations in solution.

The kinetics and mechanism of chromate and arsenate adsorption was investigated using a pressure-jump relaxation kinetic technique and X-ray absorption fine structure (XAFS) spectroscopy. Pressure-jump relaxation experiments indicated that both arsenate and chromate formed inner-sphere bidentate surface complexes with goethite. This occurred via the formation of an intermediate inner-sphere monodenate surface complex. For both oxyanions, the rate-limiting step was the reaction proceeding from the mono- to the bidentate surface complex. Rate information indicated that arsenate more favorably formed an inner-sphere bidentate surface complex on goethite than chromate. This is consistent with XAFS spectroscopy and the finding that chromate is the more mobile of the two oxyanions in the vadose zone.

The surface structure of Ni(II) sorbed on kaolinite was investigated using XAFS and transmission electron microscopy (TEM). XAFS along with

crystallographic considerations indicated that a bidentate binuclear surface complex formed at all surface site occupancies followed by Ni-hydroxide nucleation. TEM was used to examine the spatial resolution of the precipitate and indicated that Ni-hydroxide formed discrete islands or clusters over the kaolinite surface.

Chapter 1

INTRODUCTION

1.1 CELSS Concept and the Lunar Regolith

As the 21st century approaches, the National Aeronautics and Space Administration (NASA) is planning the exploration and settlement of our solar system. The most plausible first step would be to establish a permanent human colony on the moon. Three possible objectives of lunar colonization include scientific research, exploration of lunar resources for use in building a space infrastructure, and attainment of self-sufficiency in the lunar environment (Duke et al., 1985). An integral component of lunar colonization is the establishment of a controlled ecological life support system (CELSS). The basis of the CELSS concept is the integration of biological and physicochemical processes to build a system that will generate food, potable water, and a breathable atmosphere from metabolic and other wastes (in a stable and dependable manner). The central theme of a CELSS is the use of green plant photosynthesis to remove carbon dioxide and produce oxygen and potable water, which will result in food production (Averner, 1989).

The lunar regolith will play a major role in the development of lunar based agriculture by (i) acting as a soil medium and providing a solid support substrate for plant growth, and (ii) providing essential, plant-growth elements (McKay et al., 1989). Common constituents of the lunar regolith are silicate minerals (e.g., pyroxenes, olivines, feldspars), iron-titanium oxides (e.g., ilmenite), glassy materials, and

agglutinates (i.e., complex mixtures of glass and mineral fragments) (Ming and Lofgren, 1990). The primary minerals present in the lunar regolith are similar to those present in terrestrial soils and will provide many essential plant nutrients. However, unlike terrestrial soil, the lunar regolith is devoid of water and organic matter. In addition, the potentially toxic elements, Cr and Ni, are present at levels that are unusually high compared to terrestrial soils. Therefore, the successful use of the lunar regolith for plant growth systems is dependent on a thorough understanding of many geochemical processes.

A voluminous amount of research exists on rock and mineral dissolution in terrestrial aqueous environments. However, little research exists on aqueous dissolution of lunar materials retrieved during the Apollo missions. Keller and Huang (1971) compared the dissolution of an Apollo 12 lunar dust to a pulverized basalt in water, CO_2-charged water, 0.01 M acetic acid, and 0.01 M salicylic acid. They found that the lunar dust was more soluble in the organic acids than the pulverized basalt. Therefore, under typical terrestrial weathering environments the lunar soil should readily yield inorganic plant nutrients. However, increased dissolution may yield concentrations of trace metals (such as Cr and Ni) that are toxic to bacteria and plants. If lunar soils are to be used as a substrate for plant growth it will be necessary to understand their geochemistry in aqueous environments. One area of lunar geochemistry that needs to be studied is the dissolution kinetics of lunar constituents and the potential release of toxic trace metals such as Cr and Ni. Understanding the mechanism and rate of dissolution and quantifying the amount and redox state of potentially toxic trace metals is necessary before lunar soils can be successfully used as a medium for plant growth. Additional dissolution studies on lunar materials are limited because of the small quantities retrieved during the Apollo missions.

Consequently, it is necessary to develop and use terrestrial simulants for geochemical research. Simulants have been developed with one or more physical and/or chemical properties of the lunar regolith. Ming and Lofgren (1990) examined the formation of minerals during hydrothermal alterations of a synthetic lunar basaltic glass. Potential ion-exchange minerals such as zeolites and phyllosilicates were synthesized. With lunar simulants, research can be conducted and protocols established without exhausting the precious stock of lunar samples.

To date, two types of lunar simulants have been produced for use in research; glass simulants and a basalt simulant. Several batches of glass simulants have been produced by commercial glass companies. These glass simulants are high titanium glasses that have been developed to represent similar glasses retrieved from the lunar mare (lunar lowland region) regions. The basalt simulant is a high titanium terrestrial analog that was mined from a quarry in Duluth, Minnesota. The basalt simulant has similar mineralogy and chemical composition as basalts retrieved by the Apollo 11 mission. Both simulants were ground and dry sieved into eight particle size fractions that were representative of Apollo 11 soils. Efforts were made to keep the simulants as reduced and free of water as possible. However, both simulants contained small quantities of water which was unavoidable.

1.2 Methodologies

1.2.1 Silicate Dissolution Kinetics

There are three basic types of experiments that can be used to measure the kinetics of dissolution/weathering reactions: batch techniques, flow or column methods, and mixed flow techniques. Batch techniques are widely used by geochemists and soil chemists because of their simplicity. The traditional batch

technique involves placing a mineral and solution in a vessel such as a centrifuge tube or bottle. The vessel is agitated using a shaker or stirrer for a certain time interval, and the suspension is usually centrifuged or filtered to obtain a clear supernatant for subsequent analysis (Sparks, 1989).

Several problems are associated with batch reactors. First, the reaction rates are not measured directly and, in most studies, the concentration versus time data are fit to the integrated form of the presumed rate law. If the fit is good, the reaction mechanism is interpreted from the differential rate law (Rimstidt and Dove, 1986). This may not be an accurate procedure, because several rate laws may fit experimental data with high correlation coefficients (Inskeep and Bloom, 1985). Also, dissolution of many minerals is incongruent and new concentration versus time patterns are produced each time a new phase begins to form. Lastly, sample grinding and preparation produces excessively reactive surfaces due to supersoluble (ultrafine) particles adhering to larger grains, mineral dislocations and stressed areas. These surfaces often react more rapidly than the bulk solid (Petrovich, 1981a,b).

A second problem with batch techniques is not removing dissolved species. This can cause secondary precipitation of mineral phases that may limit or inhibit further dissolution of the mineral (Holdren and Adams, 1982). A third problem associated with batch techniques is changes in the solid to solution ratio after sampling. This may alter the solution composition and affect the overall dissolution kinetics (Rimstidt and Dove, 1986). Although there are inherent problems associated with batch techniques they are still the method of choice for dissolution studies. Batch techniques can provide important initial rate information as well as information concerning secondary weathering products. Additionally, several of the above problems can be overcome with small modifications in the experimental procedure.

Flow or column techniques have been used infrequently to study the kinetics of mineral dissolution (Correns and von Engelhardt, 1938; Manley and Evans, 1986). Flow techniques involve placing the mineral in a column or tube and leaching it with a reacting solution. The reacting solution is equilibrated with the mineral and subsequently displaced by a second aliquot of the same solution. This procedure is repeated over a period of time. The advantages of the column technique are a fairly constant solution to solid ratio, removal of dissolved species and the simulation of a natural weathering/leaching environment.

The use of the mixed flow reactor method for measuring dissolution reaction rates has increased in recent years (Wollast and Chou, 1985; Mast and Drever, 1987; Rimstidt and Dove, 1986). The fluidized bed reactor has been used extensively in the chemical industry to study the kinetics of physical and chemical processes involving a solid phase and a gas or liquid phase (Sparks, 1989). The fluidized bed reactor maintains a suspension of solid particles through fluid flow. The fluid flow is adjusted such that its velocity equals the settling rate of the solid particles. Because the suspension is quite dense, the settling rates of different-sized particles are normalized by frequent collisions with other particles. Particles that escape the fluidized bed to the lower density of the overlying solution quickly fall back. The fluidized bed reactor is best suited to a well-defined particle size fraction (Sparks, 1989).

Other types of mixed flow reactors have been used to study mineral dissolution rates. Rimstidt and Dove (1986) developed a mixed flow reactor to study the rate of wollastonite hydrolysis. Their reactor consisted of a one liter reaction kettle, motorized stirrer, peristaltic pump and pH meter. The reacting solution is pumped through the reaction kettle at a constant rate until a steady state is achieved.

Evolution of the reaction toward a steady state is monitored using an electrode or spectrophotometer flow cell. Once the reaction has reached a steady state, effluent is collected and saved for detailed chemical analysis.

The mixed flow reactor eliminates many of the disadvantages associated with traditional batch systems. Measurements are made after the reactor has achieved a steady state. Therefore, actual reaction rates are determined. This eliminates the problem of deciding which integrated rate law to choose to fit the data. The mixed flow reactor allows one to separate rapidly dissolving "disturbed surfaces" and ultra-fine grains created during sample preparation from the easily identifiable slower reaction rate of the bulk solid (Rimstidt and Dove, 1986). Also, the precipitation of secondary phases is usually avoided because their concentration is maintained at levels well below saturation.

1.2.2 Kinetics of Metal Sorption on Oxide and Clay Surfaces

Unlike silicate dissolution kinetics, the kinetics of metal sorption on soil constituent surfaces is often too rapid to be measured using traditional batch and flow techniques. Kinetic methods that can be used to measure these rapid reactions are relaxation techniques such as pressure jump. With the pressure jump technique the equilbrium of a system is perturbed by a rapid change in the pressure. Kinetic information is obtained by measuring the time it takes for the system to re-equilibrate ("relaxation time"). The pressure perturbation is small enough that measurements are made close to the final equilibrium during the relaxation period. Due to this small pressure perturbation, concentration changes are minute and it is necessary to use a very sensitive detection measurement such as conductivity (Sparks, 1989). Relaxation methods are an attractive kinetic technique because the use of a small perturbation

reduces all rate expressions to first order equations. Therefore, the rate equations are linearized, which simplifies elucidation of intricate reaction mechanisms (Sparks, 1989). Relaxation kinetic methods have been used successfully in ascertaining rates and mechanisms of metal ion sorption on soil constituents (Hayes and Leckie, 1986; Zhang and Sparks, 1989, 1990a,b; Grossl et al., 1994).

1.2.3 Spectroscopic and Microscopic Techniques

A myriad of spectroscopic and microscopic techniques is available for probing mineral surfaces. However, no single technique is a panacea for investigating dissolution and sorption reactions. Researchers investigating the dissolution of mineral surfaces often use a combination of surface spectroscopies and microscopies to examine changes in mineral surfaces. X-ray photoelectron spectroscopy (XPS), Auger electron spectroscopy (AES), elastic recoil detection (ERD), Rutherford backscattering analysis (RBS), secondary ion mass spectrometry (SIMS), and resonant nuclear reaction (RNR) are several techniques that are used to examine changes in mineral surface chemistry. These techniques are extremely surface sensitive and have been employed in conjunction with electron microscopies to determine the presence of leached mineral surfaces. Transmission electron microscopy (TEM) is capable of atomic resolution and can detect changes in mineral surfaces. Additionally, energy dispersive spectroscopy (EDS), which is an electron spectroscopy coupled with the TEM, can provide quantitative elemental analysis of mineral surfaces. Therefore, information gleaned from these techniques can provide insight into the mechanism of silicate and glass dissolution.

The above techniques are widely used by geochemists to examine mineral surfaces. However, these techniques are less useful for examining the sorption of

metals on soil constituent surfaces. Many surface spectroscopies require the use of high vacuums which may alter the structural environment of the sorbing metal. Additionally, these techniques provide little information on the local structural/chemical environment of the sorbing species.

X-ray absorption fine structure spectroscopy (XAFS) has been used to investigate the sorption of heavy metals on oxide surfaces (Charlet and Manceau, 1992; Fendorf et al., 1994). XAFS has the distinct advantage over other surface spectroscopies in that systems can be investigated in situ and it can provide information on the structural environment of the sorbed metal. XAFS is a powerful technique for investigating environmentally significant sorption reactions. However, it also has many limitations. Access to a synchrotron source may be difficult to obtain. Also, multiple chemical environments, such as those found in soils, may be difficult to resolve. Finally, user friendly data analysis packages are hard to find or are unavailable.

1.3 Research Objectives

Both the Minnesota lunar simulant (MLS-1) and glass simulant (batch 2D) were used in the following research. Research objectives were achieved using a combination of kinetic techniques, surface microscopies (TEM and SEM), and spectroscopies. The original objectives of this research were to examine the dissolution of the simulants under terrestrial weathering conditions and to quantify the release and redox state of Cr and Ni present. However, upon receiving the simulants it became clear that the quantities of Cr and Ni were at concentrations too small to be practically quantified in conventional dissolution experiments. Therefore, the original objectives of the research were modified. The first objective then became to only

examine the rate and mechanism of dissolution for the two lunar simulants when subjected to a terrestrial weathering environment. This information is important because it provides insight into the rate of lunar regolith weathering, the mechanism of dissolution under a wide range of experimental conditions, the formation of secondary weathering products, and the potential release of toxic metals.

The second objective was to take information gleaned from the dissolution studies, such as the nature of secondary weathering products, and examine the kinetics and mechanisms of Cr and Ni sorption in the presence of these precipitates. This information is extremely important because released Cr and Ni may be sorbed or undergo redox reactions which may render the metals more or less toxic than their original form. The above information will provide an understanding of the geochemistry of the lunar regolith in a terrestrial environment and the fate and nature of potentially released Cr and Ni.

The first objective was accomplished by investigating the long-term dissolution of both lunar simulants at pH 3, 5, and 7 and in the presence of citric and oxalic acid. Aqueous analytical data was supplemented by transmission and scanning electron microscopies (TEM and SEM) to observe changes in the mineral surfaces. The second objective was achieved by examining the sorption kinetics of Cr and Ni on secondary weathering products. Initial dissolution studies indicated that Fe-oxides and kaolinite may form early in dissolution. Hence, these surfaces were chosen for the sorption studies. The sorption of chromate on goethite was investigated using a pressure-jump relaxation technique and XAFS. These techniques provide complimentary information on sorption mechanisms. Chromate was chosen as the sorbate because the presence of Mn in lunar soils may be involved with the oxidation of released Cr. Additionally, chromate is the more mobile and toxic form of Cr.

Finally, the sorption of Ni on kaolinite was investigated employing batch studies and the use of XAFS and TEM to ascertain the sorption mechanism.

1.4 References

Averner, M.M. 1989. Controlled ecological life support system. pp. 145-153. *In* D.W. Ming and D.L. Henninger (eds.), Lunar base Agriculture: Soils for Plant Growth. Soil Science Society of America, Madison, WI.

Charlet, L. and A.A. Mancaeu. 1992. X-ray absorption spectroscopic study of the sorption of Cr(III) at the oxide-water interface: I. Molecular mechanism of Cr(III) oxidation on Mn oxides. J. Colloid Interface Sci. 148:425-442.

Correns, C.W., and W. Von Engelhardt. 1938. Neue Untersuchungen ueber die Verwitterung des Kalifeldspates. Chemie der Erde 12:1-22

Duke, M.B., W.W. Mendell, and B.B. Roberts. 1985. pp. 57-68. Strategies for a permanent lunar base. In W.W. Mendell (ed.), Lunar bases and space activities of the 21st Century. Lunar and Planetary Institute, Houston

Fendorf, S.E., G.M. Lamble, M.G. Stapleton, M.J. Kelley, and D.L. Sparks. 1994. Mechanisms of chromium(III) sorption on silica. 1. Cr(III) surface structure derived by extended X-ray absorption fine structure spectroscopy. Environ. Sci. Technol. 28:284-289.

Grossl, P.R., D.L. Sparks, and C.C. Ainsworth. 1994. Rapid kinetics of Cu(II) adsorption/desorption on goethite. Environ. Sci. Technol. 28:1422-1429.

Hayes, K.F., and J.O. Leckie. 1986. Mechanism of lead ion adsorption at the goethite/water interface. p. 114-141. *In* J.A. Davis and K.F. Hayes (ed.) Geochemical processes at mineral surfaces. ACS Symp. 323. 190th Meet. Am. Chem. Soc., 8-13 Sep. 1985, Chicago. ACS, Washington, DC.

Holdren, G.R. Jr., and J.E. Adams. 1982. Parabolic dissolution kinetics of silicate minerals: An artifact of nonequilibrium precipitation processes? Geology 10:186-190.

Inskeep, W.P., and P.R. Bloom. 1985. An evaluation of rate equations for calcite precipitation kinetics at pCO_2 less than 0.01 atm and pH greater than 8. Geochim. Cosmochim. Acta 49: 2165-2180.

Keller, W.D., and W.H. Huang. 1971. Response of Apollo 12 lunar dust to reagents simulative of those in the weathering environment of Earth. Proceedings of the Second Lunar Science Conference, Vol. I, pp. 973-981, The M.I.T. Press, Cambridge.

Manley, E.P., and L.J. Evans. 1986. Dissolution of feldspars by low-molecular-weight aliphatic and aromatic acids. Soil Science 141:106-112.

Mast, M.A., and J.I. Drever. 1987. The effect of oxalate on the dissolution rates of oligoclase and tremolite. Geochim. Cosmochim. Acta 51:2559-2568.

Ming, D.W., and G.E. Lofgren. 1990. Crystal morphologies of minerals formed by hydrothermal alteration of synthetic lunar basaltic glass. *In* L.A. Douglas (ed.), Soil micromorphology: A basic and applied science. Developments in soil science 19, Elsevier Science Publishers B.V. Amsterdam.

McKay, D.S., and D.W. Ming. 1989. Mineralogical and chemical properties of the lunar regolith. pp. 45-69. *In* D.W. Ming and D.L. Henninger (eds.), Lunar base Agriculture: Soils for Plant Growth. Soil Science Society of America, Madison, WI.

Petrovich, R. 1981a. Kinetics of dissolution of mechanically comminuted rock-forming oxides and silicates I. Deformation and dissolution of quartz under laboratory conditions. Geochim. Cosmochim. Acta 45:1665-1674.

Petrovich, R. 1981b. Kinetics of dissolution of mechanically comminuted rock-forming oxides and silicates II. Deformation and dissolution of oxides and silicates in the laboratory and at the earth's surface. Geochim. Cosmochim. Acta 45:1675-1686.

Rimstidt, J.R., and P.M. Dove. 1986. Mineral/solution reaction rates in a mixed flow reactor: Wollastonite hydrolysis. Geochim. Cosmochim. Acta 50:2509-2516.

Sparks, D.L. 1989. Kinetics of soil chemical processes. Academic Press, New York.

Wollast, R., and L. Chou. 1985. Kinetic study of the dissolution of albite with continuous flow-through fluidized bed reactor. p. 75-96. *In* J.L. Drever (ed.) The chemistry of weathering. Reidel Publishing Company, Boston.

Zhang, P.C., and D.L. Sparks. 1989a. Kinetics and mechanism of molybdate adsorption/desorption at the goethite/water interface using pressure-jump relaxation. Soil Sci. Soc. Am. J. 53:1028-1034.

Zhang, P.C., and D.L. Sparks. 1989b. Kinetics and mechanism of sulfate adsorption/desorption at the goethite/water interface using pressure-jump relaxation. Soil Sci. Soc. Am. J. 54:1266-1273.

Zhang, P.C., and D.L. Sparks. 1990. Kinetics and mechanism of selenite and selenate adsorption/desorption at the goethite/water interface using pressure-jump relaxation. Environ. Sci. Technol. 24:1848-1856.

Chapter 2

DISSOLUTION KINETICS OF A LUNAR GLASS SIMULANT AT 298 K: THE EFFECT OF pH AND ORGANIC ACIDS

2.1 Introduction

2.1.1 Glass Dissolution Kinetics

Numerous studies have examined the dissolution of both natural (White, 1983; Berger et al., 1987; Crovisier et al., 1987) and synthetic glasses (Rana and Douglas, 1961; Boksay et al., 1967; El-Shamy et al., 1972; Boksay and Bouquét, 1975; Doremus, 1975; Lanford et al., 1979; Bunker et al., 1983; Bunker et al., 1988). Unlike the debate concerning the dissolution mechanism of crystalline silicates (surface reaction hypothesis vs. leached layer hypothesis), the general consensus is that the leached layer hypothesis describes the dissolution of most silicate glasses (Douglas and El-Shamy, 1967; Doremus, 1975; Lanford et al., 1979). Several researchers have shown that the development of a leached layer in silicate glasses follows a two step process (Douglas and El-Shamy, 1967; Hench and Clark, 1979; Mularie et al., 1979; Bunker et al., 1983). In the first step, the release kinetics of alkali and alkaline earth cations from the glass follows the parabolic rate law, while the second stage is best described by a linear rate equation. Several investigations have attributed the first step to a diffusion-controlled process involving the ion-exchange of protons in the bulk solution with charge balancing cations (e.g. Na^+) in

the glass. The second step has been described by the uniform dissolution of the glass Si framework (Douglas and El-Shamy, 1967; Hench and Clark, 1979).

However, recent studies have shown that the dissolution process of silicate glasses may be more complex than can be described by the above simplified model (Bunker et al., 1983; Bunker et al., 1988; Casey and Bunker, 1990). Similar to the above model (Douglas and El-Shamy, 1967; Hench and Clark, 1979) the first step involves the diffusion of reactive solutes (H_2O and H^+) into the bulk glass which partly hydrolyze the structure and exchange with alkali and alkaline earth cations. However, it is unclear as to the nature of the diffusing solutes. During the second stage, although alkali release is linear with time, the molar ratios of glass constituents found in solution are different from those in the bulk glass indicating incongruent dissolution. Investigations have indicated that the silica-rich leached layer, created by the ion exchange process, repolymerizes into a porous silica network. Solute diffusion through this layer is rapid relative to hydrolysis. Therefore, the overall rate of cation leaching from the glass is controlled by hydrolysis of the bulk glass and not the diffusion of solutes through a leached layer (Casey and Bunker, 1990). The kinetics and magnitude of these leaching reactions are affected by temperature, solution composition, and structure of the solid (Casey et al., 1988).

2.1.2 Objectives

A great deal of information exists in the literature on the dissolution of glasses at different pH values. However, there is little information on the dissolution of either naturally occuring or synthetic glasses in the presence of naturally occurring organic acids. Additionally, lunar soils differ substantially from terrestrial soils and information gleaned from these studies is not directly transferable. Therefore, the

objectives of this study are to examine the rate and mechanism of dissolution for a high Ti simulated lunar glass under rhizosphere conditions. This involves examination of glass dissolution at pH values of 3, 5, and 7. The influence of naturally occurring organic acids (citric and oxalic) was also examined at pH 7. All of these studies were conducted in batch reactors.

2.2 Materials and Methods

2.2.1 Solid Material

Experiments were conducted using a synthetic lunar basaltic glass produced by Corning Glass Company, Corning, New York (Fig. 2.1). The chemical composition of the glass was determined by electron microprobe analysis (Table 2.1) and is similar to high titanium glasses found in the lunar mare regions . Subsequent Mössbauer spectroscopy indicated that the iron content of this glass is primarily in the Fe^{+2} state. The bulk glass was ground in a corundum grinding jar and dry sieved into eight particle size fractions (Table 2.1). No additional effort was made to separate fines adhering to the grains. Investigations on the dissolution of crystalline silicates show a significant effect of fines on the kinetics of dissolution (Holdren and Berner, 1979). However, White and Claassen (1980) showed that the dissolution rates of amorphous silicates do not appear to be affected by such material other than by increasing surface area. The different sieve fractions were then combined to reproduce a grain size distribution similar to Apollo 11 mare soils (10084,853). The combined glass sample was heated to 383K to remove adsorbed water and was stored in air-tight containers in an environmental glove box purged with argon gas. The specific surface area was 0.187 m^2/g as determined by a 3 point N_2 Brunauer-Emmett-Teller (B.E.T.)

gas adsorption isotherm method. This value was in close agreement with the calculated surface area from particle size distribution.

Figure 2.1 SEM image of the high Ti lunar glass simulant.

Table 2.1 Chemical Composition, Grain Size Distribution, and Surface Area of Lunar Glass Simulant 2D.

Sieve Size	Microns	Percent
> 20 mesh	+ 850	7
> 35 mesh	+ 500	4
> 60 mesh	+ 250	8
> 100 mesh	+ 150	8
> 200 mesh	+ 75	16
> 270 mesh	+ 53	9
> 400 mesh	+ 38	16
< 400 mesh	- 38	32

Oxide	Wt %	Mol %
SiO_2	47.9	51.5
Al_2O_3	13.0	8.3
TiO_2	6.6	5.4
FeO	12.8	11.5
MnO	0.16	0.15
MgO	6.9	11.0
CaO	10.4	11.8
Na_2O	0.03	0.03
K_2O	0.05	0.03
Cr_2O_3	0.22	0.10
P_2O_5	0.15	0.07
Total	98.21	99.81

Surface area	0.187 m^2/g

2.2.2 Reacting Solutions

For the experiments conducted at pH 3 and 5, we used standard biphthalate based (0.05 M) pH-buffers (Fisher Scientific Corporation). Additionally, each buffer contained formalin to retard the growth of algae. The pH 7 solution was buffered using 1 mM $KHCO_3$. The effect of ionic strength on glass dissolution was measured by conducting pH 7 experiments at three different ionic strengths. The pH

of the buffer was adjusted using 1M HCl. Subsequently, the ionic strength was adjusted to 0.005, 0.01, and 0.05 M using $NaNO_3$.

Solutions for the organic acid experiments were prepared using reagent grade citric and oxalic acids (Sigma Corporation) and ultrapure water. The concentrations of the organic acids were 2 and 20 mM, which were chosen to represent concentrations found in the plant root environment (Stevenson, 1967). The pH of all organic acid solutions was adjusted to a pH 7 with 1 M NaOH. This pH was chosen because both citric and oxalic acid are in a dissociated form. Fluctuations in pH during the experiments were adjusted by dropwise addition of 1 N NaOH or HCl. Mercuric chloride (0.02 mM) was added to each sample to prevent the microbial degradation of the organic acids. The above experimental conditions are summarized in Table 2.2.

Table 2.2 Summary of experimental conditions.

Solution	Acid Conc. (m mole L^{-1})	pH [1]	Ionic Strength (mole L^{-1})	Time Total (days)
Biphthalate	--------	3.0	0.05	365
Biphthalate	--------	5.0	0.05	365
Water	--------	7.0	0.05	365
Water	--------	7.0	0.01	
Water	--------	7.0	0.005	
Citrate	20	7.0	0.123	172
	2.0	7.0	0.0123	
Oxalate	20	7.0	0.056	172
	2.0	7.0	0.006	

[1] pH of the solution during the experiment.

2.2.3 Experimental

The batch reactor experiments were conducted in acid-washed high-density polyethylene bottles. The batch reactors were placed in an environmentally controlled incubator at 298K ± 1. The incubator was kept dark to prevent the photo-oxidation of the organic acids. The batch reactors were gently agitated (60 revs/min) on a rotating shaker between sample analyses. Approximately two hours before sampling, the reactors were allowed to settle. For each analysis, 10 mL of reacting solution was withdrawn from the top of the solution column and the sample was filtered through a 0.20 micron Gelman filter (Gelman GA-8, Gelman Sciences, Inc., Ann Arbor, MI). After the sample aliquot was filtered, an additional 10 mL of reacting solution was added back to the original reaction vessel. These sampling protocols were chosen in order to maintain constant solution/solid ratios throughout the experiment. The pH of the filtered sample was decreased to approximately pH 3 using 0.5 M HCl to prevent precipitation of metals prior to analysis. Samples were analyzed for Si, Al, Ti, Fe, Mg, Ca, and the minor elements Cr and Mn by Inductively Coupled Plasma (ICP) spectrometry. Additionally, a blank for each reacting solution was analyzed and any metal contaminants present were subtracted from the sample results.

The aqueous solution data was entered into GEOCHEM-PC (Parker et al., 1993) and MINTEQA2 (Allison et al., 1991) chemical speciation programs. These programs determined possible supersaturation of ions with respect to particular solid phases and were used in conjunction with electron microscopy to determine precipitate formation.

2.2.4 Electron Microscopy and Electron Probe Microanalysis (EPMA)

At the termination of the dissolution experiments the weathered glass particles were filtered, washed twice with deionized water, air dried, and stored under desiccation. For scanning electron microscopy (SEM), particles from the various experiments were mounted on silver tape and glued onto Al stubs using epoxy resin. The grains were coated with carbon and examined using a JEOL JSM 35 scanning electron microscope.

For the transmission electron microscopy (TEM) experiments grains from the various treatments were mounted on epoxy stubs using Embed 812, epoxy resin. Thin sections of the epoxy embedded grains were obtained using a diamond knife and mounted on a holey carbon film supported by a copper mesh grid. Likewise, the samples were coated with carbon and examined with a JEOL JEM 2000FX transmission electron microscope. Semi-quantitative compositions were obtained from the glass before and after exposure to the reacting solutions using an energy dispersive spectrometer (EDS) and a Link ExL GEN 1089 system analyzer.

For electron probe microanalysis, polished petrographic thin sections of epoxy embedded particles (<1.0 μm) were carbon coated and analyzed using a Cameca Camebax microbeam electron microprobe operated at 15 kV and 10 nA beam current. National Institute of Standards and Technology mineral standards were used for calibration.

2.2.5 Data Analysis

Numerous studies (Lagache, 1976; Busenburg and Clemency, 1976; Grandstaff, 1977; Holdren and Berner, 1979; White and Claassen, 1979; White, 1983) have described changes in aqueous chemistry as a function of time during dissolution

of silicate minerals using the parabolic and linear empirical rate equations, respectively:

$$Q = Q_0 + k_p t^{1/2} \quad (2.1)$$

and

$$Q = Q_0 + k_l t \quad (2.2)$$

where Q (moles cm^{-2}) is the mass transfer of a ion into solution per unit surface area of the glass. Q_0 (moles cm^{-2}) is the result of extrapolation of either Eqn. (2.1) or (2.2) to time zero and is a function of the initial surface ion exchange (White, 1983) and k_p and k_l are the parabolic and linear rate coefficients, respectively.

2.3 Results

2.3.1 Introduction

Experimental data for the release of Si, Al, Fe, Mg, Ca and Ti from the glass are shown in Figs. (2.2-2.9 and 2.21-2.26). Data for the pH 7 and 2 mM oxalic acid are excluded because elemental analysis were beyond detection limitations. The experimental data were applied to the linear and parabolic rate expressions (Eq{2.1} and Eq{2.2}) and the closeness of fit was indicated by the coefficient of determination (r^2). In most cases r^2 was greater than 0.97 (Table 2.3). Short term data (8 h) were excluded from fitting due to the dependence on surface ion exchange during the initial dissolution of the glass (White, 1983). Rate coefficients and coefficients of determination for all experiments are summarized in Table 2.3.

2.3.2 pH Experiments

The molar ratios of Ca, Mg, Fe, and Al to Si in solution were greater than the molar ratios in the bulk glass indicating incongruent dissolution of the surface.

The release rates of Ca, Mg, Al, and Fe from the glass at pH 3 and 5 follow a two stage process (Fig. 2.2- 2.9). The first stage is characterized by a non-linear release of these elements and is described well by the parabolic rate equation (Eq. 2.1). In the second stage, the release of these elements is linear with time (Eq. 2.2). The first stage occurs up to 4.15×10^6 s (48 days) followed by linear release until the termination of the experiment 31.5×10^6 s(365 days). Calculated rate coefficients for both stages in the pH 3 and 5 experiments showed similar trends with rate constants for the release of metals decreasing in the order Al>Ca>Mg>Fe (Table 2.3). In contrast, silica is described well by the linear rate equation (Fig. 2.8 and 2.9). Deviations in the linear release rate of silica occurred at pH 3 and 5 at time periods greater than 8.3×10^6 s (96 days). The calculated rate constant for silica release was an order of magnitude greater for the pH 3 experiment than that at pH 5 (Table 2.3). The molar ratios of aqueous Ca, Mg, Al, and Fe to Si show a decrease in the first stage and reach a steady state in the second stage (Fig 2.10 and 2.11). Slight increases in this molar ratio near the end of the experiment are due to decreases in the aqueous silica concentration. Although the molar ratios reach a steady state in the second stage they are greater than the values measured in the bulk glass. Trace quantities of Ti, Cr, and Mn were released at all pHs. Variations in the ionic strength at pH 7 did not affect the dissolution rate.

The computer codes GEOCHEM-PC and MINTEQA2 indicate that in reacting solutions silicic acid concentrations at pH 3 collected at 16.6×10^6 s (192 days) and Al concentrations at pH 5 collected at 4.2×10^6 s (48 days) are supersaturated with respect to amphorous Si and gibbsite, respectively. Therefore, it might be expected that these solid phases precipitate from solution.

Table 2.3 **Parabolic and linear rate parameters and correlation coefficients describing major element release under various experimental conditons for the lunar glass simulant. (Q_0, moles·cm^{-2}·10^{-10}; k_p, moles·cm^{-2}·s$^{1/2}$·10^{-13}; k_l, moles·cm^{-2}·s^{-1} ·10^{-16})**

		Ca				Mg				Al			
Sta.[1]	Exp.	r^2	Q_0	k_p	k_l	r^2	Q_0	k_p	k_l	r^2	Q_0	k_p	k_l
1	pH=3	.99	.964	3.31	--	.99	.859	2.73	--	.99	.705	4.15	--
1	pH=5	.99	.413	1.09	--	.99	.182	1.02	--	.99	.064	1.27	--
2	pH=3	.99	5.37	--	.601	.99	4.28	--	.580	.98	7.67	--	.669
2	pH=5	.99	2.04	--	.235	.99	1.68	--	.224	.98	2.28	--	.237
--	Citr[2]	.99	-.348	1.95	--	.99	-.446	1.78	--	.99	-1.12	2.74	--
--	Citr[3]	.99	-2.37	1.86	--	.99	-.326	1.76	--	.98	-1.00	2.67	--
--	Oxal[4]	--	--	--	--	.95	.237	1.46	--	.97	-1.06	1.90	--

1 Stage: Stage 1, parabolic release; Stage 2, linear release.
2 20 mM Citric acid.
3 2 mM Citric acid.
4 20 mM Oxalic acid.

Table 2.3 Continued

		Fe				Si[1]			Ti[1]	
Sta.[1]	Exp.	r^2	Q_0	k_p	k_l	r^2	Q_0	k_l	r^2	Q_0	k_l
1	pH=3	.99	.739	3.28	–	.99	.242	1.88	–	–	–
1	pH=5	.99	.255	.977	–	.99	.255	.888	–	–	–
2	pH=3	.99	5.82	–	.513	–	–	–	–	–	–
2	pH=5	.97	2.10	–	.116	–	–	–	–	–	–
–	Citr[2]	.98	-.528	1.79	–	.99	2.25	1.25	.99	.096	.335
–	Citr[3]	.99	-.537	1.92	–	.99	.094	1.16	.98	.112	.296
–	Oxal[4]	.98	-.203	1.70	–	.95	.338	1.32	–	–	–

1. Stage: First stage parabolic release; Second stage linear release.
2. 20 mM Citric acid.
3. 2 mM Citric acid.
4. 20 mM Oxalic acid.

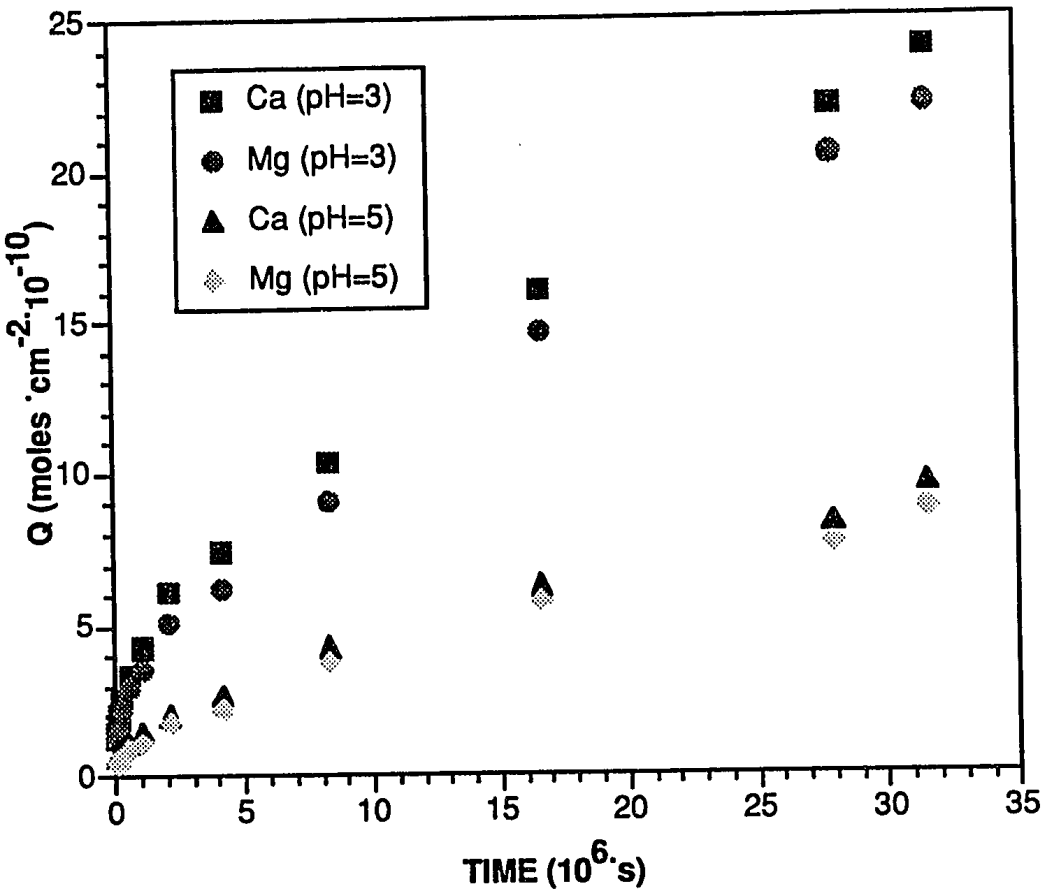

Figure 2.2 **Two stage release of Ca and Mg from the lunar glass simulant at pH 3 and 5.**

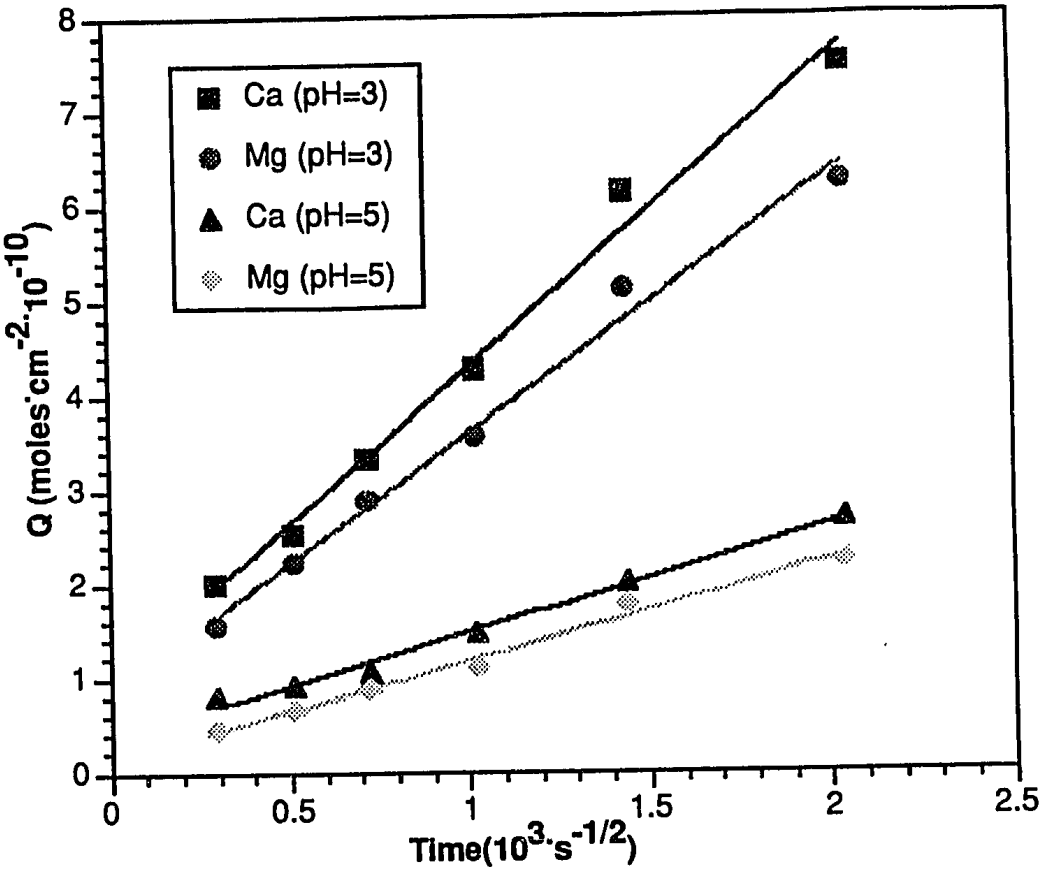

Figure 2.3 **Stage 1: parabolic release of Ca and Mg from the lunar glass simulant at pH 3 and 5.**

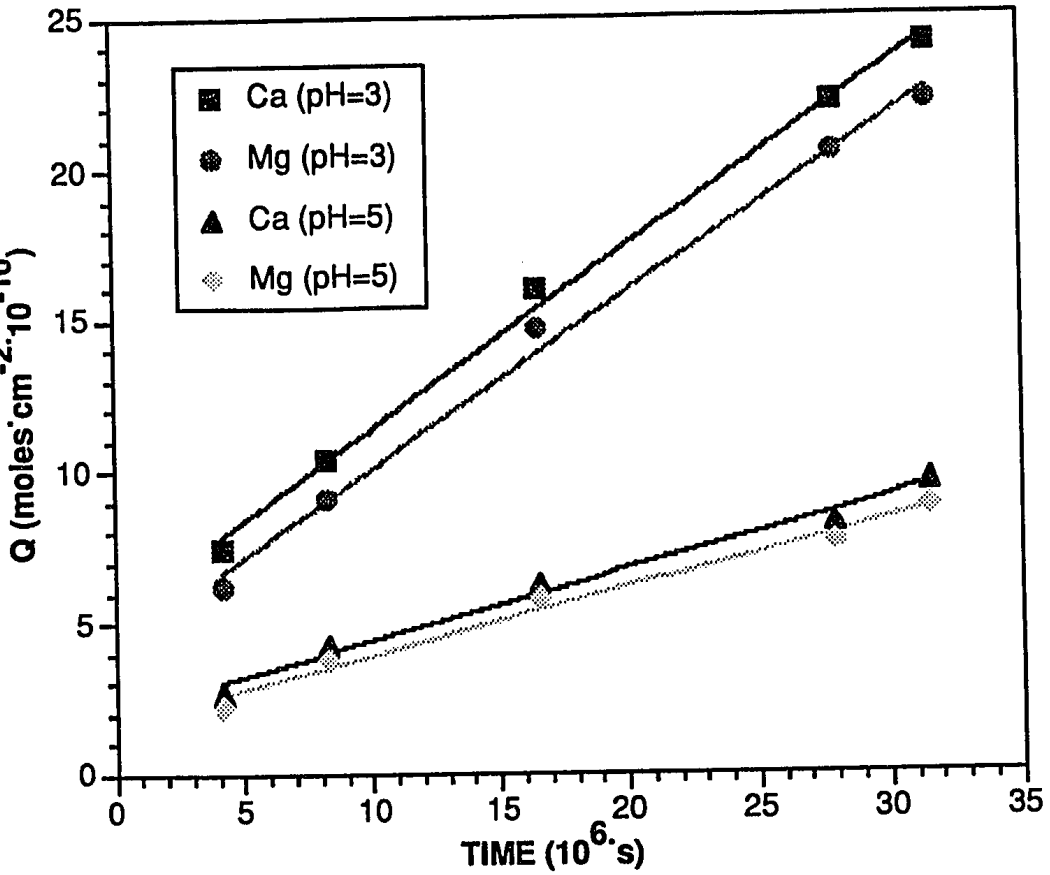

Figure 2.4 **Stage 2: linear release of Ca and Mg from the lunar glass simulant at pH 3 and 5.**

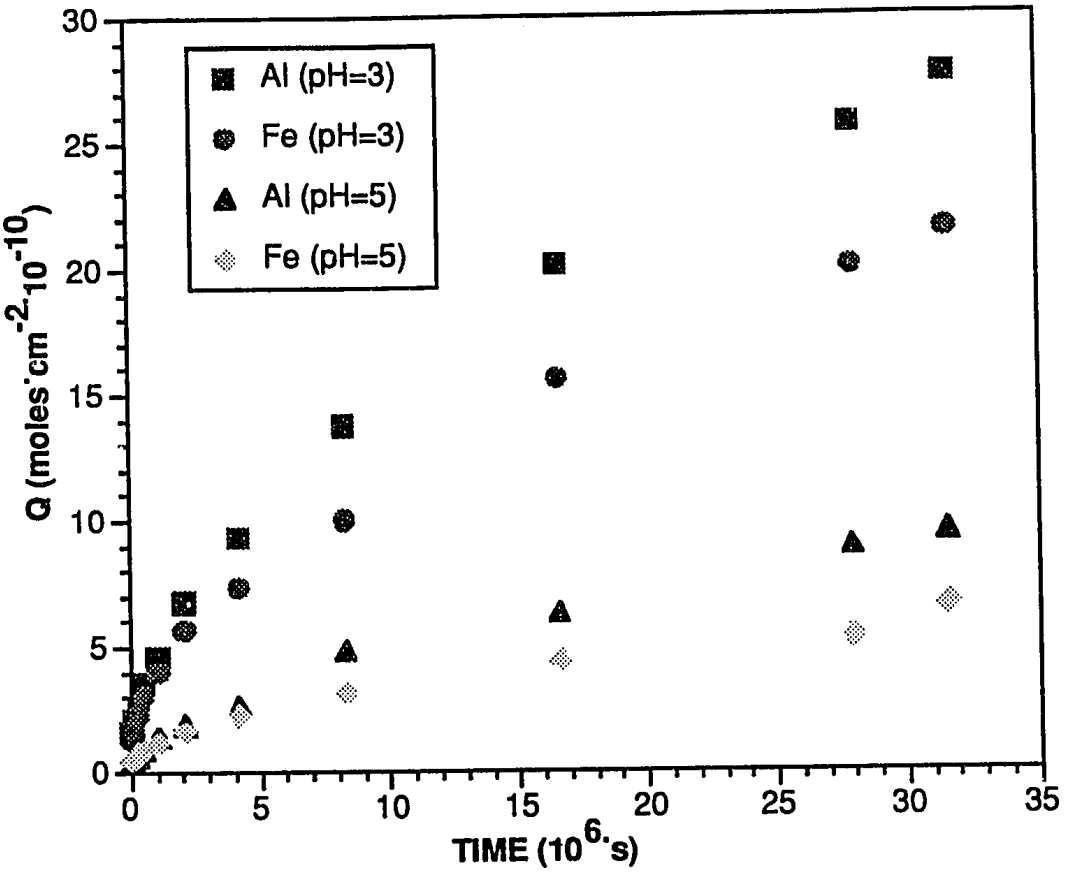

Figure 2.5 **Two stage release of Fe and Al from the lunar glass simulant at pH 3 and 5.**

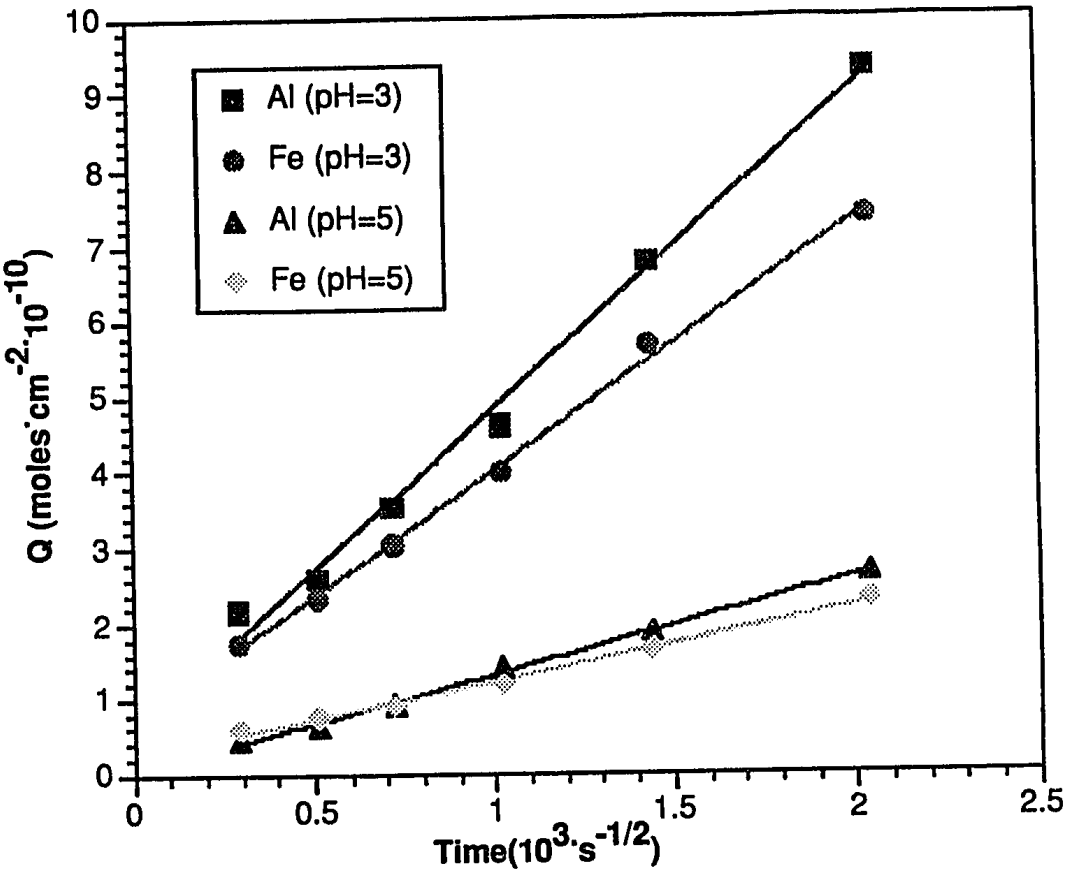

Figure 2.6 **Stage 1: parabolic release of Fe and Al from the lunar glass simulant at pH 3 and 5.**

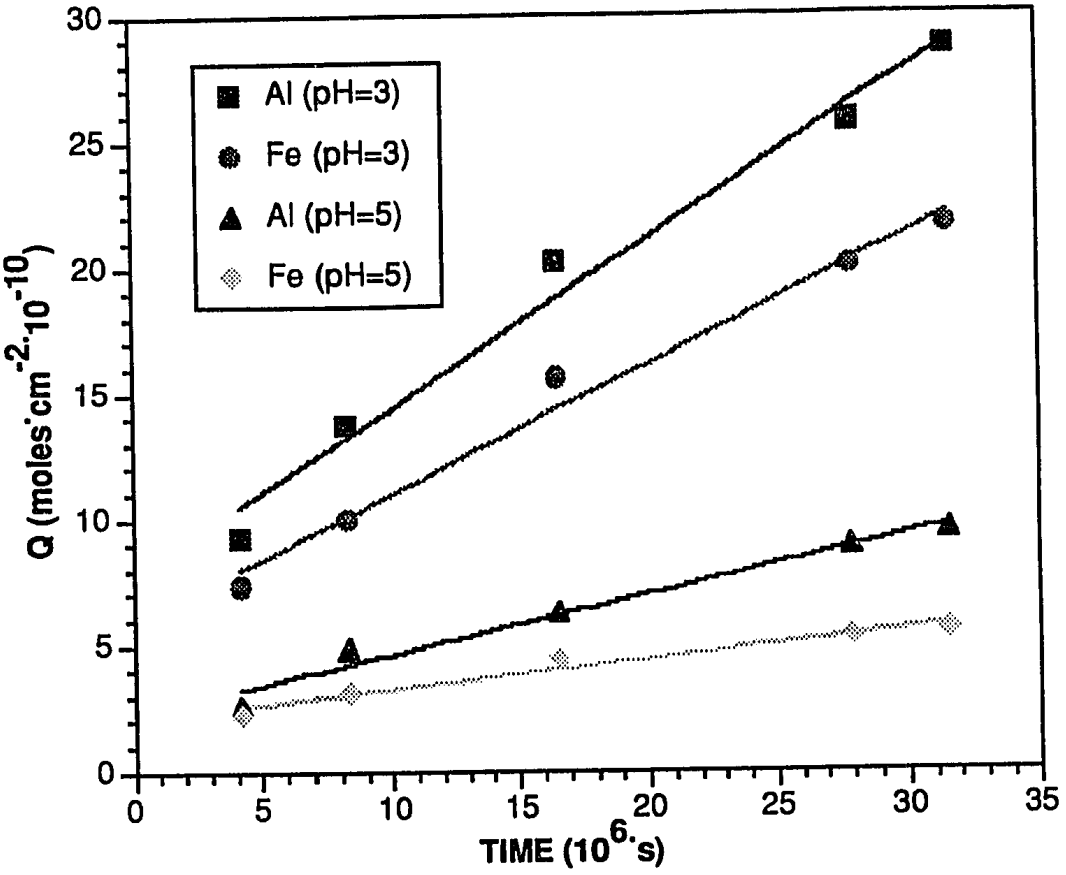

Figure 2.7 **Stage 2: linear release of Fe and Al from the lunar glass simulant at pH 3 and 5.**

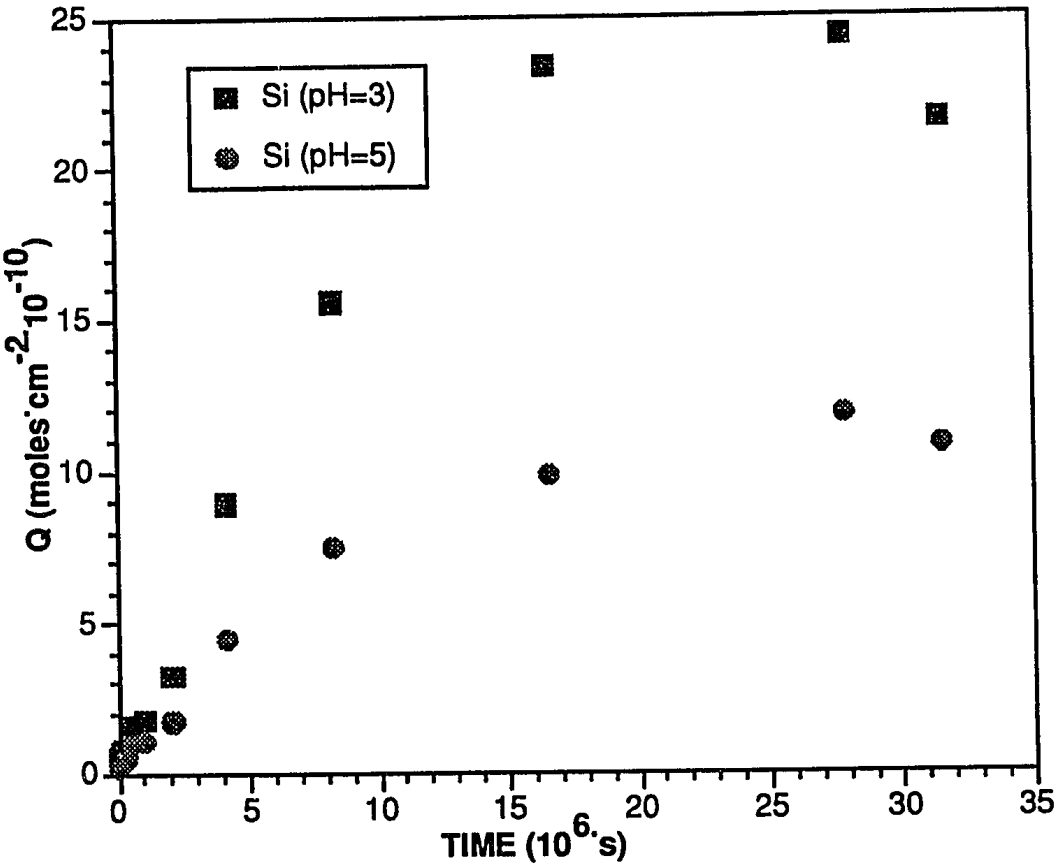

Figure 2.8 The release of Si into aqueous solution from the lunar simulant glass as a function of time at pH 3 and 5.

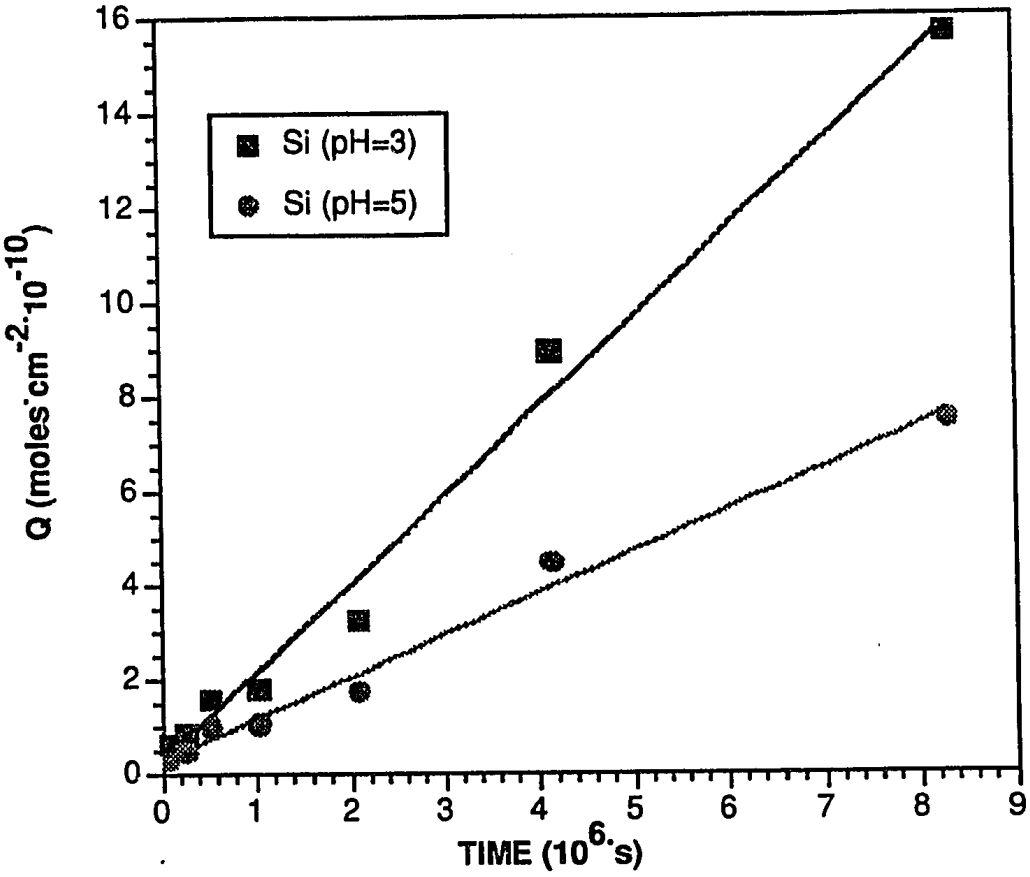

Figure 2.9 Linear release of Si for 8.3 X 10^6 s at pH 3 and 5.

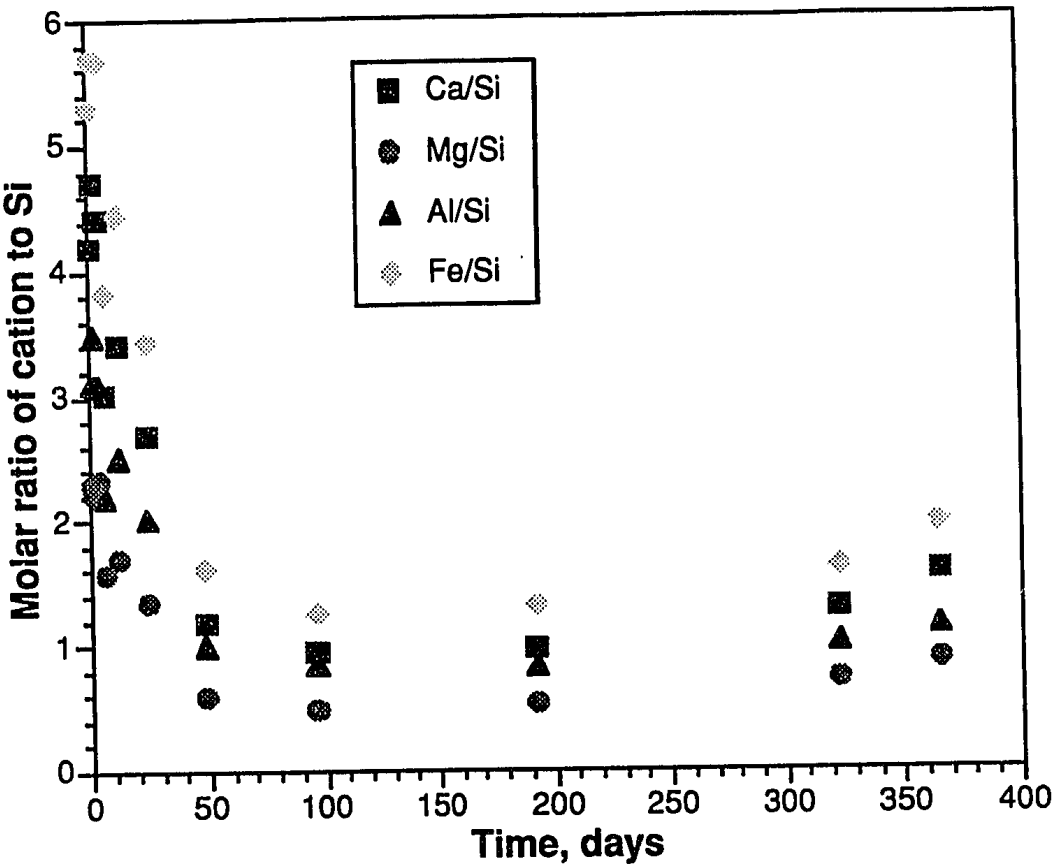

Figure 2.10 Molar ratio of major cations to Si release into aqueous solution from the lunar glass simulant as a function of time at pH 3.

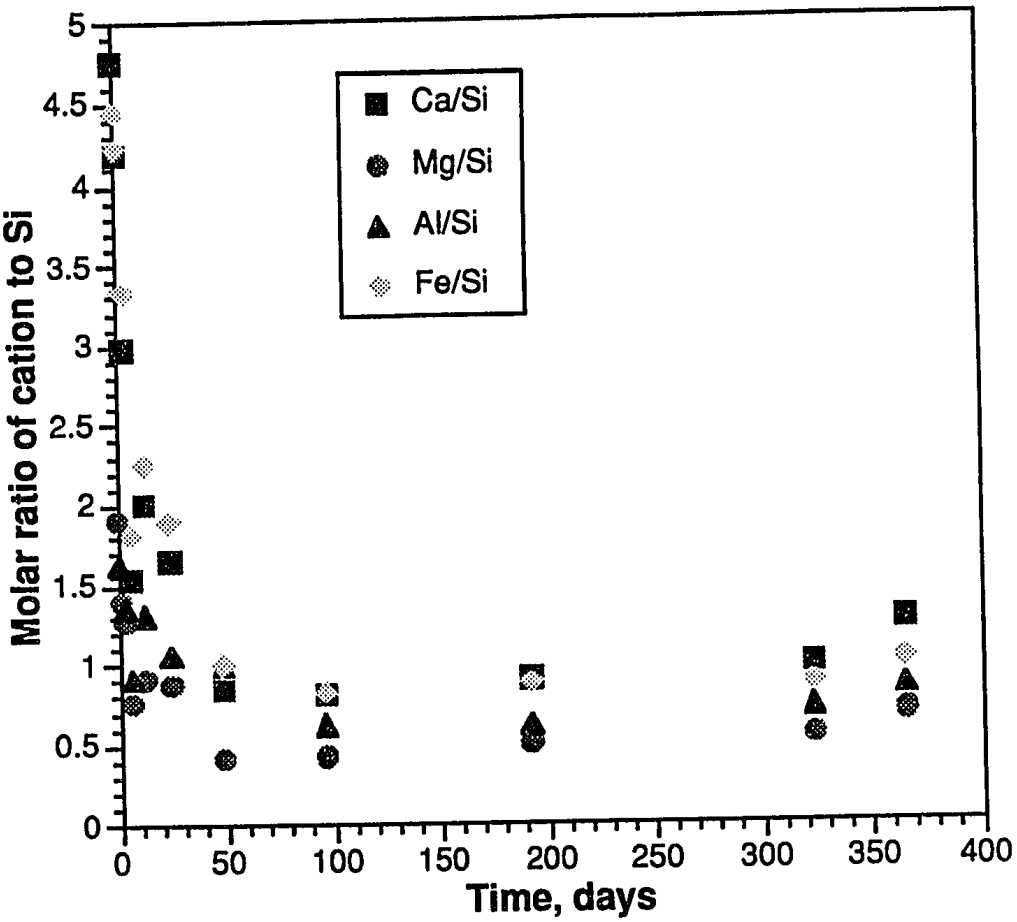

Figure 2.11 Molar ratio of major cations to Si release into aqueous solution from the lunar glass simulant as a function of time at pH 5.

Transmission electron microscopy indicated the presence of a leached layer at both pH 3 and 5 (Fig 2.12-2.19) (as indicated by the lighter edge surrounding the particle). Note that the clear striations running parallel are caused by the fracture of the glass during thin section preparation and were unavoidable. The leached layers were approximately 100 nm and 47 nm thick for the pH 3 and 5 samples, respectively. Semi-quantitative EDS spectra were obtained for both the pH 3 and 5 samples. For the pH 3 sample, a series of EDS spectra were obtained along a weathered edge of the glass particle (Fig. 2.14). Four regions were analyzed, starting from the outer leached edge and moving inward toward the unleached glass . In addition, one spectra was obtained from an unweathered sample of glass as a reference. The five spectra obtained from these regions are displayed in Figure 2.15 and 2.16. Note that the Cu peak is due to the copper grid used to hold the sample. Changes in elemental composition are determined by comparing the relative peak heights to Ti (only trace quantities of this element were found in solution). The results of the four EDS spectra are summarized below:

Region 1: Area closest to the reacting solution showing a depletion in all major elements relative to Ti. The leached region is composed of Ti and Si which are more resistant to weathering. Note a reduction in the Si peak relative to Ti indicating a depletion in Si at the surface (Fig. 2.15a).

Region 2: This region shows a depletion in all elements except silica. This leached region is similar in composition to region 1 except there is little reduction in the Si peak relative to Ti (Fig. 2.15b).

Region 3: This region shows a similar elemental composition to region 2; however, the extent of elemental depletion is less (Fig. 2.15c).

Region 4: This region shows little elemental depletion (Fig. 2.15d) and is similar to the spectra obtained from the unweathered sample of glass (Fig. 2.16).

The above results provide insight into the dissolution reaction occurring at the surface of the glass at pH 3. Calcium, Mg, Al, and Fe were depleted throughout the leached region creating a zone enriched in Ti and Si. As weathering proceeded Si was removed at the surface creating a surface zone rich in Ti. Results of EDS spectra from the pH 5 samples showed similar results: a region enriched in Ti and Si.

Transmission electron microscopy and EDS were employed to determine the presence of possible precipitates. At pH 3 the presence of an amorphous silica precipitate would be difficult to distinguish from the amorphous leached layer rich in silica already present. As expected, no amorphous silica distinct from the leached layer was observed using TEM. Transmission electron microscopy results from the pH 5 experiment did not indicate the presence of an Al precipitate which is consistent with aqueous solution data which does not show a drop in Al concentration.

Scanning electron microscopy was employed to examine the leached surfaces of the glass for crazing (i.e. cracking of the mineral surface). Crazing is caused by the build up of stress within the leached layer and can occur while the material is immersed in the reacting solution or can be caused by drying (Casey and Bunker, 1990). Figures 2.20 and 2.21 show crazing of the leached glass surface reacted at pH 3. This crazing was only observed after the glass had been dried in a dessicator for several weeks. Similar crazing was not observed for the glass reacted at pH 5.

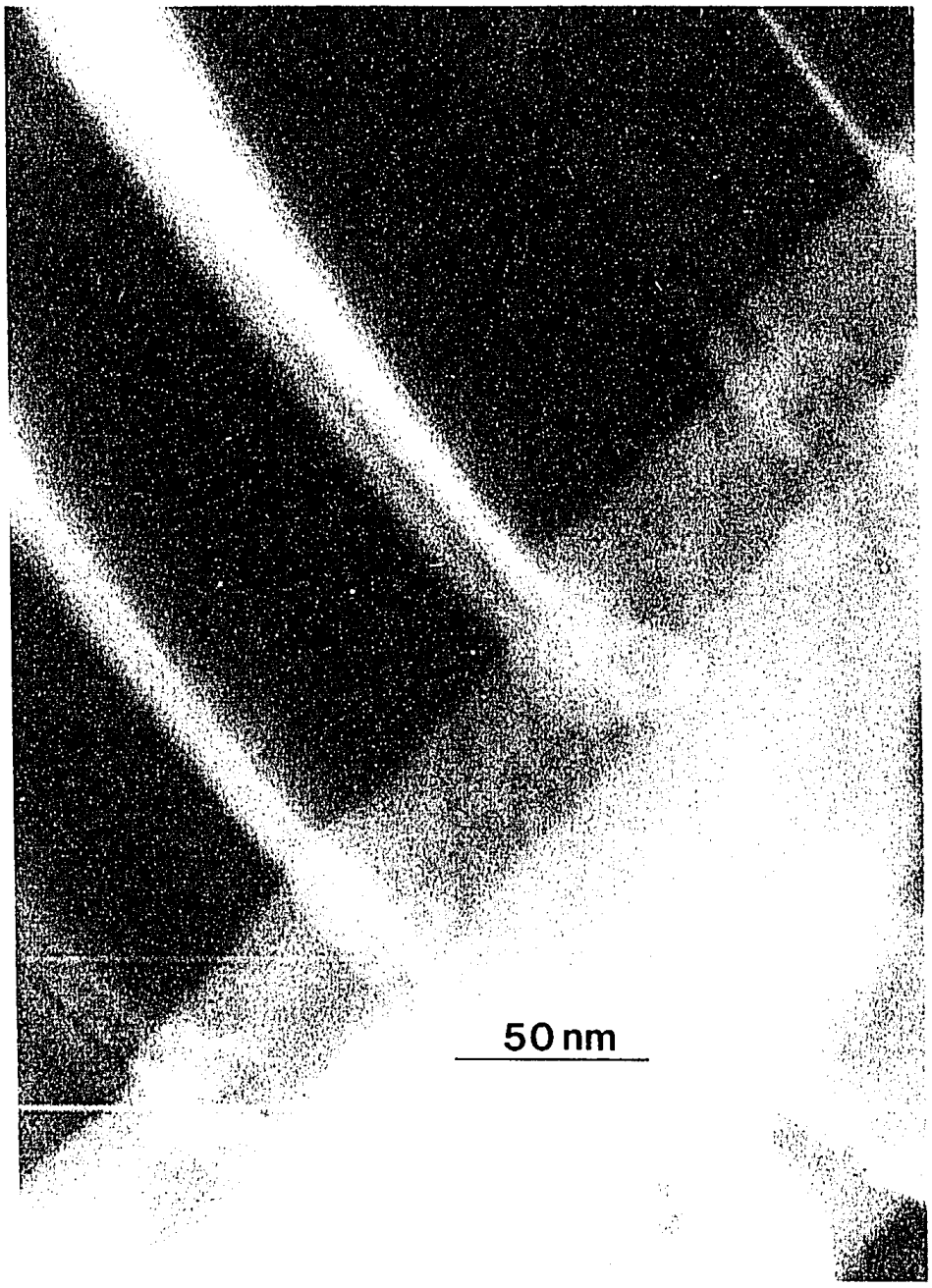

Figure 2.12 TEM image of the lunar simulant glass surface after reaction with an aqueous solution at pH 3. A leached layer is clearly visable at the outer edge of the glass particle.

Figure 2.13 TEM image of the lunar simulant glass surface after reaction with an aqueous solution at pH 3. EDS spectra were obtained from the leached corner of the particle.

Figure 2.14 High magnification TEM image of Fig. 2.13 showing the four regions where the EDS spectra were obtained.

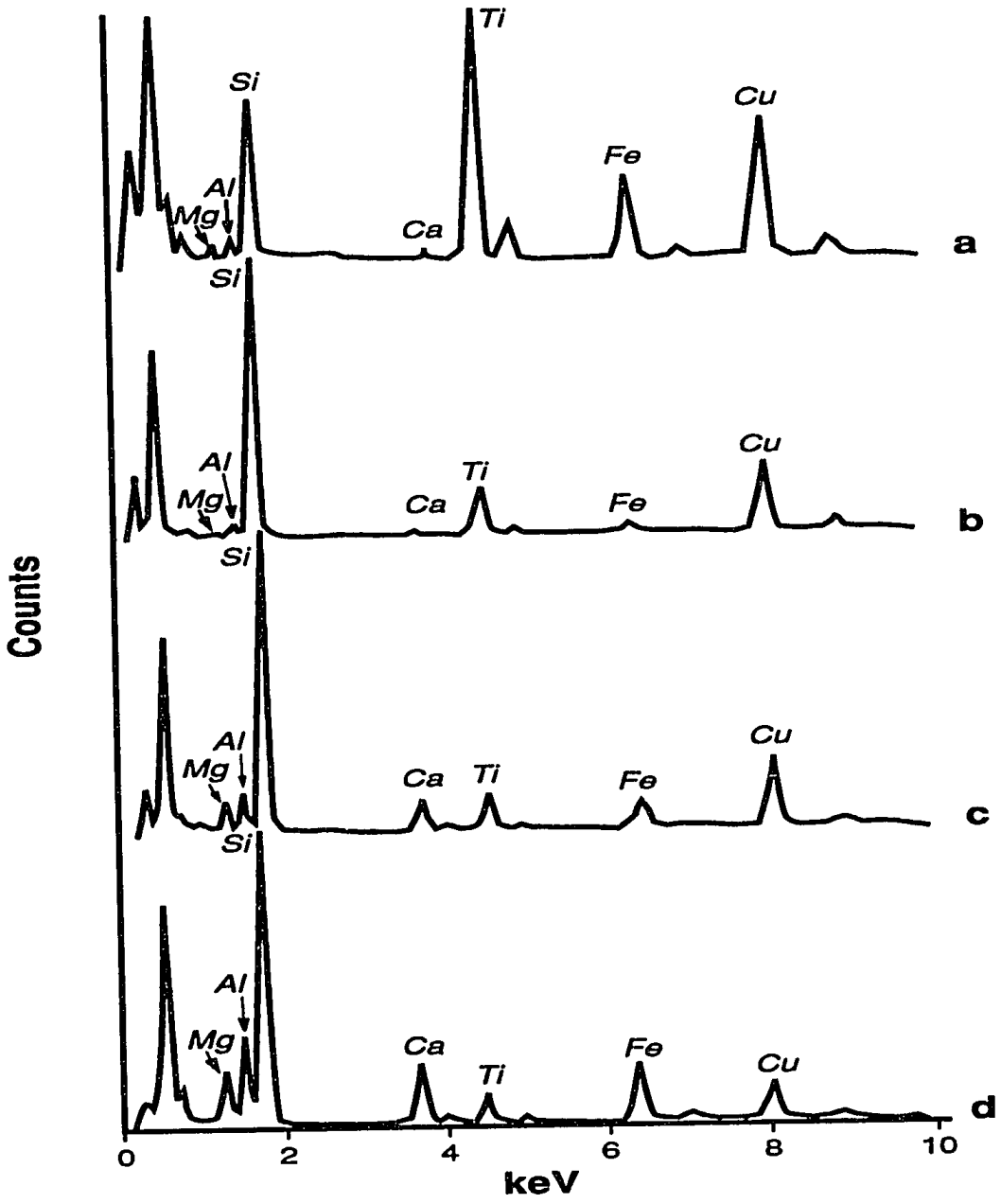

Figure 2.15 EDS spectra obtained from the glass surface depicted in Fig. 2.14. a) Region 1, b) Region 2, c) Region 3, d) Region 4.

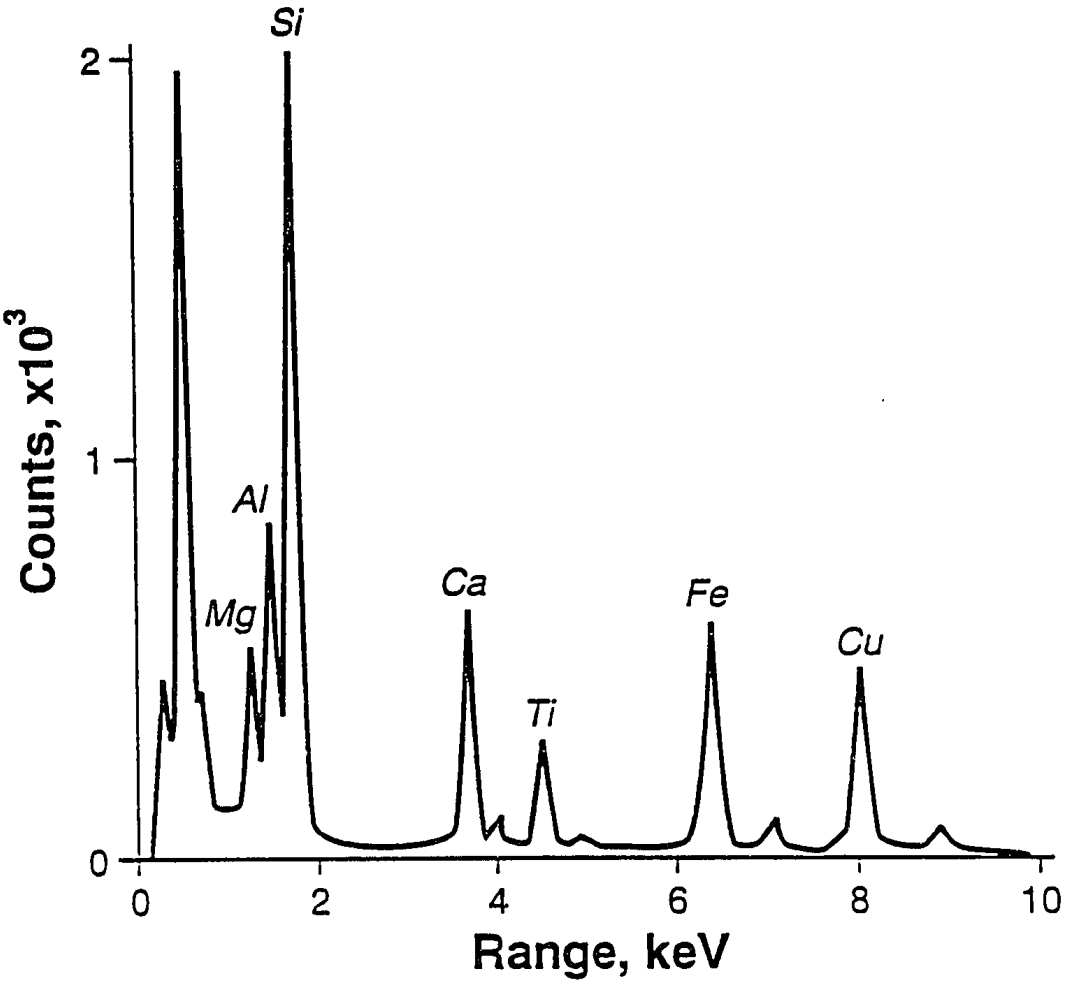

Figure 2.16 EDS spectra obtained from the unweathered bulk glass

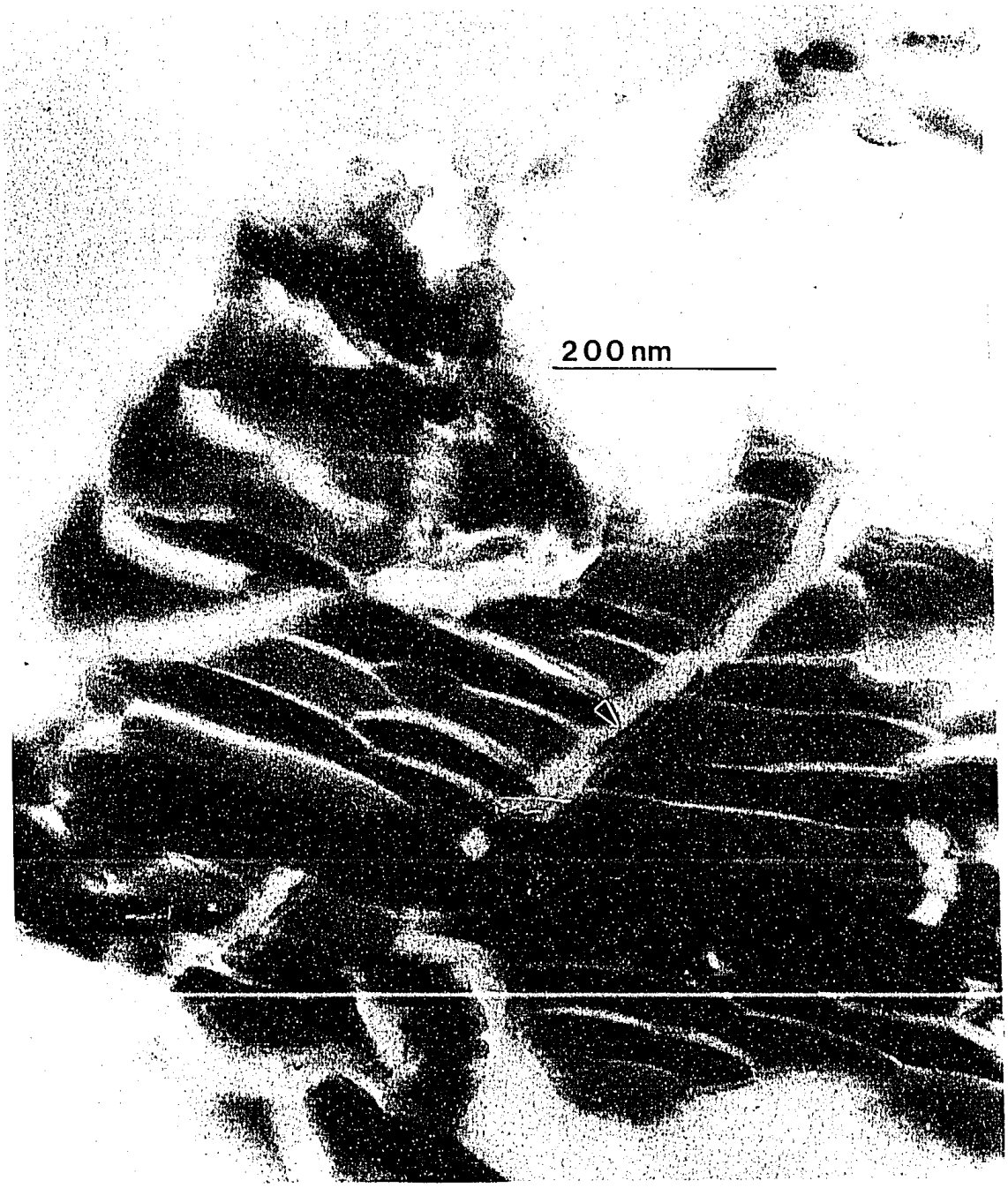

Figure 2.17 TEM image of the lunar simulant glass surface after reaction with an aqueous solution at pH 5. A leached layer is clearly visable at the outer edge of the glass particle.

Figure 2.18 High magnification TEM image of Fig. 2.17.

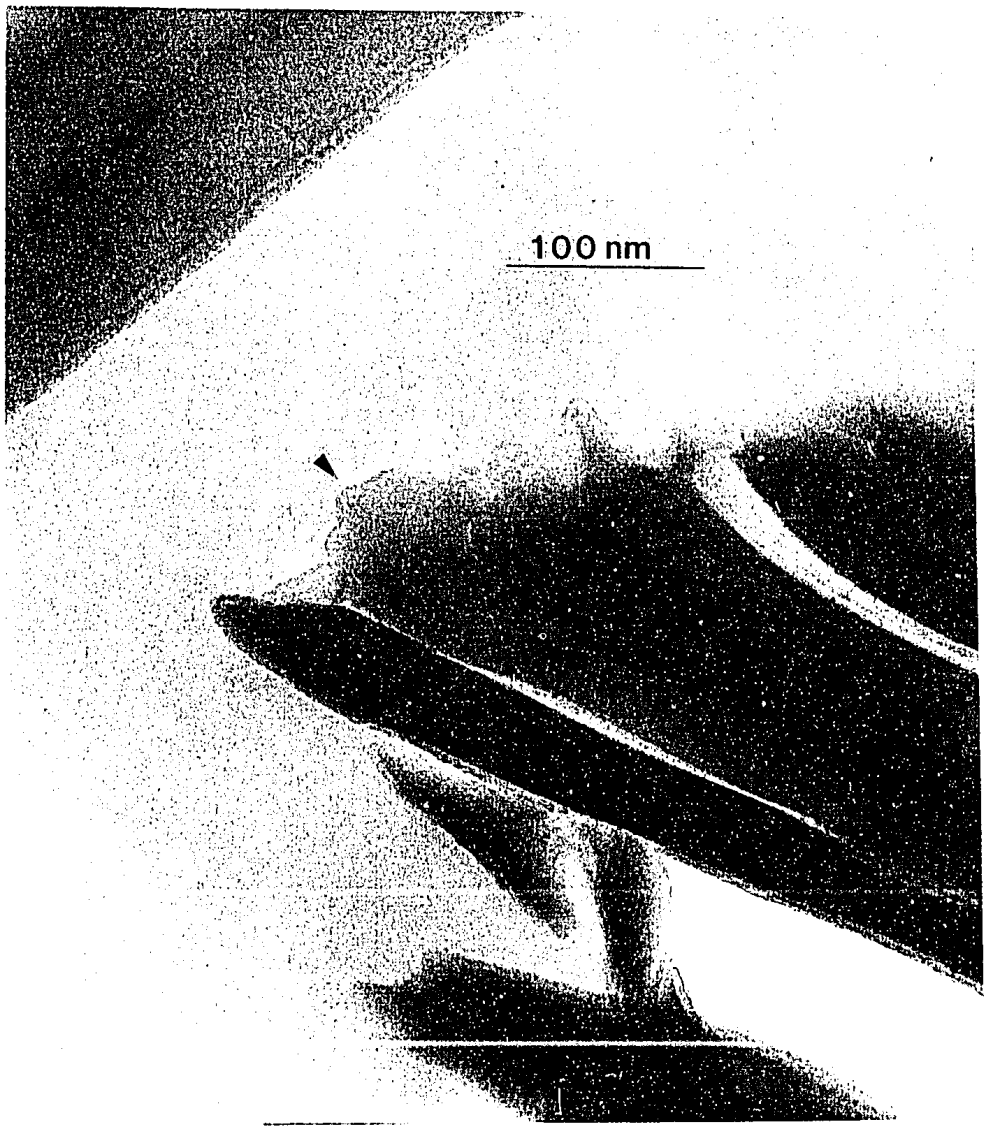

Figure 2.19 TEM image of the lunar simulant glass surface after reaction with an aqueous solution at pH 5. A non-uniform leached layer is clearly visable at the outer edge of the glass particle.

Figure 2.20 SEM image of the lunar simulant glass surface after reaction with an aqueous solution at pH 3 and storage in a dessicator showing crazing of the glass surface.

Figure 2.21 High magnification SEM image of Fig. 2.20.

2.3.3 Organic Acid Experiments

In contrast to the pH dissolution experiments, the release of Ca, Mg, Al, and Fe in the presence of citric and oxalic acid exhibited a one stage process. Dissolution of the glass in both citric and oxalic acid was congruent for the duration of the experiment. The release of these metals was described well by the parabolic rate equation (Eq. 2.1) (Fig 2.22-2.25). Calculated rate coefficients for both organic acids decreased in the order Al>Ca>Fe>Mg and were slightly greater for citrate (Table 2.3). The 2 mM citrate data is not shown because the release rates of all major elements were similar to the 20 mM citrate. Silica release in both oxalate and citrate followed a linear release rate up to 4.2 x 10^6 s (48 days) and than approached a steady state (Figs 2.26 and 2.27). Calculated rate constants for silica release are calculated from the linear portions of mass transfer plots and were similar for both organic acids (Table 2.3). Detectable amounts of Ti were released for both citric acid experiments. Similar to silica, Ti release was linear up to 4.2 x 10^6 s (48 days) and than approached a steady-state (Figs 2.26 and 2.27). Trace quantities of Cr and Mn were released in all organic acid experiments while trace amounts of Ti were released only in the oxalate experiments.

The computer codes GEOCHEM-PC and MINTEQA2 indicated that in the reacting solutions the concentration of Al at 1.04 x 10^6 s (12 days)becomes supersaturated with respect to gibbsite for both citric acid experiments and this solid phase might be expected to precipitate. Transmission electron microscopy showed the presence of a leached layer for both citrate and oxalate experiments (Fig. 2.28-2.30). Semi-quantitative EDS analyses showed the leached layer to be rich in Si and Ti

similar to the pH experiments. In contrast to the results of the computer speciation programs, a precipitate was observed for the oxalate experiment while none was observed for the citrate experiment (Fig. 2.29 and 2.30). The precipitate appears to be mainly composed of iron as verified by EDS. Attempts to obtain electron diffraction patterns from the precipitate failed.

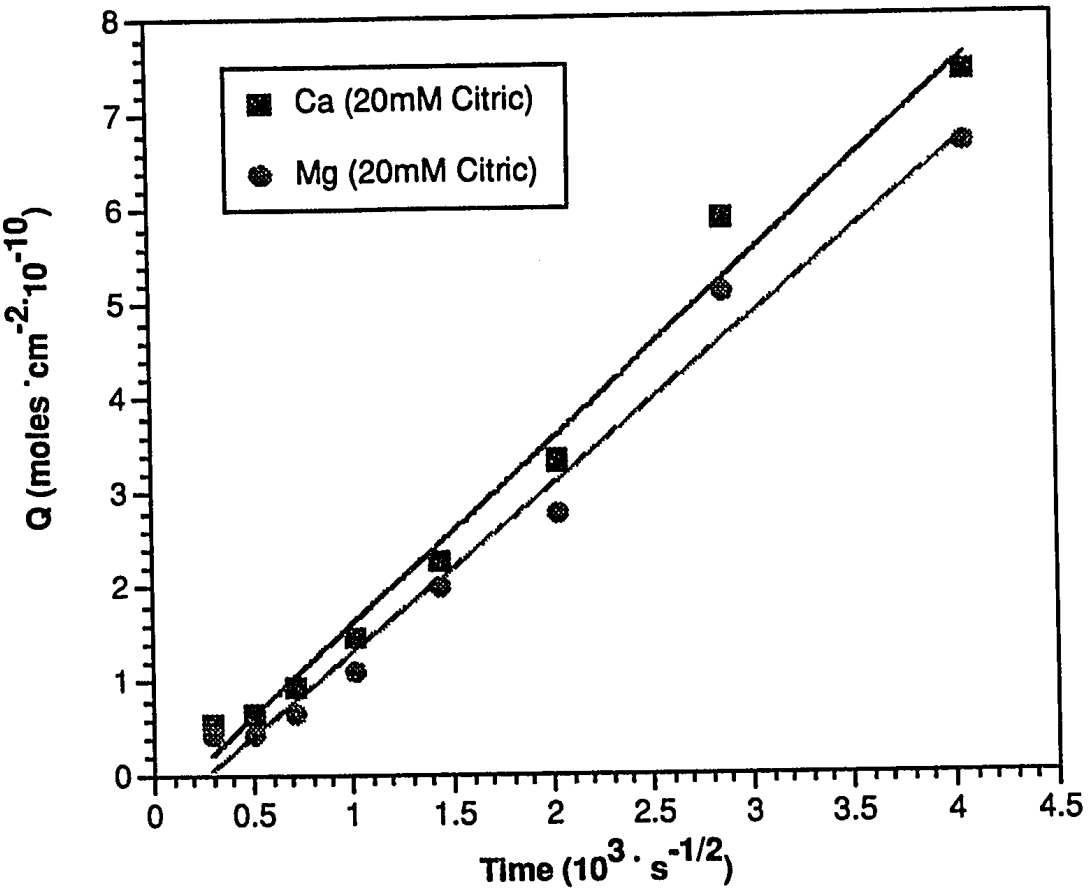

Figure 2.22 **Parabolic release of Ca and Mg into aqueous solutions from the lunar simulant glass as a function of time at 20 mM citric acid.**

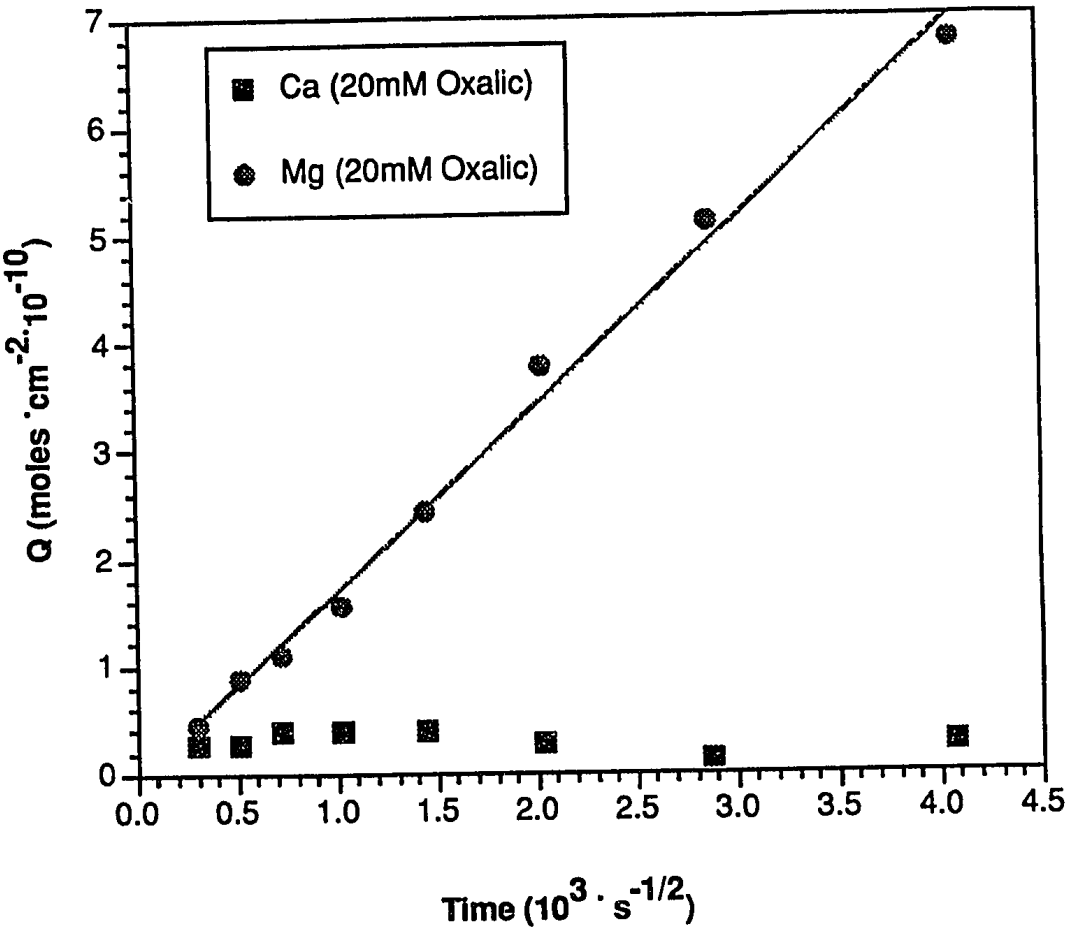

Figure 2.23 **Parabolic release of Ca and Mg into aqueous solutions from the lunar simulant glass as a function of time at 20 mM oxalic acid.**

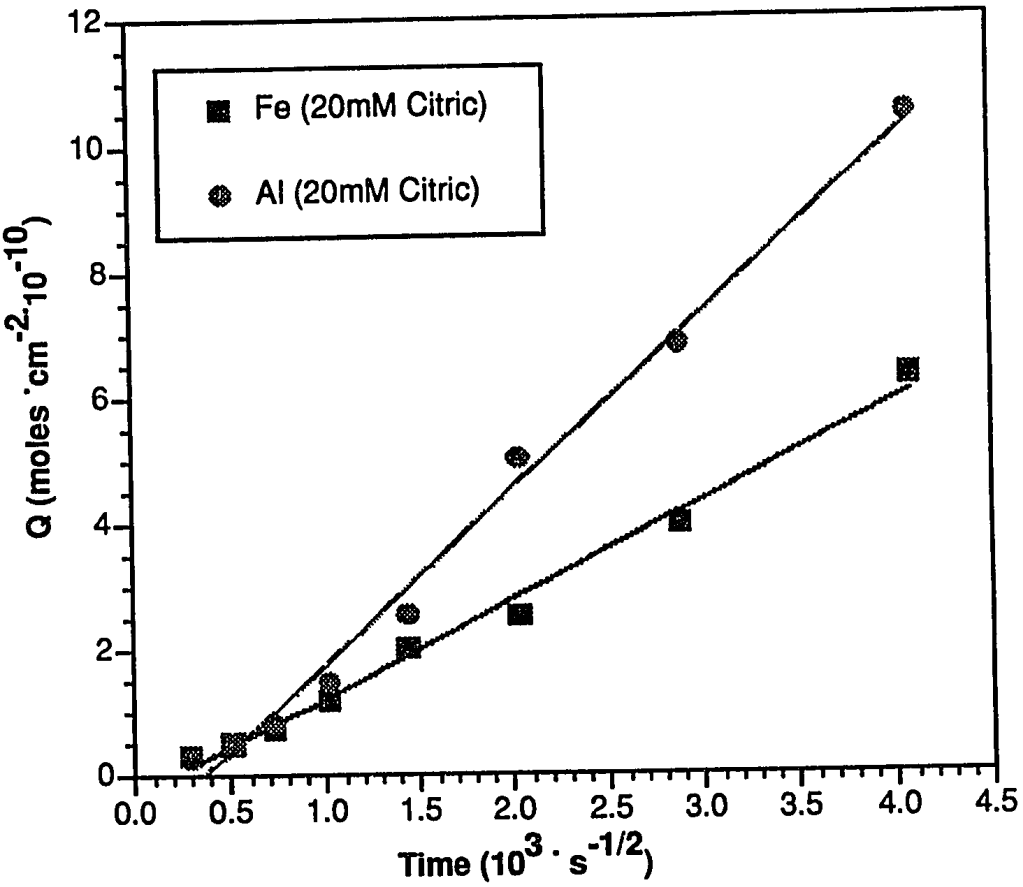

Figure 2.24 **Parabolic release of Fe and Al into aqueous solutions from the lunar simulant glass as a function of time at 20 mM citric acid.**

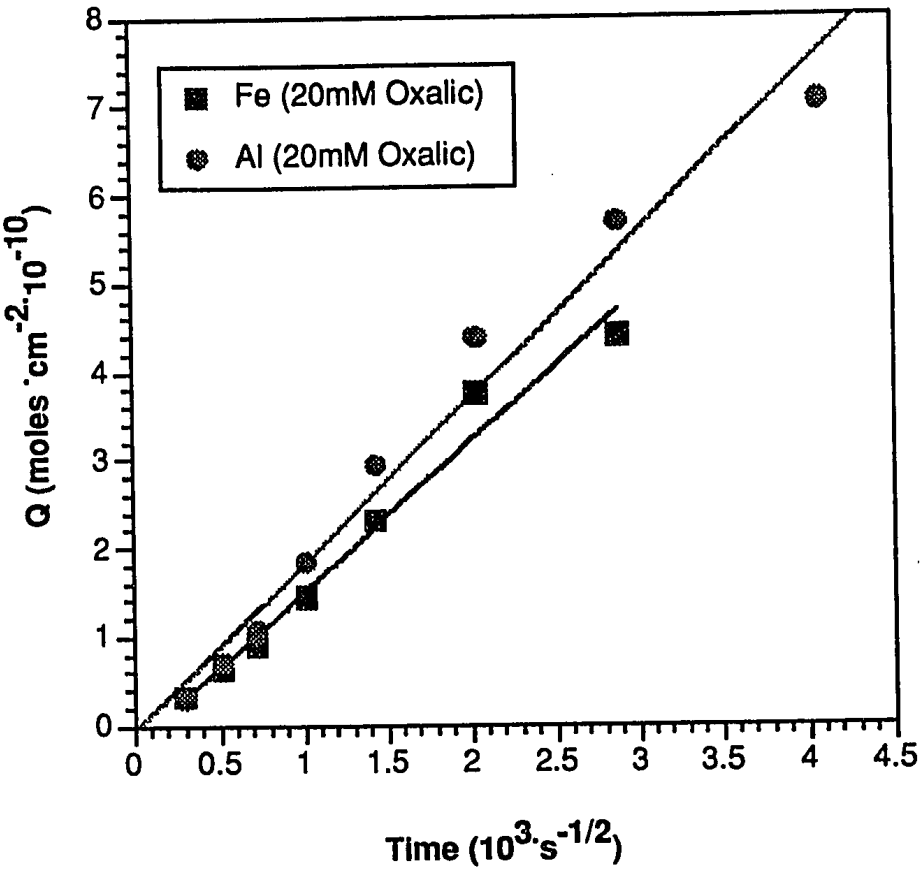

Figure 2.25 Parabolic release of Fe and Al into aqueous solutions from the lunar simulant glass as a function of time at 20 mM oxalic acid.

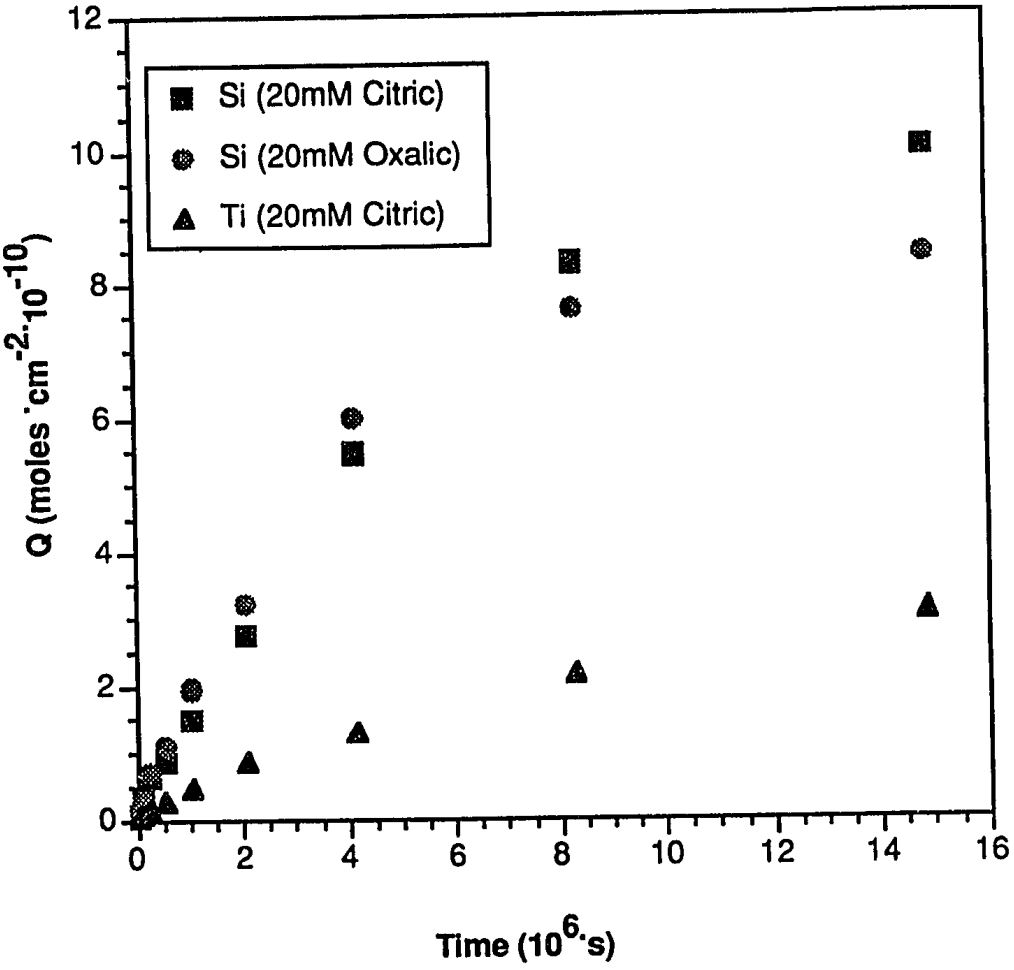

Figure 2.26 Release of Si and Ti from the lunar simulant glass at 20 mM citric and oxalic acid concentrations for 1.5 X 10^7 s.

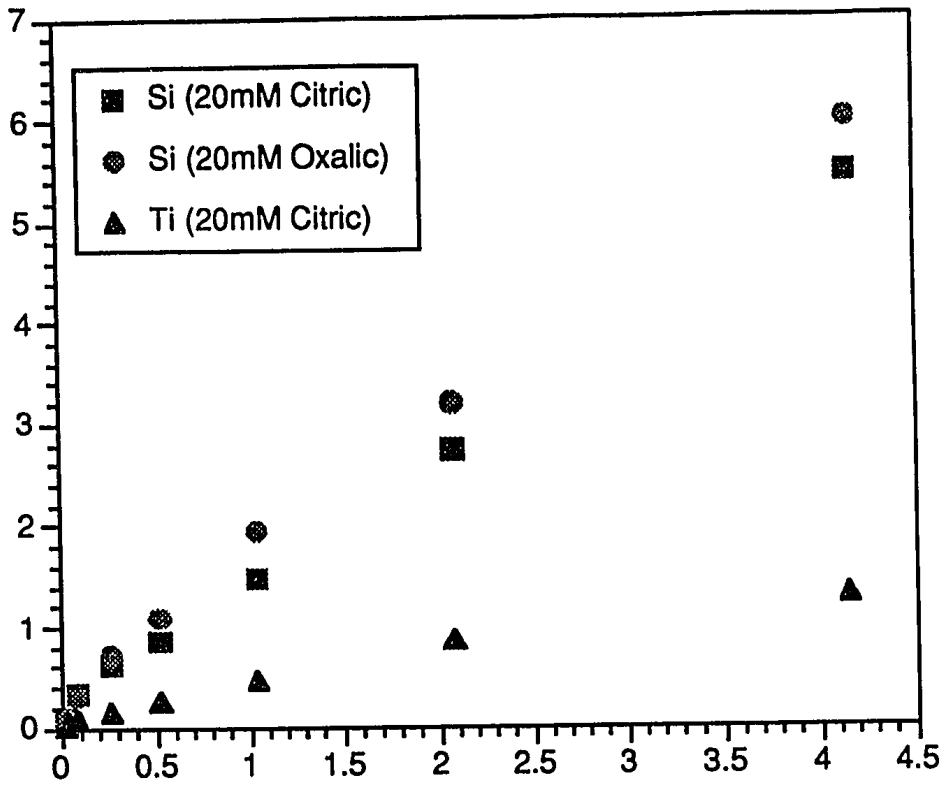

Figure 2.27 Linear release of Si and Ti at 20 mM citric and oxalic acid concentrations for 4.15 X 10^6 s.

Figure 2.28 TEM image of the lunar simulant glass surface after reaction with an aqueous 20mM citric acid solution. A leached layer is clearly visable at the outer edge of the glass particle.

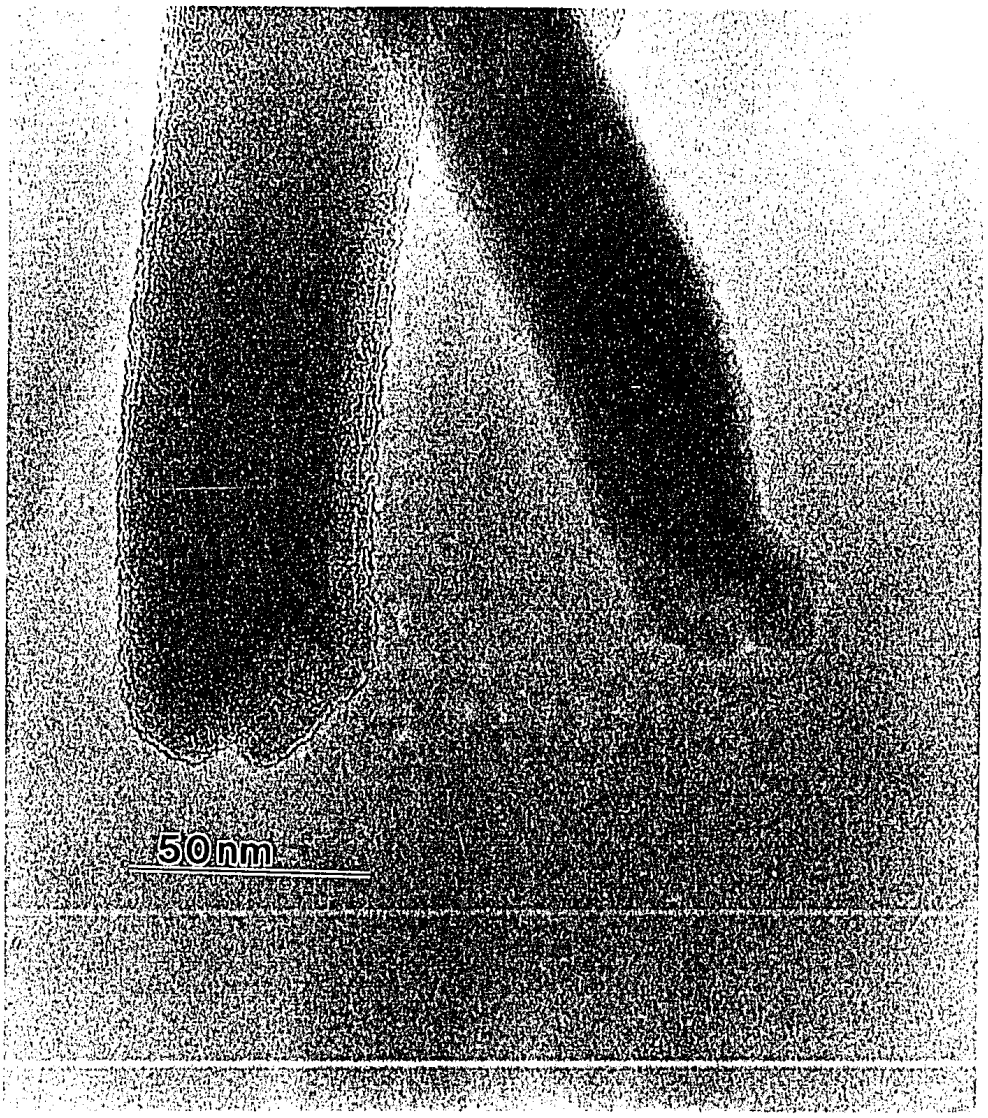

Figure 2.29 High magnification TEM image of the leached layer shown in Fig. 2.28.

Figure 2.30 TEM image of the lunar simulant glass surface after reaction with an aqueous solution at 20mM oxalic acid. Note the leached surface a) and the fibrous Fe precipitate b).

2.4 Discussion

2.4.1 pH Experiments

TEM and EDS results indicate the presence of a leached layer that is depleted in Ca, Mg, Al, and Fe and rich in Si and Ti . It is proposed that the first stage involves the diffusion of reactive solutes (H_2O or H^+) into the bulk glass. These reactive solutes are involved in hydration, ion exchange, and hydrolysis reactions. The release of Ca, Mg, Al, and Fe involves an ion exchange reaction that is coupled to hydrolysis (Barrer and Klinowski, 1975) This reaction necessitates that the bridging oxygen bond between Si and Al hydolyzes simultaneously with ion exchange of Ca^+ with H^+ as shown below,

$$\text{=Si-}\overset{\overset{Ca^+}{\vdots}}{O}\text{-Al=} + H^+ \rightarrow \text{=Si-OH} + Al(H_2O)_x^{x-3} + Ca^{+2} + H_2O \qquad (2.3)$$

This reaction is irreversible and Al is released via hydrolysis along with the ion exchange of Ca (or Mg and Fe). The aluminum in Eq. 2.3 is unstable and quickly hydrates to six-fold coordination. A similar reaction involving the simple ion exchange of the hydronium ion with Ca would account for the leaching of Ca, Mg and Fe from the glass (Casey and Bunker, 1990):

$$\text{=Si-}\overset{\overset{Ca^+}{\vdots}}{O}\text{-Al=} + H^+ \rightarrow \text{=Si-}\overset{\overset{H^+}{\vdots}}{O}\text{-Al} + Ca^{+2} \qquad (2.4)$$

We favor the first reaction since the leached layer at pH 3 and 5 is mainly composed of Si and Ti. During the coupled hydrolysis/ion-exchange reaction the

diffusion of cations through a leached layer is responsible for observed parabolic release of Ca, Mg, Al, and Fe (Rana and Douglas, 1961; Boksay et al., 1967; El-Shamy et al., 1972; Boksay and Bouquet, 1975; Lanford et al., 1979; White, 1983; Berger et al., 1987). Silica is released from the glass via a surface controlled hydrolysis reaction which follows a linear release rate.

The second stage involves the repolymerization of the silica rich leached layer creating a porous silica network (Bunker et al., 1988; Casey and Bunker, 1990). During repolymerization Si is incorporated from solution which explains the observed drop in the aqueous Si concentration. Solute diffusion through this network is fast relative to hydrolysis. Therefore, the overall rate of cation leaching from the glass is controlled by hydrolysis of the bulk glass and not diffusion of solutes through a leached layer, and consequently, release is linear. Casey and Bunker (1990) used TEM to examine the surface of a sodium-silicate glass after extensive leaching in acidic and basic solutions. They found that the repolymerization was so extensive that the texture of the leached layers resembled colloidal silica. Although TEM micrographs from both pH experiments revealed leached layers it is difficult to determine the presence of increased porosity created by repolymerization silanol groups (Fig. 5). Close examination of these micrographs did not reveal the presence of voids which would indicate increased porosity. However, this does not preclude repolymerization of the leached network. These features may only be apparent using TEM after extensive reaction and leaching.

MINTEQA2 and GEOCHEM-PC calculations indicate that reacting solutions become supersaturated with Si (with respect to amphorphous silica) and Al (with respect to gibbsite) for the pH 3 and 5 experiments, respectively. However, the presence of amorphous silica and gibbsite solid phases was not observed by TEM and

SEM analyses. As stated in the "Results" section, amorphous silica would be difficult to observe in the presence of a silica rich leached layer unless the precipitate was distinct from the leached layer. It is proposed that Si from solution was incorporated into the leached layer during repolymerization causing the observed drop in the aqueous solution concentration. Above pH 4 aqueous Al concentrations are controlled by the precipitation of microcrystalline gibbsite. We speculate that the absence of a precipitate at pH 5 is due to ion-ion interactions which reduce the free Al^{+3} concentration in solution, and consequently, the degree of supersaturation with respect to the solid phase. Ion-ion interactions are due to the relatively high ionic strength, resulting from the use of the pH buffer phthalate. Although experimental conditions vary, the dissolution rate of the lunar simulant glass is relatively low compared to synthetic and natural basaltic glasses (Boksay et al., 1967; White, 1983; Crovisier et al., 1987). The dissolution rate of silica from the synthetic lunar simulant was an order of magnitude lower compared to a natural perlite glass at pH values of 3 and 5 (White, 1983). The slow dissolution of silica is evident from the extensive leached layers observed at pH values ≤ 5. These characteristics can be related to the elemental composition of the glass. The presence of Ti in the glass structure increases the crosslink density and strength of the glass. This reduces the rate of dissolution of silica and maintains the structural integrity of the glass once reactive elements are removed (Petit et al., 1989). Therefore, the glass is relatively unreactive at pH values >5 and becomes extensively leached when exposed to acidic conditions for long time periods.

2.4.2 Organic Acid Experiments

The dissolution of the simulated lunar glass was accelerated in the presence of citric and oxalic acid. The increased dissolution rate could only be attributed to the organic acid since the glass was relatively unreactive at pH 7 in the absence of the organic acids. In contrast to the pH experiments, the release of Ca, Mg, Al, and Fe follows a single stage parabolic process.

We propose that the organic acids accelerate the dissolution of the simulated lunar glass through a two step process. The first step involves the chemisorption of the organic ligands on the glass surface. The adsorbed organic ligand donates a partial charge inward toward the framework of the glass. This charge transfer increases the electron density of the metal-oxygen bond which in turn weakens the framework of the glass. These bonds are now more susceptible to hydrolysis thus increasing the rate of dissolution (Bennett et al., 1988). The second step involves the chelating ability of the organic ligand. The organic ligand will form complexes with cations released during the hydrolysis reactions occurring at the surface of the glass. These complexation reactions reduce the activity of the cation in solution, increasing the diffusion gradient and consequently the dissolution of metals from the glass. Additionally, the disruption of the glass framework will promote increased hydration of the bulk glass aiding in the release of network modifying cations and hydrolysis of Al. Deviations in the linear release of Si and Ti may be due to sites that are more resistant to hydrolysis that dominate at long time periods.

The dissolution rate of the glass was greatest in citric acid (2 and 20 mM) followed by 20 mM oxalic acid. As mentioned previously the 2 mM oxalic acid had little effect on dissolution of the glass. These differences in dissolution rates for the two organic acids and concentrations we attribute to size and functional group

differences between the molecules. The citric acid molecule contains three carboxylic acid groups while the oxalic contains two. Additionally, citric acid contains 4 more carbon atoms making it a much larger molecule than oxalate. The lunar glass simulant has a very small surface area (Table 1) and at 2 mM citric acid, the sorption capacity of the glass may be exceeded. Therefore, at 20 mM citric acid, insignificant increases in the dissolution rate were observed. By comparison, 2 mM oxalic acid concentration may only cover a fraction of the glass surface while at 20 mM a large portion of the surface area may be covered. Consequently, little dissolution occurred at 2 mM oxalic acid. Grossl and Inskeep (1992) observed similar differences in sorption behavior with organic acids on octacalcium phosphate.

Transmission electron microscopy and SEM revealed the presence of precipitates only for the 20 mM oxalate experiment. MINTEQA2 and GEOCHEM-PC calculations indicate that both the citric and oxalic acid experiments were supersaturated with respect to gibbsite. Complexation of Al by organic acids is probably responsible for the absence of gibbsite precipitation.

The low concentration of aqueous Ca^{+2} in the 20 mM oxalate experiment may be explained by the precipitation of Ca-oxalate. Calcium-oxalate crystals were not observed with either TEM or SEM. However, microcrystalline precipitates that had not settled out of the solution column may have been trapped on the 0.2 μm filter during sampling resulting in small quantities of aqueous Ca^{+2} in the supernatant.

The presence of a fibrous precipitate was detected in the 20 mM oxalate experiments using TEM. Qualitative EDS analysis of this precipitate showed that it was high in Fe indicating the presence of a Fe-hydroxide precipitate. Additionally, a drop in aqueous Fe concentration was observed during the last sampling period. The morphology of the precipitate is similar to a Mg-Fe hydroxide precipitate observed

from the dissolution of a basaltic glass in seawater (Crovisier et al., 1987). Since the majority of Fe present in the glass is in the ferrous state, oxidation of Fe is responsible for the precipitation of an Fe(III) hydroxide. The Fe-hydroxide precipitate can form in two ways (Siever and Woodford, 1978): i) oxidation of Fe^{+2} in solution, followed by homogeneous precipitation of Fe-hydroxide and clumping of the precipitate on the surface of the leached silicate layer and ii) oxidation of Fe^{+2} and formation of Fe(III)-hydroxide directly on the surface of the leached silicate layer. We favor the second mechanism for the formation of the Fe(III)-hydroxide precipitate. Although the batch reactors were kept in an environmentally controlled incubator in the dark, the batch reactors were removed periodically for solution sampling. We propose that photoxidation of the oxalic acid may have occurred, not only reducing its concentration but also oxidizing Fe^{+2} to Fe^{+3}. Consequently, an Fe(III) precipitate formed at pH 7.

2.5 Conclusions

1) Dissolution of the synthetic lunar basaltic glass proceeds via a two stage process at pH values 3 and 5. The first stage involves release of Ca, Mg, Al, and Fe following a parabolic relationship and the release of Si following a linear relationship. Dissolution is incongruent which creates a leached layer rich in Si and Ti and depleted in Ca, Mg, Al, and Fe. During the second stage, repolymerization of the Si-rich leached layer scavenges Si from solution and creates a porous network which is no longer a diffusional barrier to the release of cations. During the second stage , hydrolysis of the Si and Al framework, not diffusion through the leached layer, is the rate-limiting step for release of cations. Eventually, the size of the leached layer will become great enough where diffusion of cations will again become rate limiting.

2) Dissolution of the synthetic lunar basaltic glass in the presence of organic acids proceeds by a one stage process. The release of Ca, Mg, Al, and Fe follows a parabolic relationship while the release of Si is initially linear followed by an approach to a steady state. Diffusion of cations through a Si/Ti rich leached layer is the rate-limiting step. A two step mechanism involving surface adsorption of the organic ligand and subsequent hydrolysis of the surface and chelation of cations in solution is proposed for the dissolution of the glass.

3) Differences in the rate of dissolution for the organic acids are related to the size of the organic ligand and the number of carboxylic acid groups.

2.5.1 Implications for Use as a Plant Growth Substrate

Reductions in pH and the presence of organic acids will rapidly weather glasses present in the lunar regolith. Elements that are rapidly released form lunar glasses will precipitate as secondary phases as the soil solution becomes supersaturated with respect to a particular solid phase. Dissolution results indicate that Fe oxides and hydroxides may be some of the first solid phases to precipitate. Additionally, Mn released during dissolution may precipitate as Mn-oxides. Released Cr and Ni will be involved in sorption/redox reactions which may render them more/less toxic to plants. Understanding the fate of released Cr and Ni is essential to determining their potential toxicity in the CELSS environment. Kinetic and atomic/molecular level investigations will provide information on sorption mechanisms necessary for predicting the fate and potential toxicity of released Cr and Ni.

2.6 References

Allison, J.D., D.S. Brown , and K.J. Novo-Gradac 1991. MINTEQA2/PRODEFA2, a geochemical assesment model for environmental systems: version 3.0 user's guide. Environmental Research Laboratory Office of Research and Development. U.S. EPA, Athens, GA.

Barrer, R.M. and J. Klinowski . 1975. Hydrogen mordenite and hydronium mordenite. J. Chem. Soc. Faraday Trans. 71:690-698.

Bennett, P.C., M.E. Melcer, D.I. Siegel, and J.P. Hassett. 1988. The dissolution of quartz in dilute aqueous solutions of organic acids at 25°C. Geochim. Cosmochim. Acta 52:1521-1530.

Berger, G.,J. Schott and M. Loubet . 1987. Fundamental processes controlling the first stage of alteration of a basalt glass by seawater: an experimental study between 200 and 320°C. Earth Planet. Sci. Lett. 84:431-445.

Boksay , Z. and G. Bouquet. 1975. On the reaction of water molecules with the silicate network in the glass phase.Phys. Chem. Glasses 16:81-82.

Boksay, Z., G. Bouquet, and S. Dobos. 1967. Diffusion processes in the surface layer of glass. Physics Chem. Glasses 8:140.

Bunker, B.C., G.W. Arnold, E.K. Beauchamp, and D.E. Day 1983. Mechanisms for alkali leaching in mixed-Na-K silicate glasses. J. Non-Crystalline Solids 58:295-322.

Bunker, B.C., D.R. Tallant, T.J. Headley, G.L. Turner and R.J. Kirkpatrick 1988. The structure of leached sodium borosilicate glass. Phys. Chem. Glasses 29:106-120.

Busenberg, E. and C.V. Clemency. 1976. The dissolution kinetics of feldspars at 25° C and 1 atm. CO_2 partial pressure. Geochim. Cosmochim. Acta 40:41-49.

Casey, W.H., and B.C. Bunker.1990. Leaching of mineral and glass surfaces during dissolution. *In* M.F. Hochella, Jr. and A.F. White (eds.) Mineral-Water Interface Geochemistry. Rev. in Mineral. 23:397-426.

Casey, W.H., H.R. Westrich, and G.W. Arnold. 1988. The surface of Labradorite feldspar reacted with aqueous solutions at pH = 2,3, and 12. Geochim. Cosmochim. Acta 52:2795-2807.

Correns, C.W., and W. Von Engelhardt. 1938. Neue Untersuchungen ueber die Verwitterung des Kalifeldspates. Chemie der Erde 12:1-22.

Crovisier, J.L. , J. Honnorez, and J. P. Eberhart 1987. Dissolution of basaltic glass in seawater: Mechanisms and rate. Geochim. Cosmochim. Acta 51: 2977-2990.

Doremus, R.H. 1975. Interdiffusion of hydrogen and alkali ions in a glass surface J. Non-Crystalline Solids 19:137.

Douglas, R.W. and T.M. El-Shamy. 1967. Reactions of glasses with aqueous solutions. J. Am. Ceram. Soc. 50:1-8.

El-Shamy, T.M., J. Lewins and R.W.Douglas, 1972. The dependence on the pH of the decomposition of glasses by aqueous solutions. Glass. Tech. 13:81-87.

Grandstaff, D.E. 1977 Some kinetics of bronzite orthopyroxene dissolution. Geochim. Cosmochim. Acta 41:1097-1103.

Grossl, P.R. and W.P. Inskeep 1992. Kinetics of octacalcium phophate crystal growth in the presence of organic acids. Geochim. Cosmochim. Acta 56:1955-1961.

Hench, L.L. and D.E. Clark. 1979. Physical chemistry of glass surfaces. J. Non-Crystalline Solids 28:83-105.

Holdren, G.R. Jr., and J.E. Adams. 1982. Parabolic dissolution kinetics of silicate minerals: An artifact of nonequilibrium precipitation processes? Geology 10:186-190.

Holdren, G.R. and R.A. Berner. 1979. Mechanisms of feldspar weathering. I. Experimental studies. Geochim. Cosmochim. Acta 43:1164-1171.

Inskeep, W.P., and P.R. Bloom. 1985. An evaluation of rate equations for calcite precipitation kinetics at pCO_2 less than 0.01 atm and pH greater than 8. Geochim. Cosmochim. Acta 49: 2165-2180.

Isard, J.O. 1967. The dependence of glass-electrode properties on composition. In G. Eisenman (ed.) Glass Electrodes for Hydrogen and Other Cations. Marcel Dekker, New York.

Lagache, M. 1976. New data on the kinetics of dissolution of alkali feldspars at 200°C in CO_2 charged water. Geochim. Cosmochim. Acta 40:157-161.

Lanford, W. A., K. Davis , P. Lamarche , T. Laursen, and R. Groleau 1979. Hydration of soda-lime glass. J. Non-Crystalline Solids 33:249-266.

Manley, E.P., and L.J. Evans. 1986. Dissolution of feldspars by low-molecular-weight aliphatic and aromatic acids. Soil Science 141:106-112.

Mast, M.A., and J.I. Drever. 1987. The effect of oxalate on the dissolution rates of oligoclase and tremolite. Geochim. Cosmochim. Acta 51:2559-2568.

Motschi, W. 1983 Cu(II) boung to hydrous surfaces, EPR measurements characterize surface coordination. Naturwissenschaften. 70:519-520.

Mularie, W.M., W.F. Furth and A.R.C. Westwood.1979. Influence of surface potential on the kinetics of glass reactions with aqueous solutions. J. Mater. Sci. 14:2659-2664.

Parker, D.R., W.A. Norvell , and R.L. Chaney. 1993. GEOCHEM-PC: A chemical speciation program for IBM and compatible computers. *In* R.H. Loeppert et al. (ed.) Soil Chemical Equilbrium and Reaction Models. SSSA, Madison, WI.

Petrovich, R. 1981a. Kinetics of dissolution of mechanically comminuted rock-forming oxides and silicates I. Deformation and dissolution of quartz under laboratory conditions. Geochim. Cosmochim. Acta 45:1665-1674.

Petrovich, R. 1981b. Kinetics of dissolution of mechanically comminuted rock-forming oxides and silicates I. Deformation and dissolution of oxides and silicates in the laboratory and at the earth's surface. Geochim. Cosmochim. Acta 45:1675-1686.

Rana, A.R. and R.W. Douglas. 1961. The reaction between glass and water, Part 2. Discussion of the results.Phys. Chem. Glasses 2:196-205.

Siever, R. and N.Woodford. 1979. Dissolution kinetics and the weathering of mafic minerals. Geochim. Cosmochim. Acta 43:17-724.

Sparks, D.L. 1989. Kinetics of soil chemical processes. Academic Press, New York.

Stevenson, F.J. 1967 Organic acids in soil. p. 119-146.*In* A.D. McLaren and G.H. Peterson (eds.) Soil Biochemistry Marcel Dekker Inc., New York.

Stevenson, F.J. and M.S. Ardakani. 1972. Organic matter reactions involving micronutrients in soils. p. 79-114. *In* J.J. Mortvedt et al. (ed.) Micronutrients in Agriculture. SSSA, Madison, WI.

Stumm, W., G. Furrer , E. Wieland, and B.Zinder. 1985. The effects of complex-forming ligands on the dissolution of oxides and alumino-silicates. p. 55-74.*In* J.I. Drever (ed.) The Chemistry of Weathering. Reidel Publishing Co., New York.

Thorseth, I.H., H.Furnes, and M. Heldal.1992. The importance of microbiological activity in the alteration of natural basaltic glass. Geochim. Cosmochim. Acta 56:845-850.

Thorseth, I.H., H. Furnes, and O. Tumyr. 1991. A textural and chemical study of Icelandic palagonite of varied composition and its bearing on the mechanism of the glass-palagonite transformation. Geochim. Cosmochim. Acta 55:731-749.

White, A. F. 1983. Surface chemistry and dissolution kinetics of glassy rocks at 25° C. Geochim. Cosmochim. Acta 47:805-815.

White, A.F., and H.C. Claassen. 1980. Kinetic model for the short-term dissolution of a rhyolitic glass. Chem. Geol. 28:91-109.

Wollast, R., and L. Chou. 1985. Kinetic study of the dissolution of albite with continuous flow-through fluidized bed reactor. p. 75-96. *In* J.L. Drever (ed.) The chemistry of weathering. Reidel Publishing Company, Boston.

Chapter 3

DISSOLUTION KINETICS OF A LUNAR BASALT SIMULANT AT 298 K: THE EFFECT OF pH AND ORGANIC ACIDS

3.1 Introduction

3.1.1 Mechanisms of Silicate Dissolution

Although considerable research has been conducted on silicate dissolution the basic processes involved at the reaction interface are still poorly understood and are controversial. The possible mechanisms of primary silicate dissolution can be categorized into three main hypotheses.

1. Formation of a precipitate at the crystal surface (Correns and Von Englehardt, 1938; Correns, 1940; Wollast, 1967; Helgeson, 1971; Busenberg, 1978; Holdren and Adams, 1982).

2. Formation of a leached or altered layer at the mineral surface (Correns, 1961, 1963; Luce et al. 1972; Paces, 1973; Busenburg and Clemency, 1976; Chou and Wollast, 1984).

3. Dissolution via a surface-controlled reaction (Lagache et al., 1961; Lagache, 1965, 1976; Petrovic et al., 1976; Berner, 1978; Holdren and Berner, 1979; Schott et al., 1981; Dibble, 1981; Stumm et al., 1985).

The first hypothesis postulates that amorphous or crystalline precipitates forming at the solid-liquid interface inhibit subsequent silicate dissolution. The secondary precipitate then acts as a diffusion barrier for solutes moving to and from reaction sites and could potentially become rate-limiting. Precipitation of secondary phases may occur under conditions where reacting solutions become oversaturated with respect to dissolved species such as Fe, Al and Si (Busenberg, 1978; Holdren and Adams, 1982). A precipitated layer is a reasonable explanation for the observed non-linearity of dissolution found by many researchers. However, this hypothesis has been discounted by most researchers because avoidance of secondary precipitates by maintaining an under-saturated reacting solution does not eliminate non-linear kinetics (Chou and Wollast, 1984). Additionally, electron microscopy studies of mineral surfaces weathered in natural soil environments have provided little evidence of a coherent precipitated layer which would provide a diffusional barrier (Wyart et al., 1963; Berner and Holdren, 1979).

Although significant progress has been made in understanding the dissolution of silicate minerals, controversy still surrounds the leached layer versus surface-controlled reaction hypothesis (Berner et al., 1985; Chou and Wollast, 1985). Early evidence of a leached layer came from dissolution studies where silicate surfaces dissolved incongruently; alkali and alkaline earth cations and Al are removed from the silicate preferentially, leaving behind a layer residually enriched in Si (Luce et al., 1972; Chou and Wollast, 1984, 1985; Holdren and Speyer, 1985, 1986). Several researchers have proposed that H^+ or H_3O^+ exchanges with alkali or alkaline earth cations at the silicate surface leaving behind an altered or leached layer.

Continued release of cations from the interior of the mineral requires diffusion through this altered layer.

Additional evidence of an altered or leached layer came from dissolution studies where the rate of dissolution was non-linear. Many researchers investigating silicate dissolution have observed the initial rate of weathering to decrease by an order of magnitude within the first day. The parabolic rate law has often been applied to these data indicating that diffusion is the rate limiting-step (Luce et al., 1972; Grandstaff, 1977). Thus, the fit of the parabolic rate law along with incongruent dissolution has provided evidence for the existence of the leached layer.

Numerous investigators have examined the dissolution of silicate minerals using spectroscopic and microscopic techniques and found no evidence of an altered or leached layer (Holdren and Berner, 1979; Petrovic et al., 1976; Schott et al., 1981). These investigators suggested that dissolution of silicate minerals proceeds by a surface- controlled reaction. Further, frequent observations of etch pits from laboratory and naturally weathered silicate minerals indicate preferential weathering at crystal defects, along twin boundaries and at dislocations that intersect the surface (Grandstaff, 1978; Berner and Holdren, 1977; Holdren and Berner, 1979; Schott et al., 1981). The presence of etch pits indicates a surface controlled reaction mechanism since minerals weathered through diffusion should show smooth, rounded surfaces (Berner, 1978).

Lastly, several investigators have shown that the non-linear rate observed by many researchers may be an artifact of sample preparation. Holdren and Berner (1979) and Schott et al. (1981) pre-treated samples ultrasonically with a HF/H_2SO_4 mixture to remove small and ultrafine particles. They observed linear rates of

dissolution and concluded that the non-linear rates observed by many researchers were due to the rapid dissolution of small and ultrafine particles.

Transition state theory has been applied to the surface-controlled reaction hypothesis where the rate-limiting step is the breakdown of activated complexes (Rimstidt and Barnes, 1980; Lasaga, 1981; Aagaard and Helgson, 1982; Murphy and Helgeson, 1987). Transition state theory dates back to a series of papers by Henry Erying (Erying, 1935a,b; Glasstone et al., 1941). A basic tenet of the theory is that in proceeding from reactants to products, the species must travel over a potential energy barrier. The activated complex sits at the top of this barrier (or potential energy maximum) and must be overcome before products are formed.

Although early studies using spectroscopic and microscopic techniques did not identify the presence of leached layers more than a few Å thick (Petrovic et al., 1976; Schott and Berner, 1983), more recent studies have determined the presence of altered layers as deep as 5000 Å (Petit et al., 1987a,b, 1990; Schott and Petit, 1987; Nesbitt and Muir, 1988; Mogk and Locke, 1988; Casey et al., 1988, 1989; Goossens et al., 1989; Shotyk and Nesbitt, 1992). Various spectroscopic techniques such as secondary ion mass spectrometry (SIMS), X-ray photoelectron spectroscopy (XPS), auger electron spectroscopy (AES), elastic recoil detection (ERD), Rutherford backscattering analysis (RBS), and resonant nuclear reaction (RNR) have been used to probe the surface of various silicate minerals. In addition to providing direct evidence of altered surface layers, these techniques have provided insight regarding the mechanisms of silicate dissolution.

Recent data from spectroscopic techniques indicates that dissolution of silicate minerals cannot be explained by simple models like surface reaction or diffusion exchange of H^+ with cations. Schott and Petit (1987) used (RNR) and

(SIMS) to examine the surface of weathered diopside and albite. RNR allows hydrogen depth profiling while SIMS provides complimentary information on other elements. They found evidence for a hydrated layer up to 1000Å thick coupled with a decrease in constituent elements (e.g., Ca and Mg). The researchers suggested that an important step in the dissolution of silicates may be the diffusion of molecular water into the crystal and its reaction with the silicate network to produce a hydrated silicate. They emphasized that crystal dislocations should play a major role in water diffusion. Also, the breakdown of the silicate network via hydrolysis should allow for more diffusion of free molecular water in the structure.

Casey et al. (1988, 1989) investigated the surface chemistry of dissolving labradorite feldspar at various pH conditions using (ERD) and (RBS) spectroscopies. These spectroscopic techniques were used to determine depth profiles of hydrogen, silicon, aluminum and calcium. The investigators found that at low pHs (1-3), hydrogen infiltrates many unit cells into the feldspar surface. Infiltration of hydrogen proceeds simultaneously with reactions that remove Al, Ca, and Na. At near neutral (5-7) and basic pHs there was no evidence for hydrogen infiltration suggesting that dissolution proceeds at the immediate aqueous interface. Additionally, under some conditions, the silica-rich surface may repolymerize to eliminate hydrogen from the structure. The researchers suggested that the rate-controlling step for dissolution may involve electrophilic attack of bridging oxygens by water.

In a recent study Hellmann et al. (1990), examined the formation of leached layers on albite surfaces under hydrothermal conditions using XPS. The investigators found leached zones depleted in Na, Al, and O. The thickness of these leached zones varied with pH and correlated qualitatively with the energetics of interaction of H-containing species (H^+>H_3O+>OH->H_2O) with bridging oxygen

linkages. It was also observed that a reduction in O/Si ratios in the severely leached layers was consistent with repolymerization of the silica rich surface as hypothesized by Casey et al. (1988, 1989). These data suggest that the rate-controlling step for dissolution may involve attack of bridging oxygens by H-containing species.

The above research reveals that the rate-controlling step in silicate dissolution may be more complex than a simple surface-controlled reaction or diffusion through an altered or leached layer. Recent data provided by surface sensitive spectroscopic techniques suggests that the dissolution of silicate minerals may occur through the infiltration of H-containing species and subsequent attack on bridging oxygens. The creation of charged aluminol groups ($Al\text{-}OH_2^+$) may weaken bonds, subsequently causing a release of Al. The breakage of these bonds may be the rate-determining step (Hellmann et al., 1990). The dissolution of silicate minerals will vary with pH, temperature and nature of the mineral. Therefore, the rate-determining step may also vary depending on experimental conditions and mineral type.

3.1.2 Ligand Promoted Dissolution

It has long been recognized that organic acids exuded by plants and microorganisms can accelerate the dissolution of silicate minerals (Duff et al., 1962; Schalscha et al., 1967). However, the role of organic acids in silicate mineral dissolution has received much less attention than dissolution in dilute aqueous systems. There is a growing recognition of the importance of organic acids and chelates in the weathering process. These compounds are ubiquitous in the natural weathering environment and some researchers feel that the processes of mineral weathering may be completely controlled by biological activity through CO_2 production and excretion of organic acids (Krumbein and Dryer, 1985; Eckhardt, 1985).

Huang and Keller (1970) and Huang and Kiang (1972) examined the effect of several organic acids on the dissolution of a variety of rock forming silicate minerals. They found that dissolution was enhanced by the organic acids which was related to their ability to form stable Al- and Ca- complexes. However, the authors failed to buffer pH, making it difficult to separate out the effects of pH from those of complexation. In a similar study Manley and Evans (1986) examined the effect of several low-molecular-weight aliphatic and aromatic acids on the dissolution of several feldspars. They found that the amount of aluminum released appeared to be related more to the strength of the acid than to its ability to form complexes with aluminum. Again the authors failed to buffer pH making the interpretation of the results difficult.

Tan (1980) and Boyle et al. (1974) investigated the effect of humic/fulvic acids and organic acids on the dissolution of micas. Boyle et al. (1974) proposed that

dissolution of biotite by organic acids was due to the chelating ability of the organic acid. In contrast Tan (1980) concluded that the enhanced dissolution observed for muscovite and biotite was related to an increase in the proton availability from humic and fulvic acids.

Inorganic ligands, such as fluoride, have been observed to enhance the rate of silicate dissolution (Amrhein and Suarez, 1988; Shotyk and Nesbitt, 1992). Amrhein and Suarez (1988) applied the surface complexation model (Furrer and Stumm, 1986) to the dissolution of anorthite in the presence of fluoride and oxalate. They found that the dissolution rate in the presence of the ligands increased linearly with decreasing pH. In the absence of these ligands the dissolution rate was nearly pH independent. The rate of dissolution was linearly related to the surface concentration of absorbed ligands and the authors concluded that pH and complexing ligands have a synergistic effect on feldspar dissolution.

Several investigators have observed an increased rate of quartz dissolution in the presence of organic ligands (Jorgensen, 1976; Bennett et al., 1988). The addition of polyphenolic catechols increased the dissolution rate of quartz. These compounds are known to complex silica and it was suggested that the observed increase in dissolution was due to a surface complexation reaction. Bennett et al. (1988) also observed an increase in the rate of quartz dissolution in the presence of several aliphatic organic acids. The possibility of silica-organic complexes was investigated using UV-difference spectroscopy. Results suggested that several of the organic acids complex with silica via an electron-donor acceptor complex.

Oxalate has been observed at fairly high concentrations in soil solutions (Graustein, 1975). This organic acid is known to complex metals such as Al and may play an integral role in the natural weathering of silicate minerals. Antweiler and

Drever (1982) examined the importance of organic acids on the weathering of late tertiary volcanic ash. The authors conducted a field study and found that soluble organic compounds derived from vegetation controlled the release and transport of solutes by complexing with Al and Fe, and lowering pH.

Not all silicate minerals exhibit an increased rate of dissolution in the presence of organic acids. Mast and Drever (1987) examined the effect of oxalate on the dissolution rate of oligoclase feldspar and tremolite amphibole using a flow through reactor. They observed that the rates of dissolution of both minerals were essentially independent of oxalate concentration at levels up to 1 mM. Because oxalate is a strong chelator of Al it was proposed that the detachment of Si rather than Al or Mg was the rate-limiting step.

Recently, Barman et al. (1991) examined the weathering of silicate minerals that were representative of each of the six classes of silicates by organic acids. The authors investigated the effect of various organic ligands as well as the crystal structure on mineral stability sequence. It was determined that the positions of the cations in the crystals as well as the complexing abilities of the organic acids for different cations determines the solubility of silicate minerals.

The mechanism of organic acid dissolution is a combined effect involving surface processes (Stumm et al., 1985) as well as the complexing ability of the ligand (Barman et al., 1991). Many of these organic ligands are π donor ligands. Upon specific adsorption these ligands push electron density toward the surface of the mineral. This increase in electron density weakens the metal-oxygen bond of the mineral making them more susceptible to hydrolysis, thus increasing the rate of dissolution. In addition, the complexation reactions reduce the activity of the cation in

solution, increasing the diffusion gradient and consequently the dissolution of metals from the mineral.

It has been observed in both the laboratory and the field that organic and inorganic ligands can increase the rate of silicate dissolution. However, the mechanism of ligand promoted dissolution is still the subject of debate. There has been limited research on the effects of organic acids on silicate dissolution. Not only are there limited data but often the pH is not controlled to separate the effects of pH from those of complexation. Organic ligands are ubiquitous in the plant root environment and may play a dominant role in the natural weathering of silicate minerals.

3.1.3 Objectives

A myriad of studies have been published in the literature on the dissolution of silicate minerals. However, there is little research examining the effects of naturally occurring organic acids on the kinetics and mechanisms of silicate mineral dissolution. Also, lunar minerals differ substantially from terrestrial minerals and will react differently when exposed to terrestrial weathering environments. Therefore, the objectives of this study are to examine the rate and mechanism of dissolution for a lunar basalt simulant under rhizosphere conditions. This involves examination of basalt dissolution at pH values of 3, 5, and 7. The influence of naturally occurring organic acids (citric and oxalic) was also examined at pH 7. All of the studies were conducted in batch reactors.

3.2 Materials and Methods

3.2.1 Solid Material

Experiments were conducted using an igneous basalt mined from an abandoned quarry in Duluth, Minnesota . The chemical composition and mineralogy of the MLS-1 basalt are similar to lunar mare basalts returned from the Apollo 11 mission and were determined by electron microprobe and X-ray diffraction analyses, respectively (Tables 1 and 2). The most significant differences in the major element chemistry between lunar mare basalts and the MLS-1 basalt are the higher Na content and the presence of water and ferric iron in the MLS-1 basalt (Weiblen et al., 1990). The bulk MLS-1 basalt was ground in a corundum grinding jar and dry sieved into eight sieve fractions (Table 3.1). No additional effort was made to separate fines adhering to the grains. The different sieve fractions were then combined to reproduce a grain size distribution similar to Apollo 11 Mare soils (10084,853). The combined basalt sample was heated to 383 K to remove adsorbed water and was stored in air-tight containers in an environmental glove box purged with argon gas. The specific surface area was 0.683 m2/g as determined by a 3 point N2 Brunauer-Emmett-Teller (B.E.T.) gas adsorption isotherm method. This value was in close agreement with the calculated surface area from particle size distribution.

Table 3.1 Bulk chemical composition, grain size distribution, and surface area of MLS-1.

Sieve Size	Microns	Percent
> 20 mesh	+ 850	7
> 35 mesh	+ 500	4
> 60 mesh	+ 250	8
> 100 mesh	+ 150	8
> 200 mesh	+ 75	16
> 270 mesh	+ 53	9
> 400 mesh	+ 38	16
< 400 mesh	- 38	32

Oxide	Wt %	Mol %
SiO_2	45.0	49.3
Al_2O_3	15.3	9.9
TiO_2	5.2	4.3
FeO	14.2	13.0
Fe_2O_3	1.2	0.49
MgO	5.6	9.2
CaO	9.6	11.3
Na_2O	2.0	2.1
K_2O	0.34	0.24
P_2O_5	0.45	0.21
Total	98.89	100

Surface area	0.683 m^2/g

Table 3.2 Mineral Chemistry of the Minnesota Lunar Simulant

Oxide	Feldspar[1]	C-pyrox[2]	O-pyrox.[3]	Olivine	Ilmenite
SiO_2	55.67	51.88	52.74	35.07	0.02
TiO_2	0.09	0.64	0.30	0.07	50.05
Al_2O_3	28.84	1.60	-----	0.01	0.04
FeO	0.41	11.76	23.13	40.30	43.28
MgO	0.01	13.72	20.96	23.88	1.31
MnO	-----	0.29	0.49	0.52	0.50
Cr_2O_3	-----	0.03	0.02	-----	0.07
CaO	10.99	19.97	1.64	-----	0.02
Na_2O	4.03	0.24	0.02	-----	0.02
K_2O	0.03	0.01	0.01	0.01	-----

1. Plagioclase
2. Clinopyroxene
3. Orthopyroxene

3.2.2 Reacting Solutions

For the experiments conducted at pH 3 and 5, we used standard biphthalate based (0.05 M) pH-buffers (Fisher Scientific Corporation). Additionally, each buffer contained formalin to retard the growth of algae. The pH 7 solution was buffered using 1 mM $KHCO_3$. The effect of ionic strength on MLS-1 dissolution was measured by conducting pH 7 experiments at three different ionic strengths. The pH of the buffer was adjusted using 1M HCl. Subsequently, the ionic strength was adjusted to 0.005, 0.01, and 0.05 M using $NaNO_3$.

Solutions for the organic acid experiments were prepared using reagent grade citric and oxalic acids (Sigma Corporation) and ultrapure water. The concentrations of the organic acids were 2 and 20 mM, which were chosen to represent concentrations found in the plant root environment (Stevenson, 1967). The

pH of all organic acid solutions was adjusted to a pH 7 with 1 M NaOH. This pH was chosen because both citric and oxalic acid are in a dissociated form. Fluctuations in pH during the experiments were adjusted by dropwise addition of 1 N NaOH or HCl. Mercuric chloride (0.02 mM) was added to each sample to prevent the microbial degradation of the organic acids. The above experimental conditions are summarized in Table 3.3.

Table 3.3 Summary of experimental conditions.

Solution	Acid Conc. (m mole L^{-1})	pH[1]	IS (mole L^{-1})	Time (days)
Biphthalate	--------	3.0	0.05	365
Biphthalate	--------	5.0	0.05	365
Water	--------	7.0	0.05	365
Water	--------	7.0	0.01	
Water	--------	7.0	0.005	
Citrate	20	7.0	0.123	96
	2.0	7.0	0.0123	
Oxalate	20	7.0	0.056	96
	2.0	7.0	0.006	

[1] pH of the solution during the experiment.

3.2.3 Experimental

The batch reactor experiments were conducted in acid-washed high-density polyethylene bottles. The batch reactors were placed in an environmentally controlled incubator at 298K ± 1. The incubator was kept dark to prevent the photo-oxidation of the organic acids. The batch reactors were gently agitated (60 revs/min) on a rotating shaker between sample analyses. Approximately two hours before sampling, the reactors were allowed to settle. For each analysis, 10 mL of reacting solution was withdrawn from the top of the solution column and the sample was filtered through a 0.20 micron Gelman filter (Gelman GA-8, Gelman Sciences, Inc., Ann Arbor, MI). After the sample aliquot was filtered, an additional 10 mL of reacting solution was added back to the original reaction vessel. These sampling protocols were chosen in order to maintain constant solution/solid ratios throughout the experiment. The pH of the filtered sample was decreased to approximately pH 3 using 0.5 M HCl to prevent precipitation of metals prior to analysis. Samples were

analyzed for Si, Al, Ti, Fe, Mg, Ca, and the minor elements Cr, Ni and Mn by Inductively Coupled Plasma (ICP) spectrometry. Additionally, a blank for each reacting solution was analyzed and any metal contaminants present were subtracted from the sample results.

The aqueous solution data were entered into GEOCHEM-PC (Parker et al., 1993) and MINTEQA2 (Allison et al., 1991) chemical speciation programs. These programs determined possible supersaturation of ions with respect to a particular solid phase and were used in conjunction with electron microscopy to determine precipitate formation.

3.2.4 Electron Microscopy and Electron Probe Microanalysis (EPMA)

At the termination of the dissolution experiments the weathered MLS-1 particles were filtered, washed twice with deionized water, air dried, and stored under desiccation. For scanning electron microscopy (SEM), particles from the various experiments were mounted on silver tape and glued onto Al stubs using epoxy resin. The grains were coated with carbon and examined using a JEOL JSM 35 scanning electron microscope.

For electron probe microanalysis, polished petrographic thin sections of epoxy embedded particles (<1.0 μm) were carbon coated and analyzed using a Cameca Camebax microbeam electron microprobe operated at 15 kV and 10 nA beam current. National Institute of Standards and Technology mineral standards were used for calibration.

3.2.5 X-Ray Diffraction Analysis (XRD)

The ground MLS-1 basalt was mounted in cavities carved on glass slides and analyzed by a Scintag XDS 2000 X-ray diffractometer using Cu K α radiation; a software routine was used for Kβ stripping.

3.3 Results

3.3.1 pH Results

Experimental data for the quantity of Si, Al, Fe, Mg, and Ca solubilized at pH=3 and 5 are shown in Figs. 1 and 2. Data for pH 7 are excluded because elemental analyses were beyond detection limitations. Additionally, variations in ionic strength at pH=7 did not affect the dissolution rate. The release of Ca, Mg, Fe, Al, and Si from the MLS-1 at pH=3 and 5 follow a two stage process. The first stage is characterized by a rapid release rate of these elements and occurs up to 48 days. In the second stage the release rate of these elements declines and follows a more linear release rate until the termination of the experiment. Deviations in this linear release rate occurred for silica near the end of the experiment which may be due to the precipitation of amorphous silica. The quantities of major elements released into solution occurred in the following order Fe≈Mg>Si>Al>Ca for pH=3. The order was similar for the pH=5 experiment except that the quantity of Al released was similar to the quantity of Fe and Mg. Trace quantities of Ti, Cr, Ni and Mn were released at all pHs.

The computer codes GEOCHEM-PC and MINTEQA2 indicate that in reacting solutions, silicic acid concentrations at pH 3 are near supersaturation with respect to amorphous silica at the termination of the experiment. Also, Al concentrations at pH 5 collected at 12 days are supersaturated with respect to gibbsite. Therefore, it might be expected that these solid phases precipitate from solution.

Scanning electron microscopy (SEM) was used to examine weathered surfaces of the MLS-1 basalt and to determine possible precipitate formation. Figures 3.3-3.7 shows weathered surfaces of pyroxene and olivine. Figure 3.3 shows a weathered clinopyroxene surface at pH=3. This sample shows the classic side-by-side alignment of etch pits which are characteristic of weathered pyroxenes. This alignment is probably due to etching of dislocations at the boundaries of basal lamellae (Berner and Schott, 1982). Eventually exfoliation of basal lamellae will take place as seen in Figure 3.4. The pH=5 pyroxene (Fig. 3.5 and 3.6) samples exhibit similar weathering although less extensive. Figure 3.5 exhibits side-by-side etching along the boundaries of the basal lamellae while these etch pits are absent in Figure 3.6. As weathering continues these etch pits fuse and exfoliation of the basal lamellae takes place. The olivine particle weathered at pH=5 (Fig. 3.7) shows extensive weathering and fragmentation. Olivine particles were not detected at pH=3 using SEM which may be due to the instability of this mineral which dissolved rapidly and fragmented into smaller particles. No precipitates were observed at either pH using SEM.

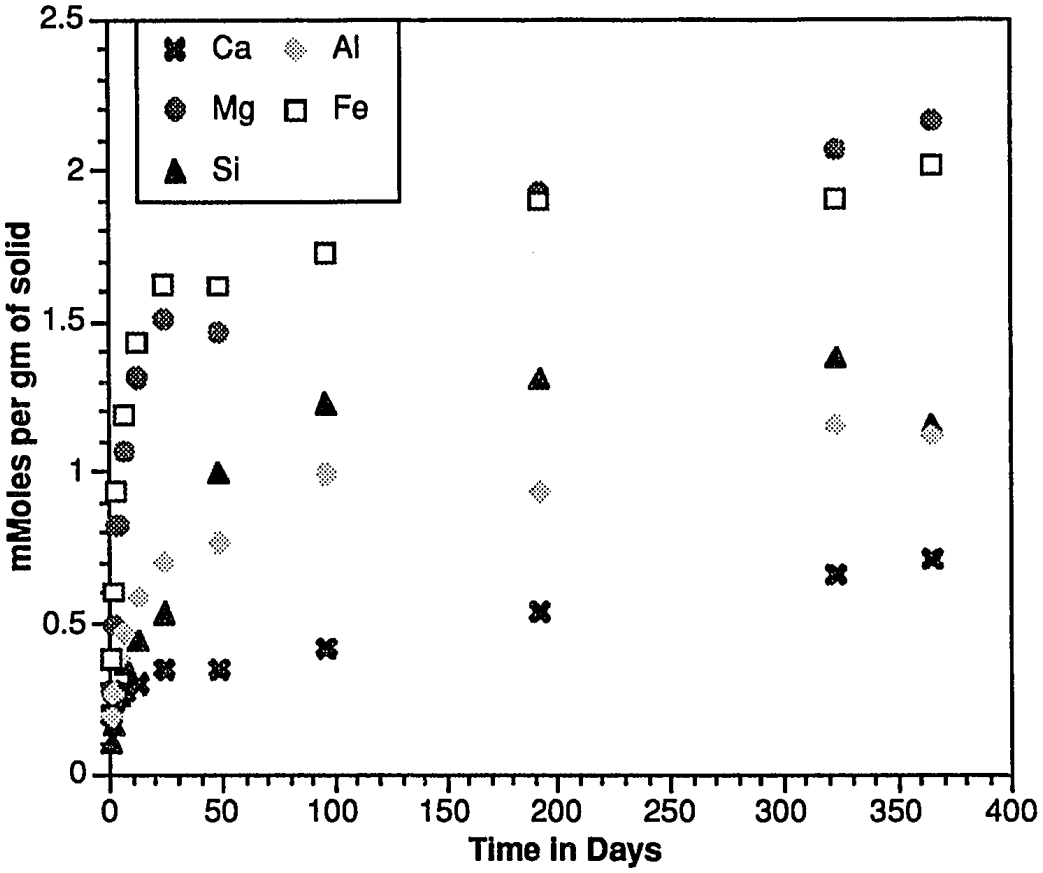

Figure 3.1 **Release of major elements into aqueous solution from the MLS-1 basalt as a function of time at pH 3.**

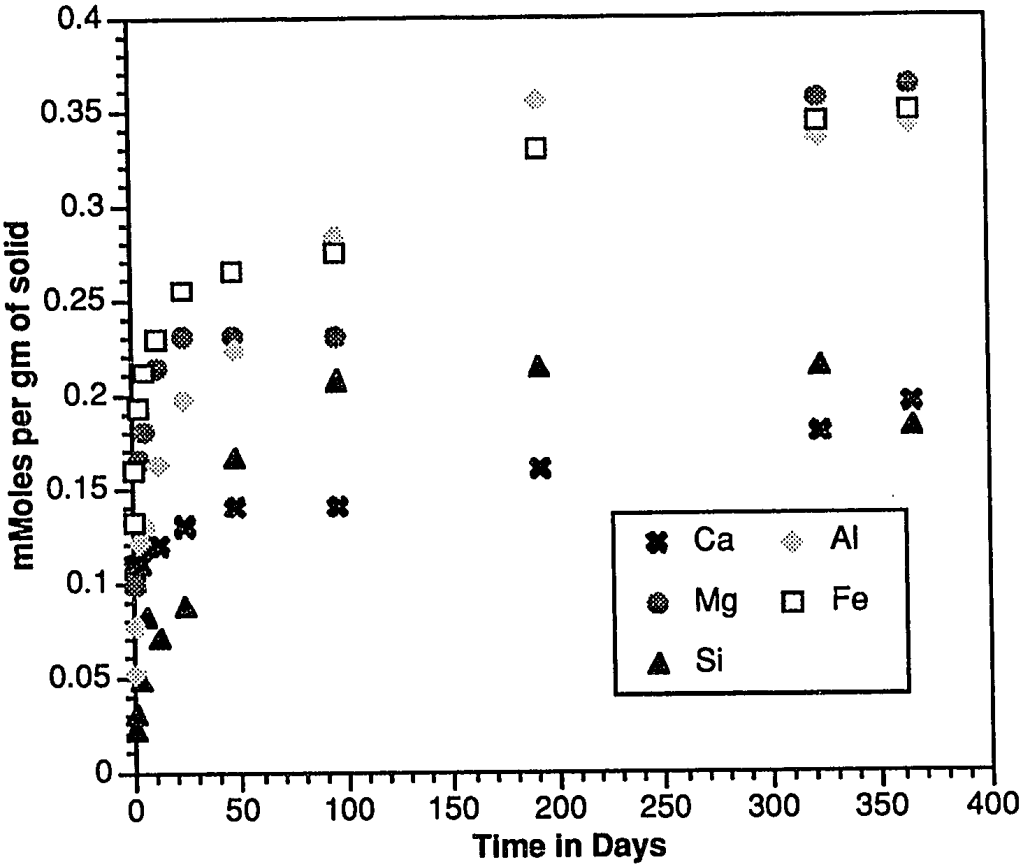

Figure 3.2 Release of major elements into aqueous solution from the MLS-1 basalt as a fuction of time at pH 5.

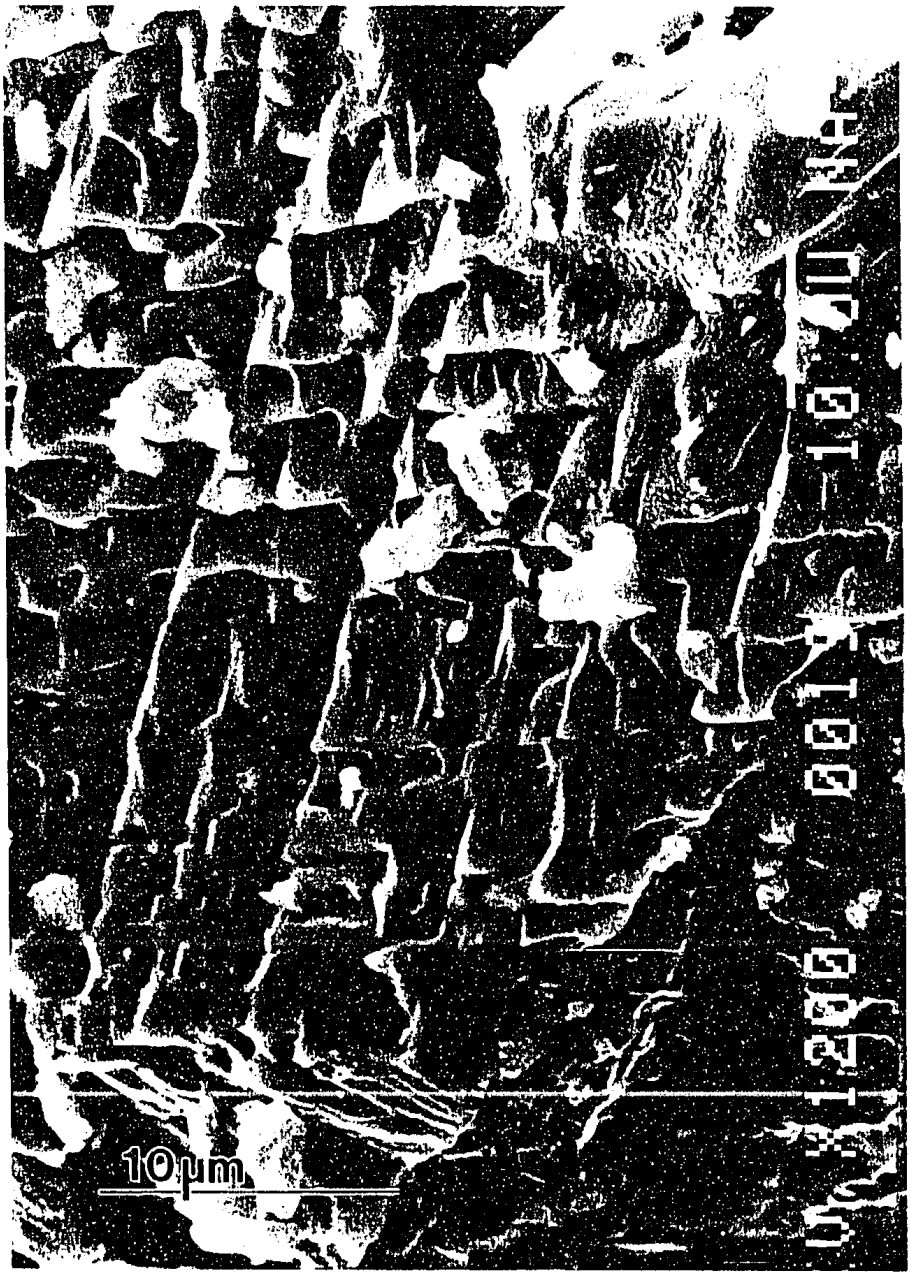

Figure 3.3 SEM image of a clinopyroxene surface weathered in an aqueous solution at pH 3. Extensive etch pits aligned in a side-by-side manner along basal lamellae are shown.

Figure 3.4 SEM image of a clinopyroxene surface weathered at pH 3. Image exhibits extensive weathering causing exfoliation along basal lamallae.

Figure 3.5 SEM image of a clinopyroxene surface weathered at pH 5. Side-by-side alignment of etch pits are visable along the basal lamallae.

Figure 3.6 SEM image of a clinopyroxene surface weathered at pH 5. The mineral surface is beginning to exfoliate along basal lamallae.

Figure 3.7 SEM image of a olivine surface weathered at pH 5. Surface exhibits extensive cracking and fragmentation.

3.3.2 Organic Acid Experiments

Experimental data for the quantity of Si, Al, Fe, Mg, and Ca solubilized at 2 and 20 mM citric acid and 20 mM oxalic acid are shown in Figs. 3.8-3.10. Data for the 2 mM oxalic acid are excluded because elemental analyses were approaching and beyond detection limitations. The release of Ca, Mg, Fe, Al, and Si from the MLS-1 at 2 and 20 mM citrate and 20 mM oxalate was initially rapid followed by a slower rate that followed a mostly linear path. Deviations in the linear rate occurred for the 20 mM oxalate experiment near the termination of the experiment. A reduction in the aqueous concentration of Fe, Al, and Si was detected during the 96 and 172 day (not shown) sampling periods. Additionally, only trace amounts of Ca were released and this quantity did not increase over time. The quantities of major elements released into solution occurred in the following order Fe≈Mg>Si>Al≈Ca for citric acid experiments. The order was similar for the 20 mM oxalate experiment except that the quantity of Al released was greater than Ca. Trace quantities of Ti, Cr, Ni and Mn were released in all organic acid experiments.

The computer codes GEOCHEM-PC and MINTEQA2 indicated that in the reacting solutions the concentration of Al at 12 days becomes supersaturated with respect to gibbsite for both citric and oxalic acid experiments and this solid phase might be expected to precipitate.

Figure 3.11-3.14 show scanning electron micrographs of weathered surfaces of pyroxene, and olivine. Similar to the pH experiments, although less extensive, the pyroxene surfaces exposed to both organic acid treatments showed side-by-side etching along the boundaries of basal lamellae (Fig. 3.11-3.13). The olivine grain exhibits a pitted or wavy surface (Fig. 3.14). This surface morphology may be

the result of etching along lattice imperfections such as cleavage planes or dislocations (Grandstaff, 1978). Precipitates were only observed for the 20 mM oxalic acid experiment. However, these materials were minute in size and difficult to identify using the EDAX system.

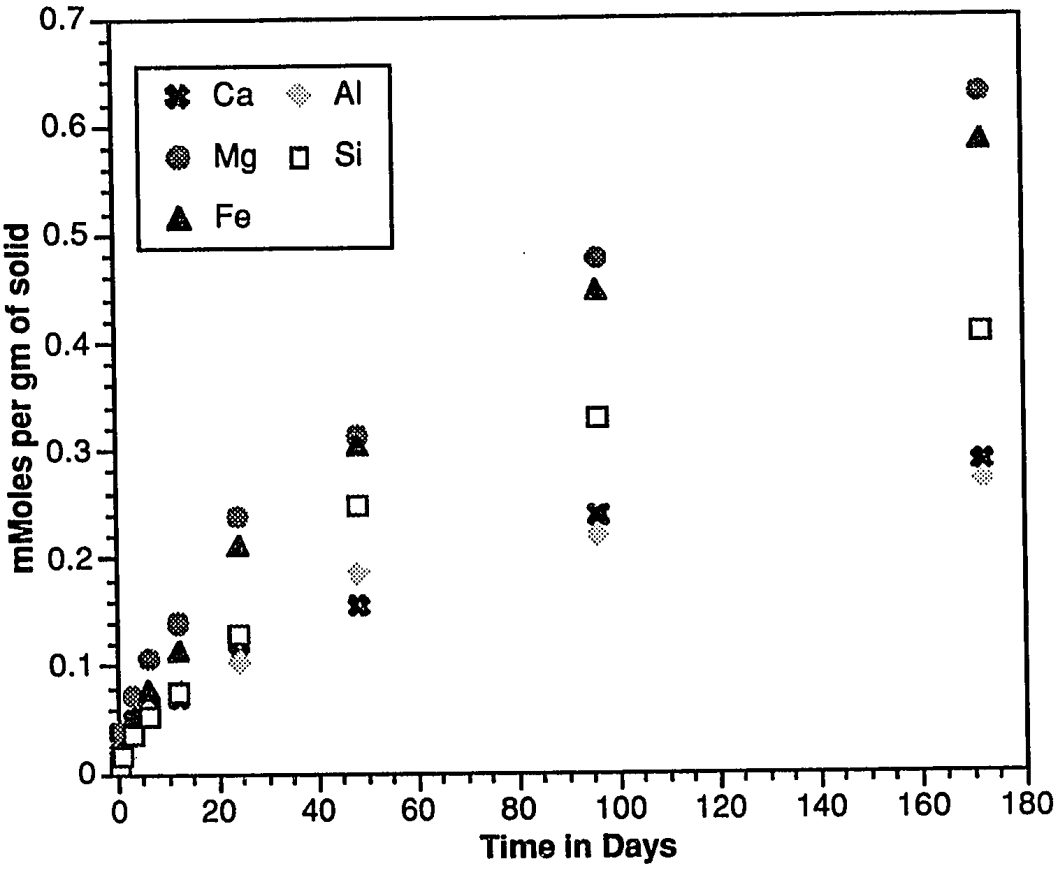

Figure 3.8 Release of major elements into aqueous solution from the MLS-1 basalt as a function of time at 20 mM citric acid.

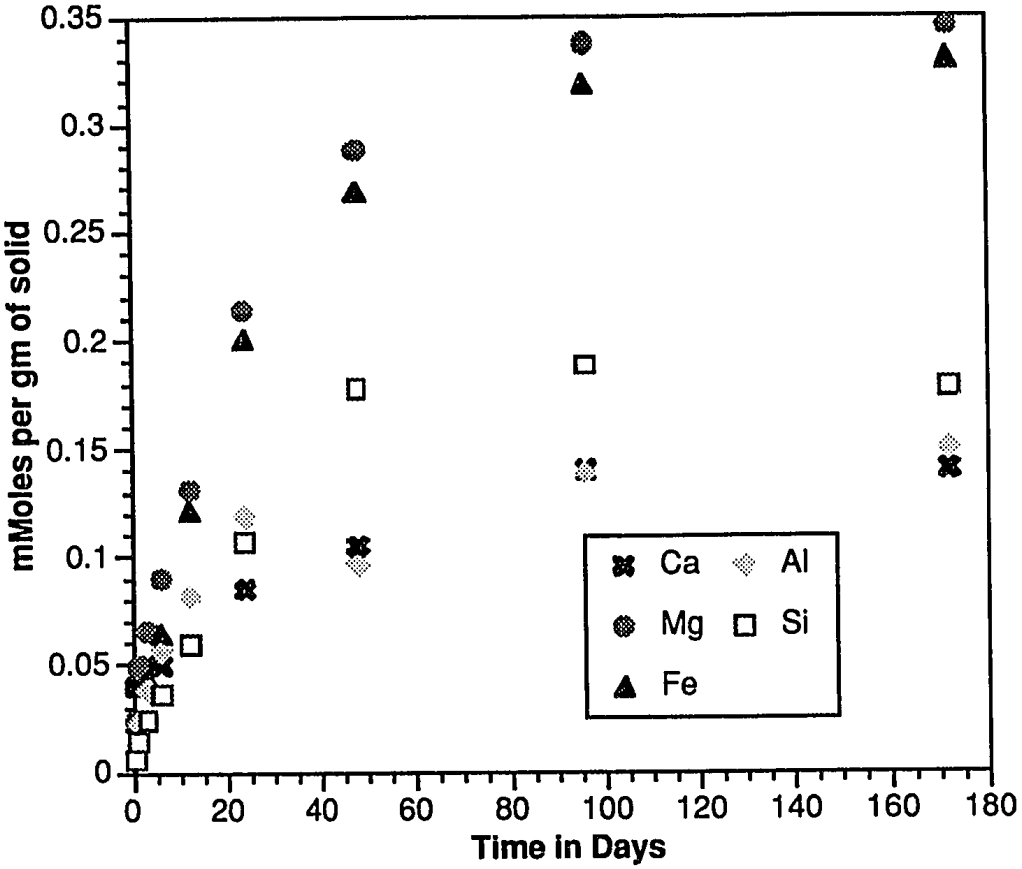

Figure 3.9 Release of major elements into aqueous solution from the MLS-1 basalt as a fuction of time at 2 mM citric acid.

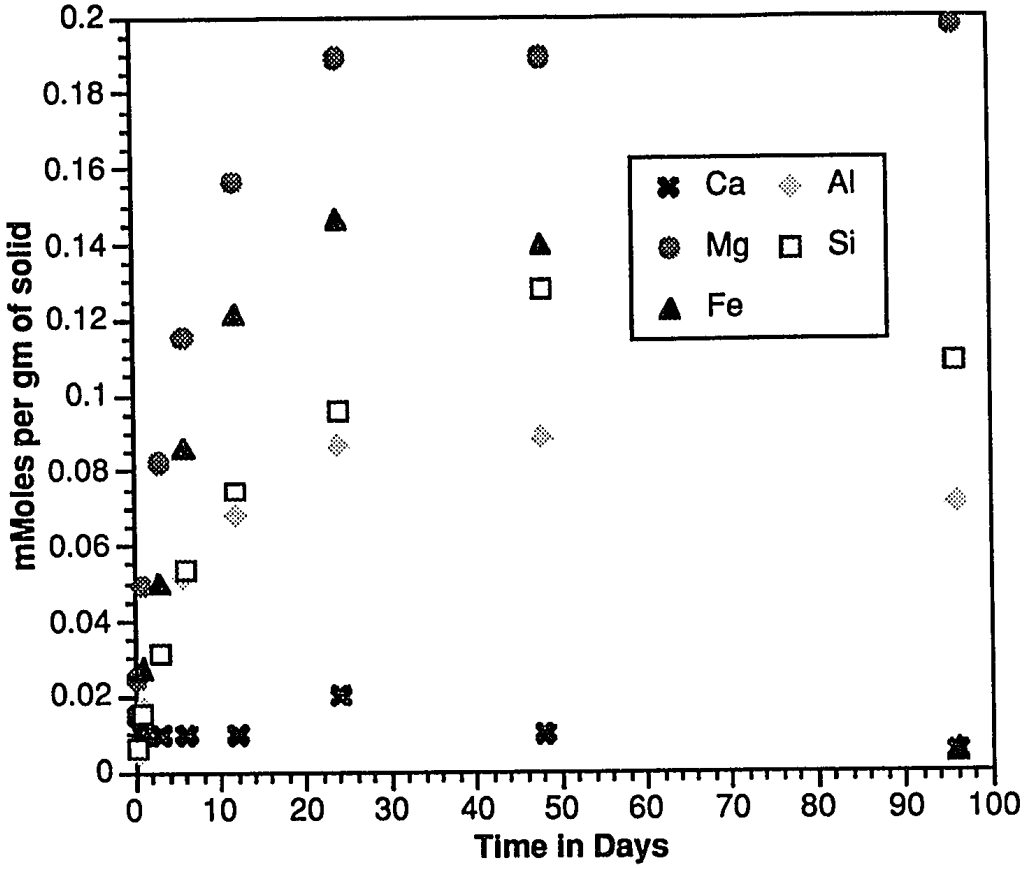

Figure 3.10 Release of major elements into aqueous solution from the MLS-1 basalt as a fuction of time at 20 mM oxalic acid.

Figure 3.11 SEM image of a clinopyroxene surface weathered at 20 mM citric acid. Etching of the surface is clearly visable along basal lamallae.

Figure 3.12 SEM image of a clinopyroxene surface weathered at 20 mM oxalic acid. Etch pits are visable along the basal lamallae although not as extensive as Fig. 3.11.

Figure 3.13 SEM image of a clinopyroxene surface weathered at 20 mM citric acid. Note the formation of etch pits along the basal lamallae.

Figure 3.14 SEM image of an olivine surface weathered at 20mM citric acid. The olivine exhibits a pitted or wavy surface.

3.4 Discussion

3.4.1 Order of Cation Release

The order of cation release can be related to the relative stabilities of the minerals composing the basalt. Olivine is the least stable of the minerals. It is composed of distinct silica tetrahedra that are balanced by Fe^{+2} and Mg^{+2}. The structure is held together predominantly by ionic forces and should rapidly weather in the presence of complexing agents and acid solutions. Pyroxenes are more stable than olivine but should also rapidly weather when exposed to organic acids and acid solutions. The MLS-1 basalt contains both ortho and clinopyroxenes. Pyroxenes consist of SiO_4 tetrahedra that are linked into chains via sharing oxygens. The chains are linked laterally by cations such as Ca, Mg, and Fe located in positions labeled M_1 and M_2. In general, the larger cations (e.g. Ca) occupy the M_2 position while the smaller cations (e.g. Mg and Fe) occupy the M_1 position. However, Mg and Fe can also occupy the M_2 position. The M_1 site is a regular octahedron and the M_2 is usually an irregular polyhedron of coordination number 8 (Klein and Hurlburt, 1985). The cation present in the M_2 site is more weakly bonded than the cation present in the M_1 site. Therefore, the Ca present in the clinopyroxene should be more mobile than the Mg or Fe. In the orthopyroxene the M_1 and M_2 can be occupied by either Fe or Mg. The plagioclase feldspar present should be less soluble than either the olivine or pyroxene minerals. Feldspars are members of tectosilicates in which all the oxygen ions in each SiO_4 tetrahedra are shared with adjacent tetrahedra (Klein and Hurlburt, 1985). This results in a mineral that is very stable. Finally, the least soluble of all

minerals present in the basalt is ilminite. Ilminite is an iron titanium oxide with a similar structure to corundum and is expected to be relatively resistant to weathering.

From the above discussion it would be expected that Fe and Mg would be released in the greatest concentrations followed by Ca and Al. In all dissolution experiments, Fe and Mg were released at greater concentrations than Ca and Al. Deviations in the expected release based on mineral stability occurred for the pH 5 experiment. Aluminum was released at similar concentrations to Fe and Mg. This may be attributed to a soluble Al bearing mineral or a greater quantity of plagioclase feldspar as compared to other minerals in this particular subsample. Additional deviations in this order may occur depending on the nature of the organic acid and its stability constant with a particular cation.

3.4.2 Dissolution Kinetics

3.4.2.1 pH Experiments

Both pH 3 and 5 experiments exhibit a two stage release process. The first stage is characterized by the rapid release of elements followed by a slower, more linear release in the second stage. The rapid release in the first stage is attributed to the fast dissolution of ultra-fine grains (Holdren and Berner, 1979; Helgeson et al., 1984) and unstable surface and subsurface features (Petrovich, 1981b) created by grinding during sample preparation. These particles have a high surface area/volume ratio and consequently have a higher free energy which makes them unstable compared to the bulk mineral (Holdren and Berner, 1979).

Following the dissolution of these ultrafine grains the release rate becomes slower and follows a more linear rate. Dissolution now occurs on the larger mineral

grains at sites of excess energy. These sites include dislocations, twinning planes, and fluid inclusions. These features were observed using SEM.

Differences in the rate of dissolution between the two experiments can be related to the hydrogen ion concentration. It is proposed that H^+ ions are involved with diffusion exchange with cations and the protonation of the surface. This protonation weakens the metal oxygen bond and enhances the release of Si from the surface. As the pH is reduced the dissolution of the silicate mineral increases (Stumm and Wieland, 1987). It must be pointed out that the above model is simplistic and silicate dissolution kinetics may be much more complex (Schott and Petit, 1987).

MINTEQA2 and GEOCHEM-PC calculations indicate that reacting solutions are near supersaturation with Si (with respect to amorphous silica) and Al (with respect to gibbsite) for the pH 3 and 5 experiments, respectively. However, the presence of amorphous silica and gibbsite solid phases was not observed by SEM analysis. Above pH 4, aqueous Al concentrations are controlled by the precipitation of microcrystalline gibbsite. We speculate that the absence of a precipitate at pH 5 is due to ion-ion interactions which reduce the free Al^{+3} concentration in solution, and consequently, the degree of supersaturation with respect to the solid phase. Ion-ion interactions are due to the relatively high ionic strength, resulting from the use of the pH buffer phthalate.

3.4.2.2 Organic Acid Experiments

The two stage dissolution process exhibited for the organic acid experiments has been observed by previous researchers (Song and Huang, 1988; Barman et al., 1991). It is proposed that the first stage is due to the rapid dissolution of ultrafine grains created during grinding of the sample, similar to the pH

experiments. After these high energy sites are depleted, dissolution occurs along dislocations, twinning planes, fluid inclusions and other high energy areas of the bulk mineral.

An additional factor affecting the initial high rates of release observed in organic acid dissolution experiments could be a diffusion controlled process involving dissolution of cations at the surface and near the surface of mineral grains that is rate limiting (Barman et al., 1991). Rapidly solubilized surface and subsurface cations form cation-organic complexes. The diffusion of these complexes is considered to be the rate limiting step. Once the surface is depleted of a large majority of its cations, then the availability of fresh surfaces caused by fragmentation, formation of defect planes, and etching becomes the rate-limiting step and linear kinetics is observed.

We propose that the organic acids accelerate the dissolution of the MLS-1 basalt through a two step process. The first step involves the chemisorption of the organic ligands on the basalt surface. The adsorbed organic ligand is a π donor and shifts electron density inward toward the framework of the mineral. This charge transfer increases the electron density of the metal-oxygen bond which weakens the framework of the mineral These bonds are now more susceptible to hydrolysis which increases the rate of dissolution (Bennett et al., 1988). The second step involves the chelating ability of the organic ligand. The organic ligand will form complexes with cations released during the hydrolysis reactions occurring at the surface of the mineral. These complexation reactions reduce the activity of the cation in solution, increasing the diffusion gradient and consequently the dissolution of metals from the minerals of the basalt. Additionally, the disruption of the mineral framework will promote increased hydration of the bulk mineral aiding in its dissolution.

Differences in the rate of dissolution between organic acids can be related to their concentration and number of functional groups. At pH 7 both organic acids are in their dissociated form. The dissolution is greater for citric acid compared to oxalic acid which is attributed to a larger number of carboxylic acid groups for the citric acid. For both citrate and oxalate greater dissolution is observed at higher concentrations.

MINTEQA2 and GEOCHEM-PC calculations indicate that both the citric and oxalic acid experiments were supersaturated with respect to gibbsite. Complexation of Al by organic acids is probably responsible for the absence of gibbsite precipitation. The 20 mM oxalic acid experiment showed a drop in the aqueous concentration of Si, Al, and Fe during the last two sampling periods (96 and 172 days). Also, SEM results indicayed the presence of precipitates. In the presence of oxalic acid at 20 mM these elements should be complexed by the organic ligand and prevented from precipitating. It is proposed that during sampling events photoxidation of oxalic acid occurred which substantially reduced its concentration. Elements that were previously complexed by the oxalate ligand are now uncomplexed and subsequently precipitate from solution. The low concentration of aqueous Ca^{+2} in the 20 mM oxalate experiment may be explained by the precipitation of Ca-oxalate. Calcium-oxalate crystals were not observed with SEM. However, microcrystalline precipitates that had not settled out of the solution column may have been trapped on the 0.2 μm filter during sampling resulting in small quantities of aqueous Ca^{+2} in the supernatant.

3.5 Conclusions

1) The order of cation release during dissolution experiments is related to the stabilities of the minerals present in the basalt. Olivine is the least stable of the minerals; consequently, Fe and Mg are released in the greatest quantities.

2) The dissolution of the MLS-1 basalt in all experiments follows a two stage process. The first stage is characterized by a rapid release of constituent elements followed by a slower, more linear rate of release. It is proposed that the first stage is due to the dissolution of ultrafine grains created during the grinding process of the basalt. During the second stage, dissolution occurs at high energy sites such as dislocations, twinning planes, and fluid inclusions, which follows a more linear rate of release. Dissolution at these sites of excess energy results in etching of the surface of the mineral which was observed using SEM. Additionally, in the organic acid experiments, the first stage may also be due to the diffusion of cation-organic complexes formed at the surface of the mineral.

3) It is proposed that dissolution in the pH experiments is caused by the diffusion exchange of H^+ ions with structural cations and protonation of the surface of the mineral. Surface protonation weakens the structure of the mineral causing breakdown and release of Si.

4) Dissolution in the presence of the organic acids proceeds via a two stage process. The first is the chemisorption of the organic ligand which shifts electron density inward toward the framework of the mineral. This charge transfer increases the electron density of the metal-oxygen bond which weakens the framework of the mineral. These bonds are now more susceptible to hydrolysis which increases the rate of dissolution. The second step involves the chelating ability of the organic

ligand which increases the diffusion gradient and subsequent dissolution of cations from the minerals of the basalt.

5) The dissolution rate in the presence of the organic acids is related to the concentration of the acid and the number of carboxylic acid functional groups.

3.5.1 Implications for Use as a Plant Growth Substrate

Reductions in pH and the release of organic ligands in the rhizosphere will rapidly weather unstable basalt minerals and release ample quantities of Ca, Mg, and Fe. These nutrients will be involved in precipitation and sorption reactions as weathering continues and should be readily available for plant uptake. The release of toxic quantities of Cr and Ni will depend on their concentration in the regolith as well as their location in primary minerals. In the MLS-1 basalt Ni is present in low concentrations and most of the Cr is found in ilminite. Therefore, only trace quantities of these metals should be released during weathering which was observed in the above dissolution studies.

A wide variety of materials compose the lunar regolith (e.g. glasses, primary minerals, agglutinates, etc.). These materials will react differently when exposed to a terrestrial weathering environment. Therefore, additional studies are necessary to understand the dissolution of the components of the lunar regolith. Also, Cr and Ni released during dissolution will be involved in sorption and redox reactions which may increase/decrease their toxicity. Thus, it is essential to determine the fate and form of these metals in the presence of secondary weathering products. The information gleaned from these studies will provide important information on the use of the lunar regolith as a plant growth medium.

3.6 References

Aagaard, P. and H.C. Helgeson. 1982. Thermodynamic and kinetic constraints on reaction rates among minerals and aqueous solutions. I. Theoretical considerations. Amer J. Sci. 282:237-285

Allison, J.D., D.S. Brown, and K.J. Novo-Gradac. 1991. MINTEQA2/PRODEFA2, a geochemical assesment model for environmental systems: version 3.0 user's guide. Environmental Research Laboratory Office of Research and Development. U.S. EPA, Athens, GA.

Amrhein, C. and D.L. Suarez. 1988. The use of a surface complexation model to describe the kinetics of ligand-promoted dissolution of anorthite. Geochim. Cosmochim. Acta. 52:2785-2793.

Antweiler, R.C. and J.I. Drever. 1982. The weathering of a late Tertiary volcanic ash: importance of organic solutes. Geochim. Cosmochim. Acta 47:623-629.

Barman, A.K., C. Varadachari, and K. Ghosh. 1992. Weathering of silicate minerals by organic acids. I. Nature of cation solubilisation. Geoderma. 53:45-63.

Bennett, P.C., M.E. Melcer, D.I. Siegel, and J.P. Hassett. 1988. The dissolution of quartz in dilute aqueous solutions of organic acids at 25°C. Geochim. Cosmochim. Acta 52:1521-1530.

Berner, R. A. and G.R. Holdren, Jr. 1979. Mechanism of feldspar weathering-II. Observations of feldspars from soils. Geochim Cosmochim. Acta 43:1173-1186.

Berner, R.A. and G.R. Holdren, Jr. 1977. Mechanisms of feldspar weathering: Some observational evidence. Geology 5:369-372.

Berner, R.A. and J. Schott. 1982. Mechanism of pyroxene and amphibole weathering II. observations of soil grains. Amer. J. Sci. 282:1214-1231.

Berner, R.A. 1978. Rate control of mineral dissolution under earth surface conditions. Amer. J. Sci. 278:1235-1252.

Berner, R.A., G.R. Holdren, Jr., and J. Schott. 1985. Protective surface layers on dissolving silicates. Comments on the paper "Study of the weathering of albite at room temperature and pressure with a fluidized bed reactor" by L. Chou and R. Wollast (Geochim. Cosmochim. Acta 48:2205-2217, 1984), Geochim. Cosmochim. Acta 49:1657-1658.

Boyle, J.R., G.K. Voigt, and B.L. Sawhney. 1974. Chemical weathering of biotite by organic acids. Soil Sci. 117:42-45.

Busenburg, E., and C.V. Clemency. 1976. The dissolution kinetics of feldspars at 25°C and 1 atm CO_2 partial pressure. Geochim Cosmochim Acta 40:41-49.

Casey, W.H., H.R. Westrich, and G.W. Arnold. 1988. Surface chemistry of labradorite feldspar reacted with aqueous solutions at pH= 2, 3, and 12. Geochim. Cosmochim. Acta 52:2795-2807.

Casey, W.H., H.R. Westrich, G.W. Arnold, and J.F .Banfield. 1989. The surface chemistry of dissolving labradorite feldspar. Geochim. Cosmochim. Acta 53:821-832.

Chou, L. and R. Wollast. 1984. Study of the weathering of albite at room temperature and pressure with a fluidized bed reactor. Geochim. Cosmochim. Acta 48:2205-2217.

Chou, L. and R. Wollast. 1985. Study of the weathering of albite at room temperature and pressure with a fluidized bed reactor. Reply to comment by R.A. Berner, G.R. Holdren, Jr., and J. Schott. Geochim. Cosmochim. Acta 49:1659-1660.

Correns, C.W. and W. Von Engelhardt. 1938. Neue Untersuchungen ueber die Verwitterung des Kalifeldspates. Chemie der Erde 12:1-22.

Correns, C.W. 1940. Die chemische verwitterrung der silikate. Naturwissenschaften 28:369-376.

Correns, C.W. 1961. The experimental chemical weathering of silicates. Clay Min. Bull. 4:249-281.

Correns, C.W. 1963. Experiments on the decompositon of silicates and discussion of chemical weathering. Clays Clay Minerals 10:443-459.

Dibble, W.E., Jr. 1981. Non-equilibrium water/rock interaction. I. Model for interface-controlled reactions. Geochim Cosmochim Acta 45:79-92.

Duff, R.B., D.M. Webley, and R.O. Scott. 1963. Solubilization of minerals by 2-ketogluconic acid-producing bacteria. Soil Sci. 95:105-114.

Eckhardt, F.E.W. 1985. Solubilization, transport, and deposition of mineral cations by microorganisms-efficient rock weathering agents. p. 161-173. *In* J.I. Drever (ed.) The Chemistry of Weathering. Reidel Publishers, Boston.

Eyring, H. 1935a. The activated complex in chemical reactions. J. Chem. Phys. 3:107-120.

Eyring, H. 1935b. The activated complex and the absolute rate of chemical reactions. Chem. Rev. 17:65-82.

Furrer, G. and W. Stumm. 1986. The coordination chemistry of weathering: I. Dissolution kinetics of Al_2O_3 and BeO. Geochim. Cosmochim. Acta 50:1847-1860.

Glasstone, S., K. Laidler, and H. Eyring. 1941. The theory of rate processes. McGraw-Hill, New York.

Gossens, D.A., J.G. Philippaerts, R. Gijbels, A.P. Pijpers, S. Van Tendeloo, and E. Althaus. 1989. A SIMS, XPS, SEM, TEM, FTIR study of feldspar surfaces after reacting with acid solutions. p. 271-274. *In* D.L. Miles (ed.) Water-Rock Interaction WRI-6. A.A. Balkema, New York.

Grandstaff, D.E. 1977. Some kinetics of bronzite orthopyroxene dissolution. Geochim Cosmochim. Acta 41:1097-1103.

Grandstaff, D.E. 1978. Changes in surface area and morphology and the mechanism of forsterite dissolution. Geochim. Cosmochim. Acta 42:1899-1901.

Graustein, W.C. 1975. On chemical weathering and forests. Geol. Soc. Amer. Abst. with programs 7:1090-1091.

Helgeson, H.C.,1971. Kinetics of mass transfer among silicates and aqueous solutions. Geochim. Cosmochim. Acta 35:421-469.

Helgeson, H.C., W.M. Murphy, and P. Aagaard. 1984. Thermodynamic and kinetic constraints on reaction rates among minerals and aqueous solutions. II. rate constants, effective surface area, and the hydrolysis of feldspar. Geochim. Cosmochim. Acta 48:2405-2432.

Hellmann, R., C.M. Eggleston, M.F. Hochella, Jr., and D.A. Crerar, 1990. The formation of leached layers on albite surfaces during dissolution under hydrothermal conditions. Geochim. Cosmochim. Acta 54:1267-1281.

Holdren, G.R., Jr. and J.E. Adams. 1982. Parabolic dissolution kinetics of silicate minerals: An artifact of nonequilibrium precipitation processes? Geology 10:186-190.

Holdren, G.R., Jr. and R.A.Berner. 1979. Mechanism of feldspar weathering. I. Experimental studies. Geochim Cosmochim Acta 43:1161-1171.

Holdren, G.R., Jr. and P.M. Speyer. 1985. pH dependent changes in the rates and stoichiometry of dissolution of an alkali feldspar at room temperature, Amer. J. Sci. 285:994-1026.

Holdren, G.R., Jr. and P.M. Speyer. 1987. Reaction rate-surface area relationships during the early stages of weathering. II. Data on eight additional feldspars. Geochim. Cosmochim. Acta 51:2311-2318.

Huang, W.H. and W.D. Keller. 1970. Dissolution of rock-forming silicate minerals in organic acids: simulated first-stage weathering of fresh mineral surfaces. Amer. Mineral. 57:2076-2094.

Huang, W.H. and W.C. Kiang. 1972. Laboratory dissolution of plagioclase feldspars in water and organic acids at room temperature. Amer. Mineral. 57:1849-1859.

Jorgensen, S.S. 1967. Dissolution kinetics of silicate minerals in aqueous catechol solutions. J. Soil Sci. 27:183-195.

Keller, W.D. and W.H. Huang. 1971. Response of Apollo 12 lunar dust to reagents simulative of those in the weathering environment of Earth. p. 973-981. Proceedings of the Second Lunar Science Conference, Vol. I, The M.I.T. Press, Cambridge.

Klein, C. and C.S. Hurlburt, Jr. 1985. Manual of mineralogy. John Wiley and Sons, New York.

Krumbein, W.E. and B.D. Dyer. 1985. The plant is alive-weathering and biology, a multi-faceted problem. p. 143-160. *In* J.I. Drever (ed.). The chemistry of weathering. Reidel Publishers, Boston.

Lagache, M. 1965. Contribution a l'etude de l'alterstion des feldspaths dans l'eau, entre 100 et 200°C, sous diverses pressions de CO_2 et application a la synthese des mineraux argileaux. Soc. Francaise Mineral. Cristallogr. Bull 88:223-253.

Lagache, M. 1976. New data on the dissolution of alkali feldspars at 200°C in CO_2 charged water. Geochim Cosmochim. Acta 40:157-161.

Lagache, M., J Wyart, and G. Sabatier. 1961. Mecanisme de la dissolution des feldspaths alcalins dans l'eau pure ou chargee de CO_2 a 200°C. C.R. Acad. Sci. Paris 253:2296-2299.

Lasaga, A.C. 1981. Transition state theory. p 135-169. *In* A.C. Lasaga and R. J. Kirkpatrick (ed). Kinetics of Geochemical Processes. Reviews in Mineralogy 8, Mineral. Soc. Amer.

Luce, R.W., R.W Bartlett, and G.A.Parks. 1972. Dissolution kinetics of magnesium silicates. Geochim. Cosmochim. Acta 36:35-50.

Manley, E.P. and L.J. Evans. 1986. Dissolution of feldspars by low-molecular-weight aliphatic and aromatic acids. Soil Science 141:106-112.

Mast, M.A., and J.I. Drever. 1987. The effect of oxalate on the dissolution rates of oligoclase and tremolite. Geochim.Cosmochim. Acta 51:2559-2568.

Mogk, D.W. and W.W. Locke. 1988. Application of auger electron spectroscopy (AES) to naturally weathered hornblende. Geochim. Cosmochim. Acta 52:2537-2542.

Murphy, W.M. and H.C. Helgeson. 1987. Thermodynamic and kinetic constraints on reaction rates among minerals and aqueous solutions. III. Activated complexes and the pH-dependence of the rates of feldspar, pyroxene, wollastonite, and olivine hydrolysis. Geochim. Cosmochim. Acta 51:3137-3153.

Nesbitt, H.W. and I.J. Muir. 1988. SIMS depth profiles of weathered plagioclase, and processes affecting dissolved Al and Si in some acidic soil solutions. Nature 334:336-338.

Paces, T. 1973. Steady-state kinetics and equilibrium between groundwater and granitic rock. Geochim. Cosmochim. Acta 37:2641-2643.

Parker, D.R., W.A. Norvell, and R.L. Chaney. 1993. GEOCHEM-PC: A chemical speciation program for IBM and compatible computers. *In* R.H. Loeppert et al. (ed). Soil Chemical Equilbrium and Reaction Models. SSSA, Madison, WI.

Petit, J.C., G. Della Mea. J.C. Dran, J. Schott, and R.A. Berner, 1987a. Mechanism of diopside dissolution from hydrogen depth profiling. Nature 325:705-707.

Petit, J.C., J.C. Dran, and G. Della Mea. 1987b. Effects of ion plantation on the dissolution of minerals. Part II: Selective dissolution, Bull. Mineral. 110:25-42.

Petrovic R., R.A. Berner, and M.B. Goldhaber. 1976. Rate control in dissolution of alkali feldspars-I. Study of residual feldspar grains by X-Ray photoelectron spectroscopy. Geochim Cosmochim. Acta 40:537-548.

Petrovich, R. 1981a. Kinetics of dissolution of mechanically comminuted rock-forming oxides and silicates I. Deformation and dissolution of quartz under laboratory conditions. Geochim. Cosmochim. Acta 45:1665-1674.

Petrovich, R. 1981b. Kinetics of dissolution of mechanically comminuted rock-forming oxides and silicates I. Deformation and dissolution of oxides and silicates in the laboratory and at the earth's surface. Geochim. Cosmochim. Acta 45:1675-1686.

Rimstidt, J.R. and H.L. Barnes. 1980. The kinetics of silica-water reactions. Geochim. Cosmochim. Acta 44:1683-1699.

Schalscha, E.B., H. Appelt, and A. Schatz. 1967. Chelation as a weathering mechanism-I. Effect of complexing agents on the solubilization of iron from minerals and granodorite. Geochim. Cosmochim. Acta 31:587-596.

Schott, J. and R.A. Berner. 1983. X-ray photoelectron studies of the mechanism of iron silicate dissolution during weathering. Geochim. Cosmochim. Acta 47:2233-2240.

Schott, J. and J.C. Petit. 1987. New evidence for the mechanisms of dissolution of silicate minerals. p. 293-315. *In* W. Stumm (ed.). Aquatic surface chemistry. Wiley Interscience, New York.

Schott, J., R.A. Berner, and E.L. Sjoberg. 1981. Mechanisms of pyroxene and amphibole weathering. I: Experimental studies of iron-free minerals. Geochim Cosmochim Acta 45:2133-2135.

Shotyk, W. and H.W. Nesbitt. 1992. Incongruent and congruent dissolution of plagioclase feldspar: effect of feldspar composition and ligand complexation. Geoderma 55:55-78.

Song, S.K. and P.M. Huang. 1988. Dynamics of potassium release from potassium-bearing minerals as influenced by oxalic and citric acids. Soil Sci. Soc. Am. J. 52:383-390.

Stevenson, F.J. 1967. Organic acids in soils. pp. 110-146. *In* A.D. McLaren and G.H. Petersen (ed.). Soil Biochemistry, vol 1. Academic Press, New York.

Stumm, W. and E. Wieland. 1987. Dissolution of oxide and silicate minerals: rates depend on surface speciation. p 367-400. *In* W. Stumm (ed.). Aquatic surface chemistry. Wiley Interscience, New York.

Stumm, W., G. Furrer, E. Wieland, and B. Zinder. 1985. The effects of complex-forming ligands on the dissolution of oxides and alumino-silicates. p. 55-74. *In* J.I. Drever (ed.). The chemistry of weathering. D. Reidel Publ. Co., Boston.

Tan, K.H. 1980. The release of silicon, aluminum, and potassium during decomposition of soil minerals by humic acid. Soil Sci. 129:5-11.

Weiblen, P.W., Murawa, M.J. and Reid, K.J. 1990. Preparation of simulants for lunar surface materials. Proceedings of Space '90. Aerospace/ASCE/Albuquerque, NM.

Weiland, E., B. Wehrli, and W. Stumm. 1988. The coordination chemistry of weathering: III: a generalization on the dissolution rates of minerals. Geochim. Cosmochim. Acta 52:1969-1981.

Wollast, R. 1967. Kinetics of the alteration of K-feldspar in buffered solutions at low temperature. Geochim. Cosmochim. Acta 31:635-648.

Wollast, R., and L. Chou. 1985. Kinetic study of the dissolution of albite with continuous flow-through fluidized bed reactor. p. 75-96. *In* J.L. Drever (ed.). The chemistry of weathering. D. Reidel Publ. Co., Boston.

Wyart, J., A. Oberlin, and C. Tchoubar. 1963. Etude en microscopeet mircodiffraction electroniques de la boehmite formee lors de l'alteration de l'albite. C.R. Seances Acad. Sci., Ser. 2. 256:554-555.

Chapter 4

OXYANION ADSORPTION/DESORPTION KINETICS ON GOETHITE USING PRESSURE-JUMP RELAXATION

4.1 Introduction

4.1.1 Relaxation Kinetics

There is considerable concern regarding trace element contamination of soils and sediments. Trace elements are defined as chemical elements whose indigenous concentrations (either in the solid or aqueous phase) are less than 100 ppm (Jurinak and Tanji, 1993). At elevated concentrations these pollutants are potentially hazardous to plant, animal and human health. High levels of trace elements have been associated with the disposal of industrial wastes, application of pesticides and sewage sludges, metal plating industries, mining industries and smelting operations. In the past, the disposal of trace element wastes often failed to consider their potential as environmental contaminants. Increased ground and surface water contamination has generated enormous public and political concern, demanding swift and proper remediation of these areas. There is now the recognition that proper disposal and clean-up methods require a better understanding of the interactions between toxins and soils.

Sorption by soils and sediments is one of the most important processes controlling trace element levels in natural waters. Significant quantities of these compounds are adsorbed on the surfaces of soil constituents such as Fe- and Al-

oxides, clays, carbonates and organic matter. This process is extremely rapid and often occurs within milliseconds (Amacher, 1991; Sparks and Zhang, 1991). Even though surface adsorption reactions occur rapidly in comparison with other chemical processes in natural environments, kinetic studies can help determine the mechanisms underlying ion adsorption on oxides (Sparks, 1989). However, conclusive mechanistic information can only be obtained in conjunction with spectroscopic experiments and adsorption modeling. Understanding the fate of inorganic contaminants in the environment requires knowledge of their interactions with the soil solid matrix (e.g., specific adsorption vs. electrostatic or non-specific adsorption). Specific adsorption is often described as the formation of inner-sphere surface complexes, which would involve the loss of at least one water molecule from the primary hydration sphere surrounding the ion, resulting in direct binding of the ion to a surface functional group. If the attraction is electrostatic, the ion maintains its primary hydration sphere when it forms an outer-sphere surface complex. Inner-sphere surface complex bonds are either covalent or ionic and they are much stronger than outer-sphere surface complexes (Sposito, 1984).

Conventional kinetic techniques, such as batch methods, cannot be used to measure the rapid rates of ion adsorption reactions. However, relaxation methods, specifically pressure-jump (p-jump) relaxation, have been successfully employed to measure the kinetics of ion adsorption/desorption reactions on soil constituents (Yasunaga and Ikeda, 1986; Sparks and Zhang, 1991). The p-jump technique is especially useful because it simultaneously supplies rate information for both adsorption and desorption processes. The p-jump method is based upon the fact that the equilibrium constant for a chemical reaction is dependent upon pressure and can be expressed by the relationship,

$$\left(\frac{\delta \ln K}{\delta \ln P}\right)_T = -\frac{\Delta V}{RT} \qquad (4.1)$$

where K is the chemical equilibrium constant, P is the pressure, ΔV is the standard molar volume change of the reaction, R is the universal gas constant, and T is the absolute temperature (Bernasconi, 1976). Therefore, a pressure perturbation shifts the equilibrium state of a chemical reaction. The system must then relax to the final equilibrium state. The relaxation is a function of all the elementary reaction steps that comprise the chemical reaction.

The use of p-jump relaxation to measure the kinetics of ion adsorption/desorption on metal oxide surfaces was pioneered by several Japanese chemists (Yasunaga and Ikeda, 1986). Their research includes some of the following adsorption/desorption kinetic studies: proton interactions with TiO_2 (Ashida et al., 1978) and Fe-oxide surfaces (Astumian et al., 1981), divalent metal ion (Hachiya et al., 1984) and uranyl (Mikami et al., 1983a) reactions with γ-Al_2O_3 surfaces, and phosphate (Mikami et al., 1983b) and chromate (Mikami et al., 1983c) adsorption reactions on γ-Al_2O_3. Hayes and Leckie (1986) were the first to use p-jump relaxation kinetics to study the adsorption/desorption behavior of a metal ion contaminant (Pb^{2+}) on goethite (α-FeOOH). Other successive studies monitored the rapid adsorption/desorption kinetics of molybdate (Zhang and Sparks, 1989), sulfate (Zhang and Sparks, 1990a), selenate and selenite (Zhang and Sparks, 1990b) and Cu^{2+} (Grossl et al., 1994) on goethite.

4.1.2 Behavior of Hexavalent Chromium

The oxidation of chromium(III) is intricately linked to the amount and form of manganese present in soils. Manganese oxides serve as electron links between Cr(III) and oxygen of the atmosphere and are the only known naturally occurring oxidant of Cr(III) (Eary and Rai, 1987). Chromium (VI) added to or formed in soils may be leached, reduced, adsorbed, precipitated, or removed by a living organism (Bartlett and James, 1988). Many of these processes occur simultaneously in soils which makes it difficult to separate them in heterogeneous soil systems. Hexavalent Cr occurs as an anion in aqueous solutions. The dichromate anion ($Cr_2O_7^{2-}$) is the dominant form in acidic solutions at high concentrations while the $HCrO_4^-$ and CrO_4^{2-} are the dominant forms at lower concentrations (Baes and Mesmer, 1976). Adsorption may be an important mechanism for removing Cr(VI) from solution especially in soils dominated by iron and aluminum oxides which have a net negative charge (Ainsworth et al., 1989; Zachara et al., 1989). Divalent CrO_4^{2-} and monovalent $HCrO_4^-$ may behave similarly to sulfate and phosphate anions becoming specifically adsorbed (Bartlett and James, 1988). However, these anions, may also be non-specifically sorbed depending on the soil mineralogy and the relation of soil pH to the zero point of charge of the colloids present in the system.

The adsorption of the chromate anion on soils and oxides has been investigated by a number of researchers (Ainsworth et al., 1989; Zachara et al., 1987, 1988, 1989; Rai et al., 1988). Chromate adsorption has been found to increase with decreasing pH as a result of protonation of surface hydroxyl sites and aqueous speciation of CrO_4^{2-}. The chromate anion is bound by soil colloids via surface coordination. However, the nature of the surface complex (e.g., inner or outer sphere)

has not been completely resolved. Indirect evidence suggests the complex is outer-sphere (Hayes, 1987; Zachara et al., 1988).

Stollenwerk and Grove (1985) investigated the adsorption and desorption of hexavalent chromium on alluvial aquifer material. They hypothesized both specific and nonspecific adsorption and concluded that Fe-oxide and hydroxide coatings present on the aquifer material controlled the surface charge. The hexavalent chromium adsorbed nonspecifically was readily desorbed by Cr-free water while specifically adsorbed Cr(VI) was very slowly released. The authors postulated that over time some of the specifically adsorbed (or fixed) Cr(VI) may actually be reduced to Cr(III) and precipitate as $Cr(OH)_3$.

The behavior of hexavalent chromium in soils and subsurface materials has not been investigated as thoroughly as in clay and oxide systems. This is due to the difficulty in separating reduction, precipitation, and adsorption reactions in heterogeneous systems. James and Bartlett (1983) examined the adsorption and reduction of various forms of hexavalent chromium with oxides and soils. They found that Cr(VI) may be removed by soils via anion adsorption or precipitation or reduction to low solubility cationic forms. The fate of the hexavalent chromium will depend on the nature of the colloids, pH of the system, presence of organic and inorganic ligands, and the presence of organic reductants. The authors found that phosphate was an adequate extractant for characterizing "exchangeable" Cr(VI). The Cr(VI) that was not extracted was termed "nonexchangeable" and consisted of precipitated, reduced, and tightly bound Cr. These nonexchangeable forms could not be separated in a heterogeneous soil system. Addition of lime to the soils decreased both the exchangeable and nonexchangeable Cr(VI) removed from the soils. The authors proposed that raising the soil pH decreased anion adsorption by reducing the positive

charge and decreased the amount of nonexchangeable Cr(VI) via reduction to Cr(III). Also, the authors examined the reduction of adsorbed Cr(VI) in the presence of gallic acid. In several of the soils, the adsorbed Cr(VI) was reduced to Cr(III) while in others little or none was reduced. The authors concluded that, in soils containing high levels of amorphous minerals and organic matter, the Cr(VI) is held in such a way that the gallic acid could not react with it.

In summary, chromium is a dynamic element in soil systems. Its mobility and toxicity will be affected by a number of factors including pH, presence of inorganic and organic complexing agents, presence of Mn-oxides, and redox state of the soil. It has been observed that Cr(III) oxidation will take place in many different soils under a wide range of factors. The sorption mechanism of Cr(VI) has been postulated through macroscopic techniques and is still the subject of debate. A thorough and complete understanding of the sorption mechanism of Cr(VI) will enable us to model and to predict its mobility. This will help to avoid potential toxicity problems in systems where it is present in high concentrations.

4.1.3 Objectives

The objective of this study is to examine the sorption behavior of chromate and arsenate (oxyanions) on goethite (α-FeOOH) using a pressure-jump relaxation technique. Goethite was chosen because high concentrations of Fe present in the lunar regolith make it a likely weathering product. Chromate was selected as the form of Cr because the presence of Mn-oxides in the lunar regolith may be involved in the oxidation of Cr released during weathering. Since Cr(VI) is the more mobile and toxic form of chromium, it is important to understand its sorption mechanisms on secondary weathering products. Arsenate sorption was evaluated in

comparison to chromate because of differences in the arsenate molecule which may affect its sorption behavior and the mechanism of retention.

4.2 Materials and Methods

4.2.1 Sample Preparation

The samples used for the p-jump kinetic studies were obtained from the same lot as those used for equilibrium adsorption studies. Sample preparation involved equilibrating a given concentration of the adsorptive (the ion in solution that has the potential of being adsorbed) with a specific quantity of the adsorbent (solid surface on which adsorption occurs) at a given pH. The adsorptives were the oxyanions chromate (Cr(VI)) and arsenate (As(V)). The adsorbent for both of these studies was goethite. In the first study 1mM chromate, as sodium chromate, was equilibrated with a 10 gL^{-1} suspension of goethite in the presence of 0.001, 0,01, and 0.1 M $NaNO_3$, added as a background electrolyte. In the second study, 1mM arsenate, as sodium arsenate was equilibrated with the same quantity of goethite and with 0.01 and 0.1 M $NaNO_3$. All reactants were prepared using American Chemical Society reagent grade chemicals.

The goethite was synthesized in our laboratory from reagent grade $Fe(NO_3)_3$ using the method described in Schwertmann and Cornell (1991). Excess salts were washed from the goethite precipitate by electrodialysis until the conductivity of the wash solution was equal to that of distilled-deionized water (~14 days). The clean goethite precipitate was then freeze-dried and stored under desiccation. It was characterized by X-ray diffraction analysis and transmission electron (Fig 4.1 and 4.2) microscopy to ensure the goethite's purity. The XRD spectra and TEM micrographs were consistent with those from goethite presented in

Figure 4.1 TEM image of goethite used for the p-jump study. Note the uniformity of the crystals.

Figure 4.2 High resolution TEM image of goethite used for the p-jump study.

Samples were prepared in a flat-bottomed water-jacketed reaction vessel (400 mL) covered with a removable Plexiglas lid containing entry ports for a stirrer, a pH electrode, N_2 gas, and burette tip (Fig 4.3). The goethite suspensions together with the adsorptive and background electrolyte were mixed with an overhead driven polyethylene propeller stirrer spinning at about 5.0 revolutions s^{-1} at a constant temperature of 298 ± 0.1 K. After the desired pH was reached, by dropwise addition of either 0.2 M HNO_3 or NaOH, 20 mL of the suspension was removed and transferred to 50 mL polypropylene centrifuge tubes which were placed on a reciprocating shaker (180 cycles min^{-1}) for 24 hours. Subsequently, the pH of the sample was checked for any drift and, if necessary, pH was readjusted to the desired value. Half of the sample (10 mL) was then set aside to be used for p-jump experiments. The remaining 10 mL were centrifuged at 20,000g, the supernatant filtered through 0.2 micron filters and analyzed for Cr or As by inductively coupled plasma spectrometry.

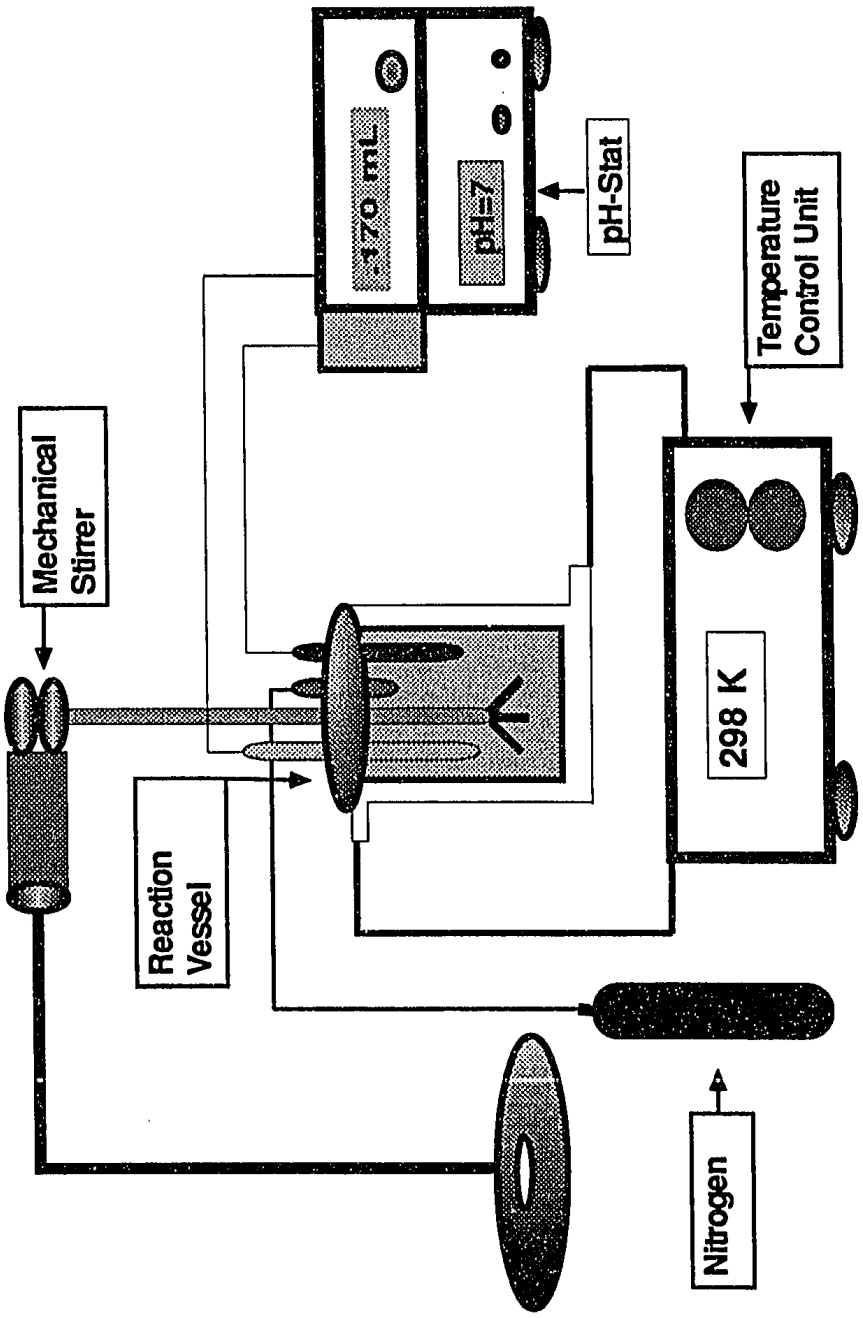

Figure 4.3 Schemetic diagram of the batch reaction vessel.

4.2.2 P-jump Instrument

The p-jump instrument used for our studies was manufactured by the DIA-LOG Company located in Duesseldorf, Germany. It is similar in design to the apparatus described in detail by Knoche (1975, 1986). To conduct a p-jump experiment it was necessary that during the course of an experiment (~ 1 hour) particle settling was kept to a minimum. Consequently, sample suspensions were sonified at least one hour prior to data collection. In fact, the greatest limitation of using the p-jump technique for oxyanion sorption investigations is that it is restricted to the use of very pure, high surface area materials.

Typically, a p-jump experiment was performed by filling a sample electrode cell with the suspension equilibrated with the adsorptive at a selected pH. For the Cr(VI) studies, p-jump experiments were run in the pH range 5.5 to 6.5. For the arsenate investigations, the pH range for the kinetic experiments was from 6.5 to 8.0. The filtered supernatant of the equilibrated suspensions was then added to the reference electrode cell. These cells have small electrodes built into their inner wall that monitor the conductivity changes occurring during the course of a relaxation experiment. Each of these cells has a capacity of about 1mL. The filled cells were then covered with a thin Teflon membrane and tightly sealed. The cells were inserted into the pressure autoclave which comprises one part of the whole pressure-jump apparatus, the other part being a system for conductivity detection (Fig. 4.4). The Teflon membrane cover constitutes a portion of the inner wall of the pressure chamber. The chamber is sealed with a thin strip of brass foil that is specifically milled to burst once the pressure within the chamber reaches approximately 13.5 MPa.

Pressure was applied to the autoclave by forcing water into the chamber with a hand operated mechanical pump. Pressure changes were transmitted to the sample suspension and reference solutions via the Teflon membrane.

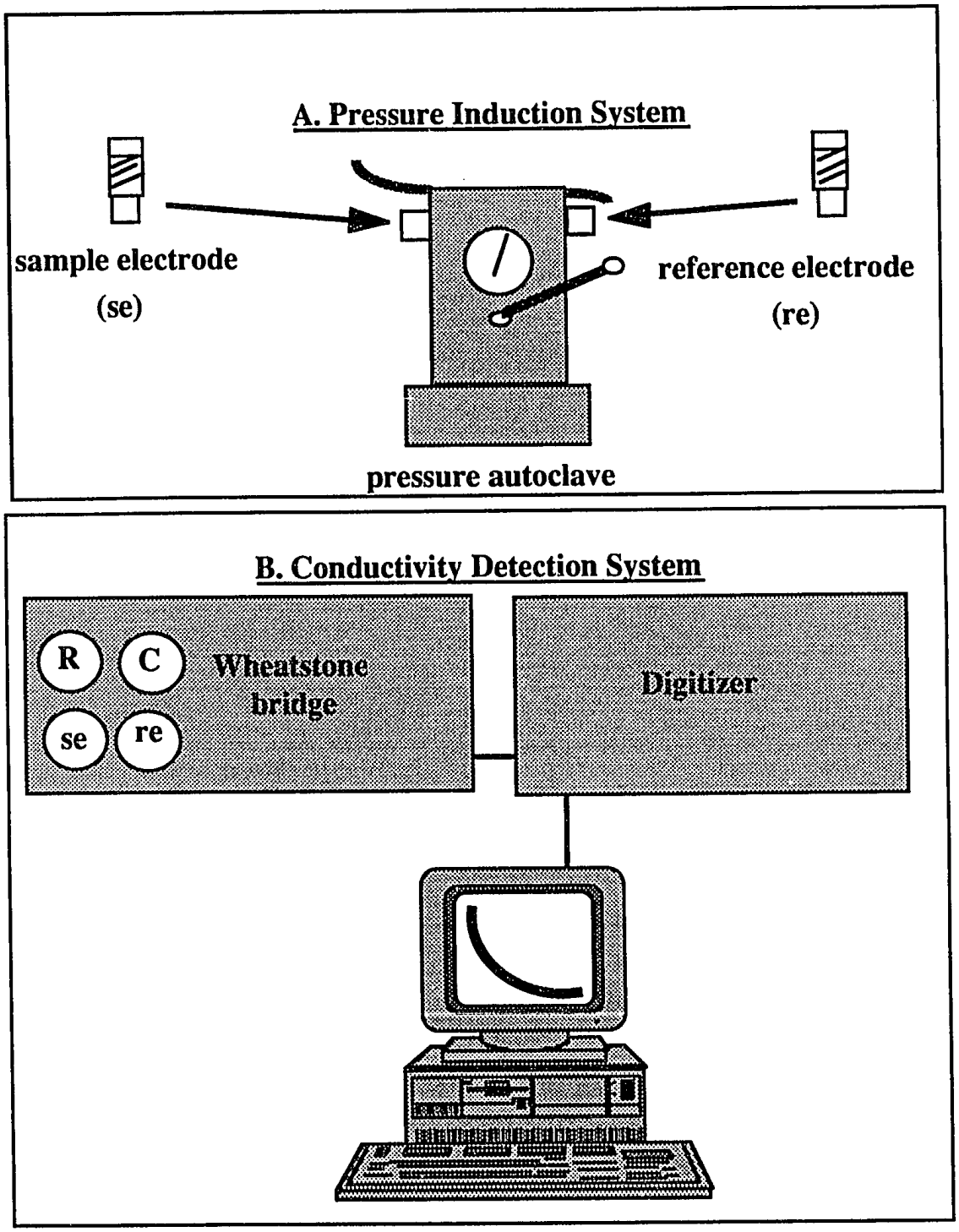

Figure 4.4 Schematic of the pressure-jump apparatus. The letters R and C represent variable resistors and capacitors, respectively.

The pressure perturbation is attained by increasing the pressure until the brass foil bursts and the pressure instantaneously (~ 60 ms) drops to ambient conditions. The sample equilibrated at the higher pressure (13.5 MPa) must now relax to the new equilibrium established at ambient pressure. The relaxation information is monitored by the conductivity detection system (Fig 4.4), which is comprised of a wheatstone bridge, a digitizer, oscilloscope, and a personal computer containing a data evaluation software program. The sample and reference electrode cells are linked to and comprise two arms of the wheatstone bridge. The other two arms are made up of variable resistors and capacitors which are adjusted to balance the bridge using the oscilloscope as a viewing screen. The bridge is balanced at ambient conditions and becomes unbalanced upon pressurization. Thus, after the brass foil ruptures, a piezoelectric capacitor triggers collection of the relaxation event which is recorded as the voltage change associated with the bridge returning to the balanced state. This information is then digitized and relayed to a microcomputer, where the relaxation curve is immediately displayed on the computer monitor. The information is plotted as the relative amplitude of the relaxation as a function of time in seconds.

The computer contains a software program provided by the manufacturer that allows for quick and direct computation of relaxation time constants or τ (tau). Tau is defined as the time it takes the relaxation to reach 1/e of the initial amplitude. The data evaluation program calculates τ by fitting and comparing the experimentally derived relaxation curve to a series of polynomial equations.

To ensure that the signals we were evaluating were only due to ion adsorption/desorption reactions, we also conducted p-jump experiments under

identical conditions, however, in the absence of either chromate or arsenate on goethite. When these were omitted no interfering relaxation signals were observed.

4.2.3 Surface Complexation Modeling

The constant capacitance model (CCM) (Stumm, 1980) was used to simulate the adsorption of chromate and arsenate on goethite. This model assumes that reacting ions are specifically adsorbed forming inner-sphere surface complexes and that background electrolyte ions do not interact with the surface forming complexes. The model also assumes that the net surface charge is a linear function of the surface potential represented by the following equation:

$$\sigma = (CSa / F)\psi \tag{4.2}$$

where σ is the surface charge ($mol_c\ L^{-1}$), C is the capacitance density ($F\ m^{-2}$), S is the specific surface area ($m^2\ kg^{-1}$), a is the suspension density of the solid ($kg\ L^{-1}$) , F is the Faraday constant (9.65×10^{-4} coulombs mol^{-1}), and ψ is the surface potential (volts). We used the CCM to predict the adsorption of chromate and arsenate on goethite as both mono- and bidentate surface species. The following surface reactions were considered by the CCM to calculate arsenate and chromate adsorption on goethite:

Surface hydrolysis reactions:

$$XOH + H^+ = XOH_2^+ \tag{4.3}$$

$$XOH = XO^- + H^+ \tag{4.4}$$

Formation of monodentate arsenate/goethite surface complexes:

$$XOH + H_3AsO_4 = XH_2AsO_4 + H_2O \quad (4.5)$$

$$XOH + H_3AsO_4 = XHAsO_4^- + H_2O + H^+ \quad (4.6)$$

$$XOH + H_3AsO_4 = XAsO_4^{2-} + H_2O + 2H^+ \quad (4.7)$$

Formation of monodentate chromate/goethite surface complexes:

$$XOH + H_2CrO_4 = XHCrO_4 + H_2O \quad (4.8)$$

$$XOH + H_2CrO_4 = XCrO_4^- + H_2O + H^+ \quad (4.9)$$

Formation of bidentate arsenate/goethite surface complex:

$$2XOH + H_3AsO_4 = X_2HAsO_4(s) + 2H_2O \quad (4.10)$$

$$2XOH + H_3AsO_4 = X_2AsO_4^-(s) + 2H_2O + H^+ \quad (4.11)$$

Formation of bidentate chromate/goethite surface complex:

$$2XOH + H_2CrO_4 = X_2(CrO_4)^o + 2H_2O \quad (4.12)$$

where XOH is a neutral site , XOH_2^+ is the protonated site, and XO^- is the deprotonated site on the goethite surface. The intrinsic conditional equilibrium constants, which estimate surface charge produced by Eqs. 4.3-4.12, are represented by Eqs 4.13-4.22:

Surface hydrolysis reactions:

$$K_{a1}(\text{int}) = \frac{[XOH_2^+]}{[XOH][H^+]}\exp(\frac{F\psi}{RT}) \tag{4.13}$$

$$K_{a2}(\text{int}) = \frac{[XO^-][H^+]}{[XOH]}\exp(-\frac{F\psi}{RT}) \tag{4.14}$$

Formation of monodentate arsenate/goethite surface complexes:

$$K_{As}^1(\text{int}) = \frac{[XH_2AsO_4]}{[XOH][H_3AsO_4]} \tag{4.15}$$

$$K_{As}^2(\text{int}) = \frac{[XHAsO_4^-][H^+]}{[XOH][H_3AsO_4]}\exp(-\frac{F\psi}{RT}) \tag{4.16}$$

$$K_{As}^3(\text{int}) = \frac{[XAsO_4^{2-}][H^+]^2}{[XOH][H_3AsO_4]}\exp(-\frac{2F\psi}{RT}) \tag{4.17}$$

Formation of monodentate chromate/goethite surface complexes:

$$K_{Cr}^1(\text{int}) = \frac{[XHCrO_4]}{[XOH][H_2CrO4]} \tag{4.18}$$

$$K_{Cr}^2(\text{int}) = \frac{[XCrO_4^-][H^+]}{[XOH][H_2CrO_4]}\exp(-\frac{F\psi}{RT}) \tag{4.19}$$

Formation of bidentate arsenate/goethite surface complex:

$$K^4_{As}(\text{int}) = \frac{[X_2HAsO_4]}{[XOH]^2[H_3AsO_4]} \tag{4.20}$$

$$K^5_{As}(\text{int}) = \frac{[X_2AsO_4^-][H^+]}{[XOH]^2[H_3AsO_4]} \exp(\frac{-F\psi_o}{RT}) \tag{4.21}$$

Formation of bidentate chromate/goethite surface complex:

$$K^3_{Cr}(\text{int}) = \frac{[X_2(CrO_4)^o]}{[XOH]^2[H_2CrO_4]} \tag{4.22}$$

The capacitance density value used in the CCM calculations was fixed at 1.06 F m^{-2} and the surface site density was 2.3 sites nm^{-2}, which was determined from chromate and arsenate adsorption isotherms. The chromate and arsenate isotherms were conducted at initial concentrations of 0.25 to 3.0 mM and pH values of 6.0 and 6.8 (arsenate only). The intrinsic surface acidity constants were $10^{7.31}$ and $10^{-8.80}$ for K_{a1} and K_{a2}, respectively (Goldberg, 1986). The least square optimization program, FITEQL Version 3.1 (Herbelin and Westall, 1994), was used to fit intrinsic surface complexation constants (Eqs. 4.15-4.22) to the experimental equilibrium adsorption data and to compute the concentrations of surface complexes. The intrinsic conditional equilibrium constants calculated for the surface reactions above are listed in Table 4.1:

Table 4.1 Intrinsic equilibrium constants calculated for Eqs (4.15)-(4.22) using FITEQL.

K_{As}^1(int)	10^{10}
K_{As}^2(int)	$10^{5.1}$
K_{As}^3(int)	$10^{0.55}$
K_{As}^4(int)	10^{17}
K_{As}^5(int)	$10^{11.4}$
K_{Cr}^1(int)	$10^{9.8}$
K_{Cr}^2(int)	$10^{4.2}$
K_{Cr}^3(int)	$10^{15.3}$

The hydrolysis reactions for arsenate and chromate along with the corresponding hydrolysis constants (K_h) are presented below:

	K_h	
$H_3AsO_4 = H_2AsO_4^- + H^+$	$10^{-2.24}$	(4.23)
$H_2AsO_4^- = HAsO_4^{2-} + H^+$	$10^{-6.94}$	(4.24)
$HAsO_4^{2-} = AsO_4^{3-} + H^+$	$10^{-11.50}$	(4.25)
$H_2CrO_4 = HCrO_4^- + H^+$	$10^{0.20}$	(4.26)
$HCrO_4^- = CrO_4^{2-} + H^+$	$10^{-6.51}$	(4.27)

4.3 Results and Discussion

4.3.1 Equilibrium Adsorption Study

The quantity of chromate and arsenate adsorbed on goethite is shown in Fig. 4.5. The adsorption envelope for arsenate was much broader than that for chromate. The differences in adsorption edges between oxyanions can be related to the degree of protonation of the molecule. Arsenate is a triprotic acid while chromate is a diprotic acid. Triprotic acids will exhibit a much broader adsorption edge over a wide pH range than a diprotic acid, which displays a steeper adsorption edge. This is because the adsorption of weak acids is strongest at pH values near their acid dissociation constants (Hingston et. al., 1971). These results are consistent with other equilibrium studies investigating oxyanion adsorption on goethite (Hingston et al., 1971; Goldberg, 1986). There was no difference between adsorption edges for both chromate and arsenate measured at different background electrolyte concentrations (Fig. 4.5). This suggests that both oxyanions form inner-sphere surface complexes with goethite. Recent X-ray absorption fine structure (XAFS) spectroscopic studies (Hayes, 1987; Waychunas et al., 1993; Fendorf et al., 1993) indicate that oxyanions predominately from inner-sphere bidentate surface complexes with goethite. Hence, we used the CCM to simulate chromate and arsenate adsorption as an inner-sphere bidentate surface complex. Overall, the simulations fit the experimental data well (Figs. 4.6 and 4.7).

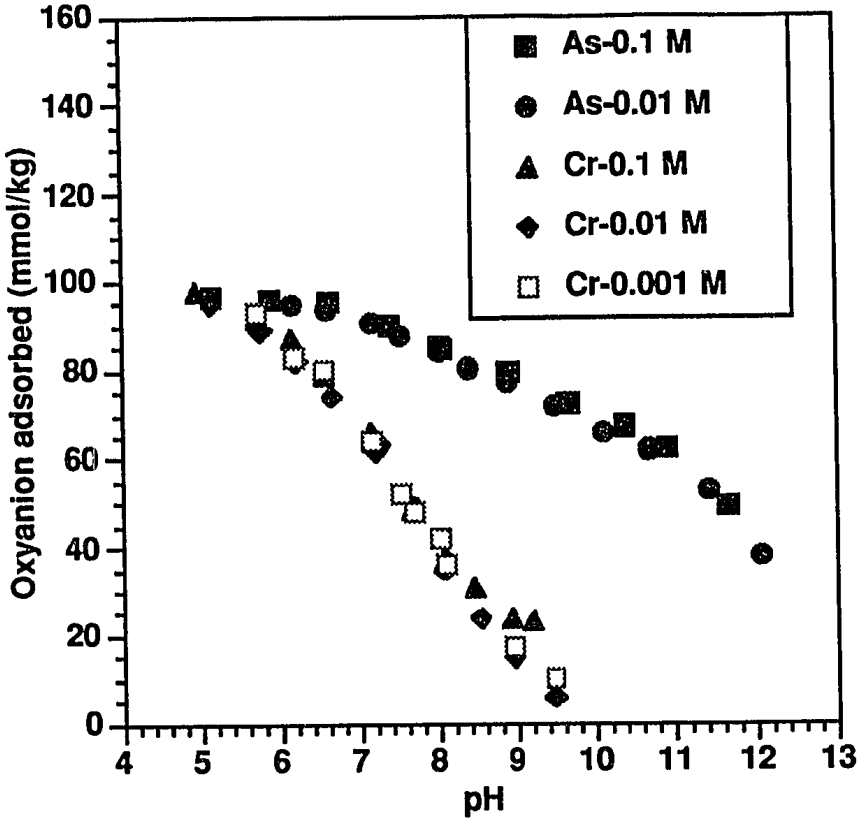

Figure 4.5 **Experimental equilibrium adsorption data for arsenate and chromate on goethite as a function of pH and ionic strength.**

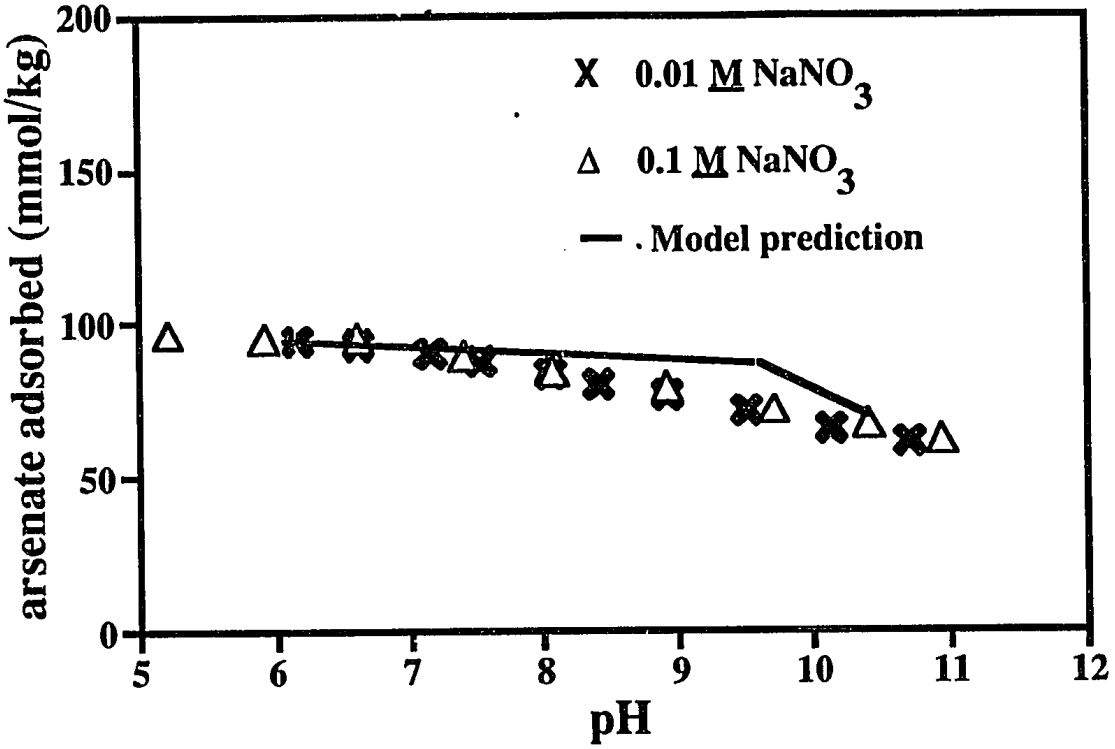

Figure 4.6 Equilibrium adsorption data for arsenate adsorption on goethite versus pH.

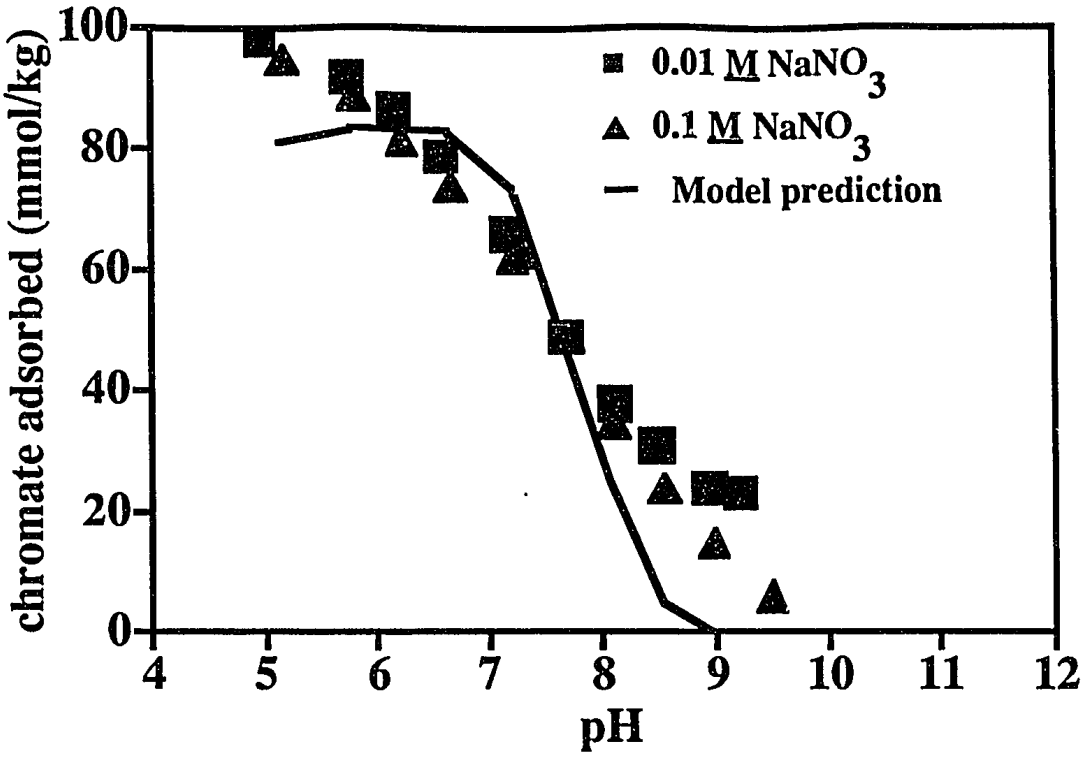

Figure 4.7 **Equilibrium adsorption data for chromate adsorption on goethite versus pH.**

4.3.2 Kinetic Study

The pressure-jump technique was used to (i) confirm the adsorption mechanism proposed from the equilibrium studies and (ii) to provide rate constants for both adsorption and desorption reactions. Pressure-jump relaxation experiments were evaluated for chromate and arsenate over the pH range 5.5 to 6.5 and 6.5 to 7.5, respectively. Additionally, p-jump experiments were conducted for chromate at initial chromate concentrations ranging from 0.5 to 2 mmol L^{-1} at a constant pH of 6. In these pH and concentration ranges we were able to confidently associate the relaxation

signals with oxyanion adsorption/desorption. A double relaxation event was observed for both chromate and arsenate adsorption/desorption on goethite (Figs. 4.8 - 4.10). For the pH experiments with both oxyanions, the slow τ values remained constant at about 50 ms. However, for chromate and arsenate the faster τ values increased from about 2.5 to 10 ms and 10 to 20 ms with increasing pH, respectively. The differences in the fast τ values between the two oxyanions can be readily observed from the plot of τ^{-1} vs. pH shown in Figures 4.8 and 4.9. A similar trend in fast and slow τ values was observed for the concentration experiment with chromate (Fig. 4.10).

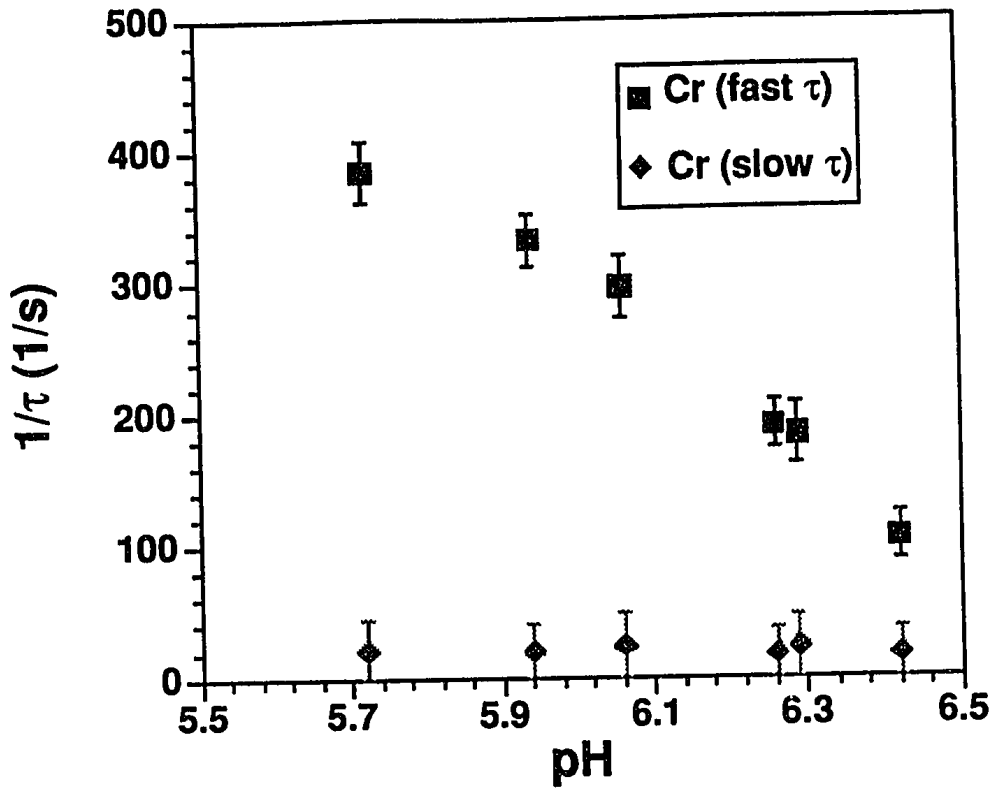

Figure 4.8 τ^{-1} values determined from p-jump experiments for chromate adsorption/desorption on goethite, as a function of pH.

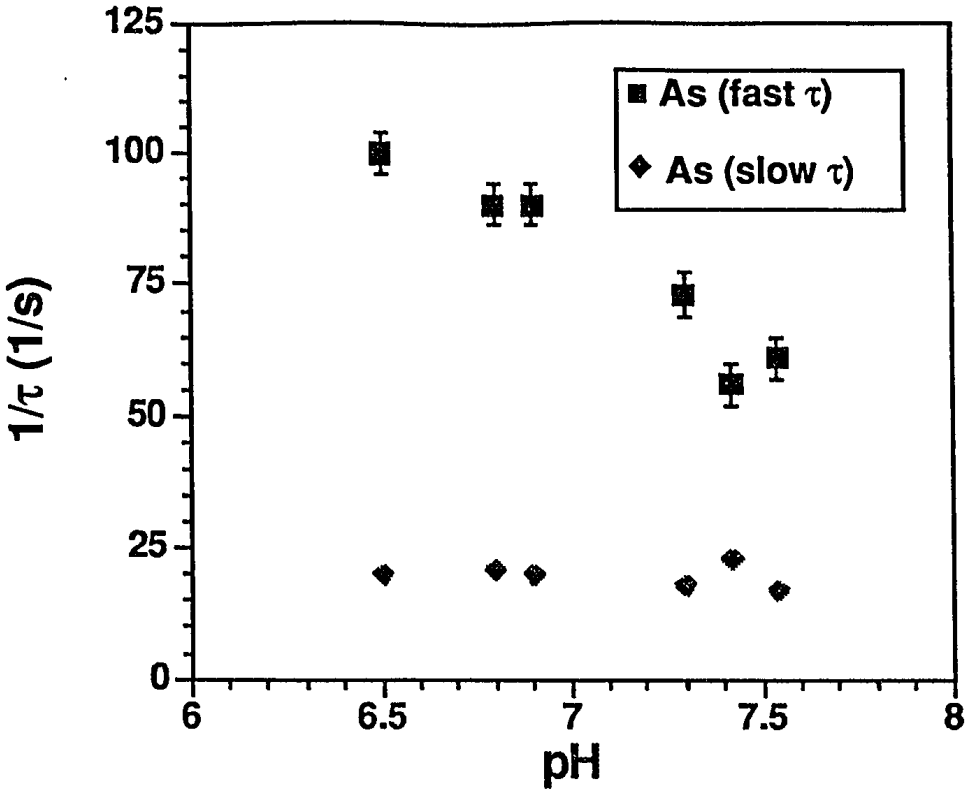

Figure 4.9 τ^{-1} values determined from p-jump experiments for arsenate adsorption/desorption on goethite, as a function of pH.

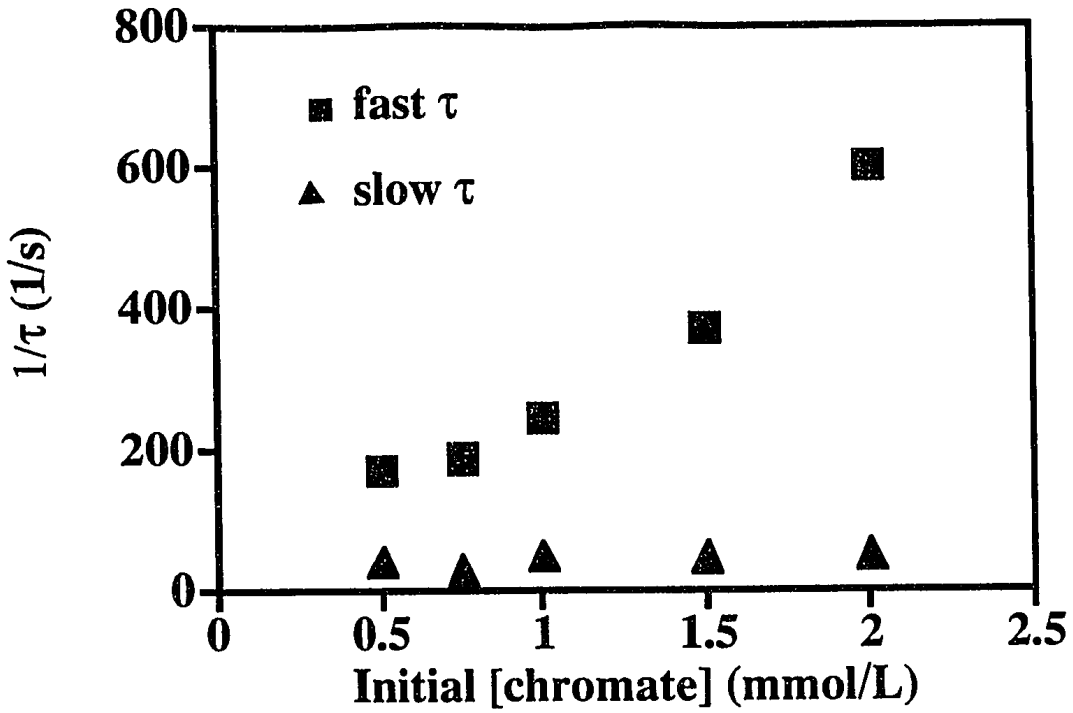

Figure 4.10 τ^{-1} **values determined from p-jump experiments for chromate adsorption/desorption on goethite, as function of initial chromate concentration.**

We propose that the mechanism for oxyanion adsorption on goethite is a two step process resulting in the formation of an inner-sphere bidentate surface complex (Fig. 4.11). The first step involves an initial ligand exchange reaction of the aqueous oxyanion ($HCrO_4^-$ or $H_2AsO_4^-$) with goethite, forming an inner-sphere monodentate surface complex. This first step produces the signals associated with the fast τ values. The next step involves a second ligand exchange reaction, resulting in the formation of an inner-sphere bidentate surface complex. This step produces the signal associated with the slow τ values.

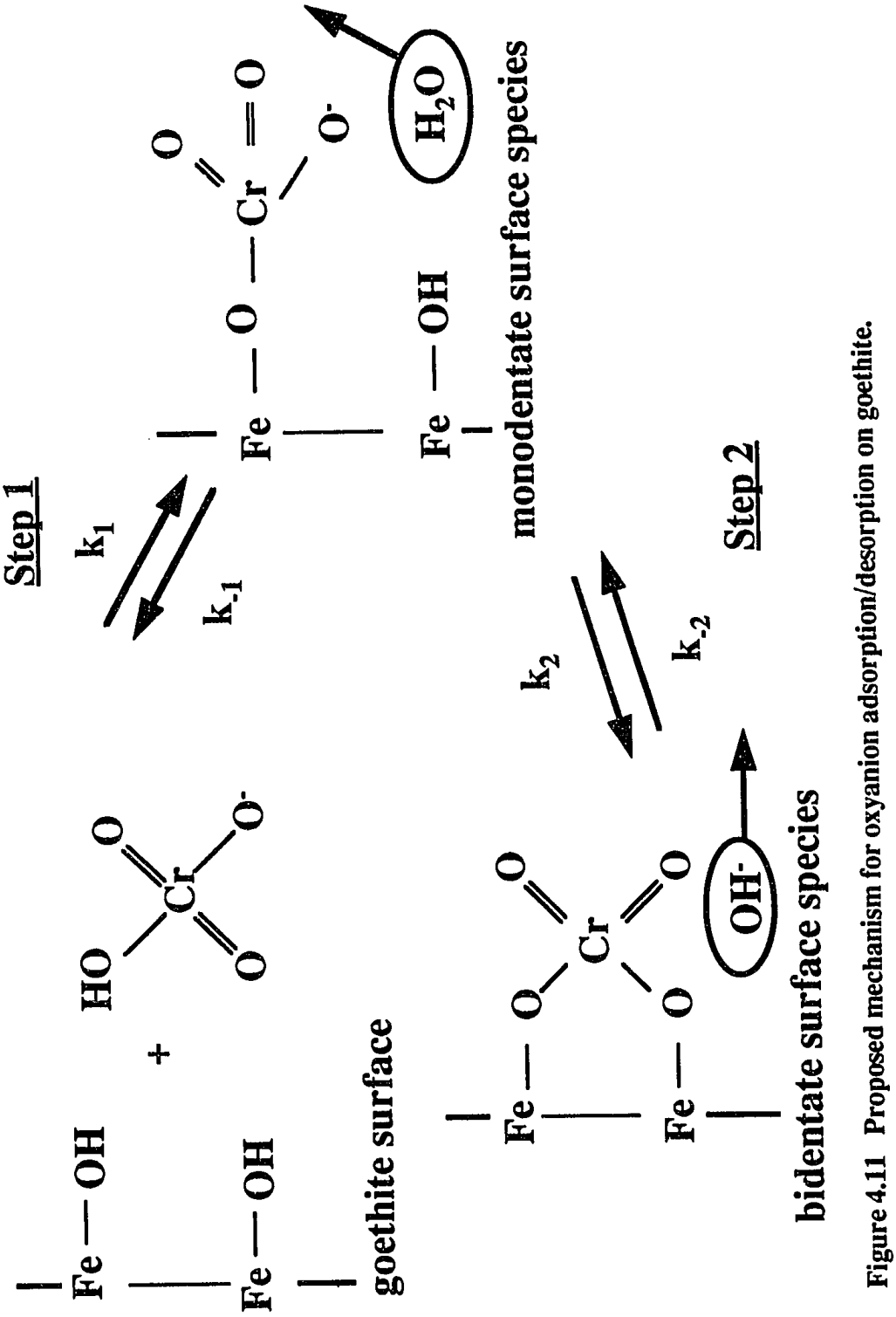

Figure 4.11 Proposed mechanism for oxyanion adsorption/desorption on goethite.

To determine if the mechanism displayed in Figure 4.11 was plausible and consistent with our kinetic data, the following linearized rate equations relating τ^{-1} values to the concentrations of reactive species were used:

$$\tau_{fast}^{-1} + \tau_{slow}^{-1} = k_1([XOH] + [\text{ion species}]) + k_{-1} + k_2 + k_{-2} \tag{4.28}$$

$$\tau_{fast}^{-1} \cdot \tau_{slow}^{-1} = k_1[k_2 + k_{-2}]\{[XOH] + [\text{ion species}]\} + k_{-1}k_{-2} \tag{4.29}$$

where the ion species is $HCrO_4^-$ or $H_2AsO_4^-$. The derivation of these equations was obtained from Bernasconi (1976) and is based on the two-step reaction system (A + B $\leftrightarrow$ C $\leftrightarrow$ D). If the mechanism portrayed in Figure 4.11 is accurate than a plot of $\tau_f^{-1} + \tau_s^{-1}$ and $\tau_f^{-1} \cdot \tau_s^{-1}$ as a function of the concentration term ([XOH] + [ion species]) should be linear. Plots of Eqs. 4.28 and 4.29 were linear suggesting that the proposed mechanism was plausible (Figs. 4.12 - 4.15).

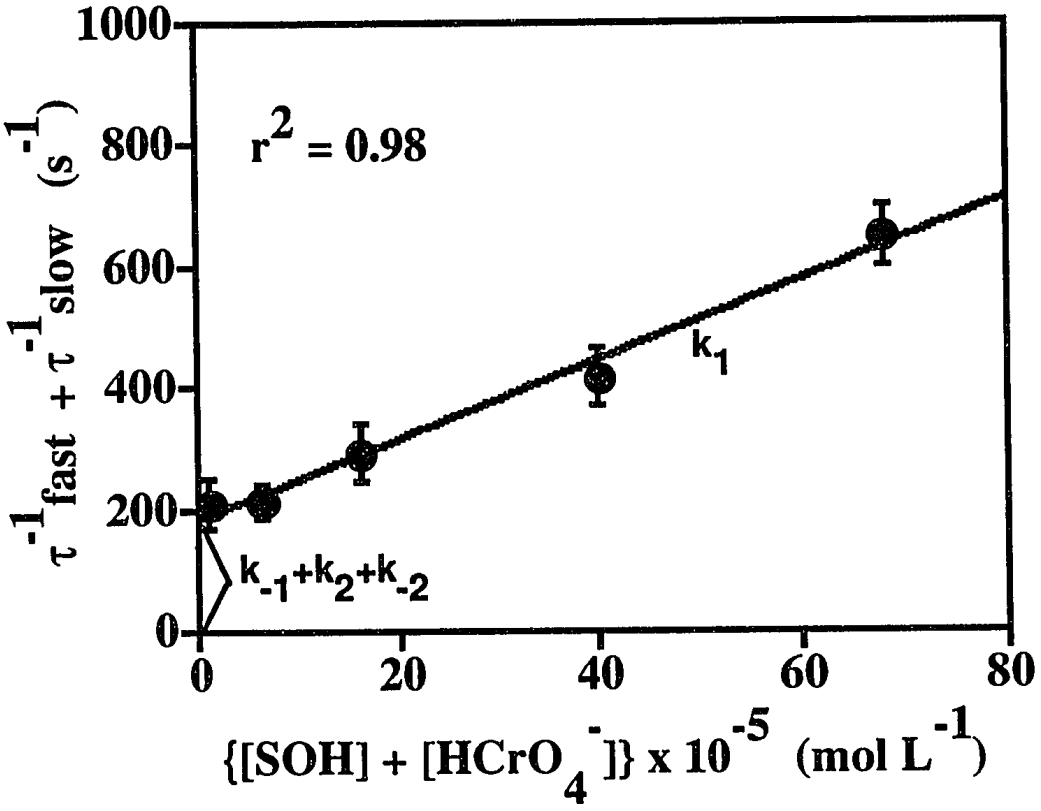

Figure 4.12 Evaluation of linearized rate equations (Eqs. 4.28 and 4.29) for the mechanism displayed in Fig. 4.11 for chromate.

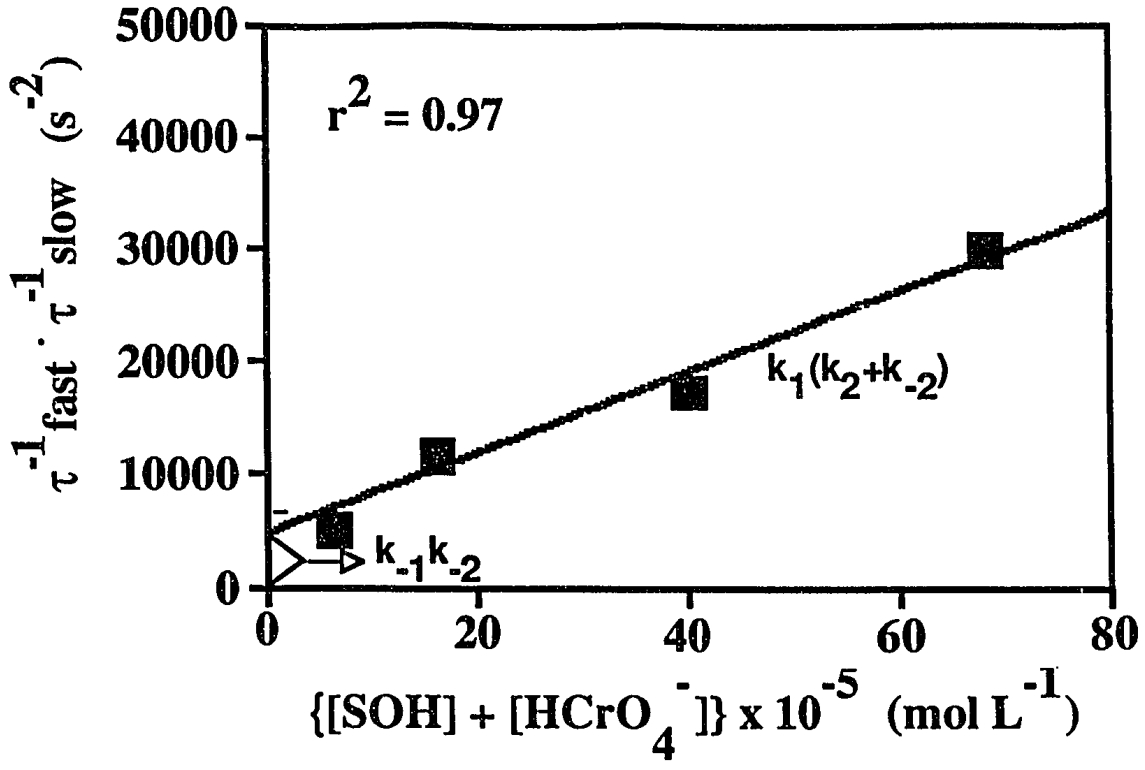

Figure 4.13 Evaluation of linearized rate equations (Eqs. 4.28 and 4.29) for the mechanism displayed in Fig. 4.11 for chromate.

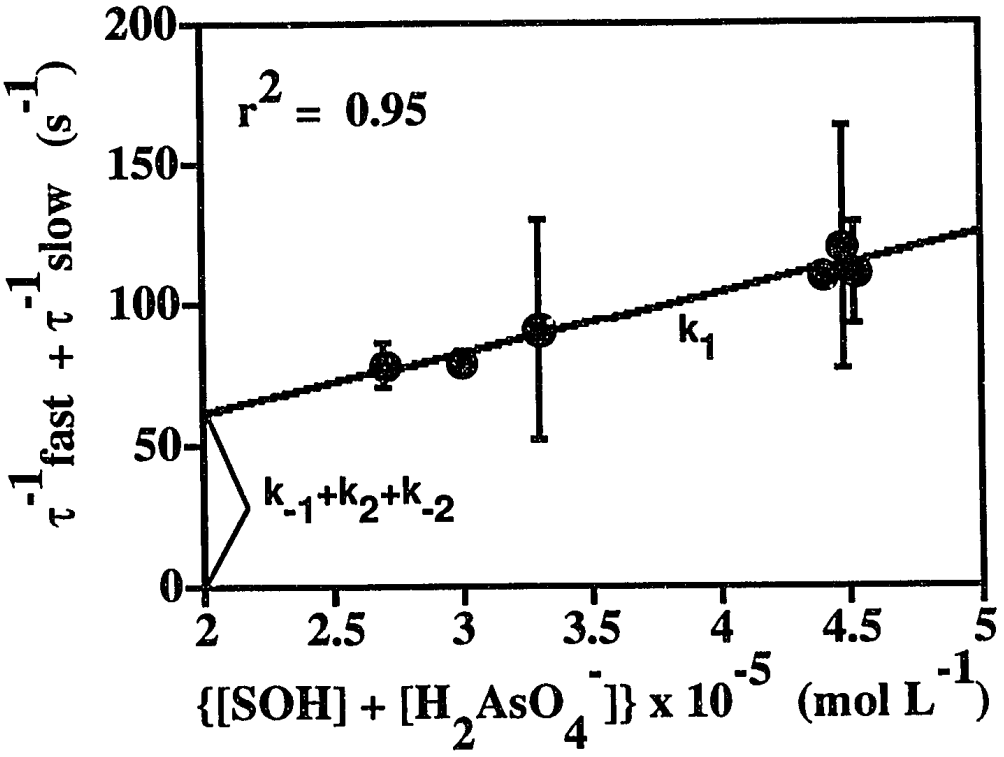

Figure 4.14 Evaluation of linearized rate equations (Eqs. 4.28 and 4.29) for the mechanism displayed in Fig. 4.11 for arsenate.

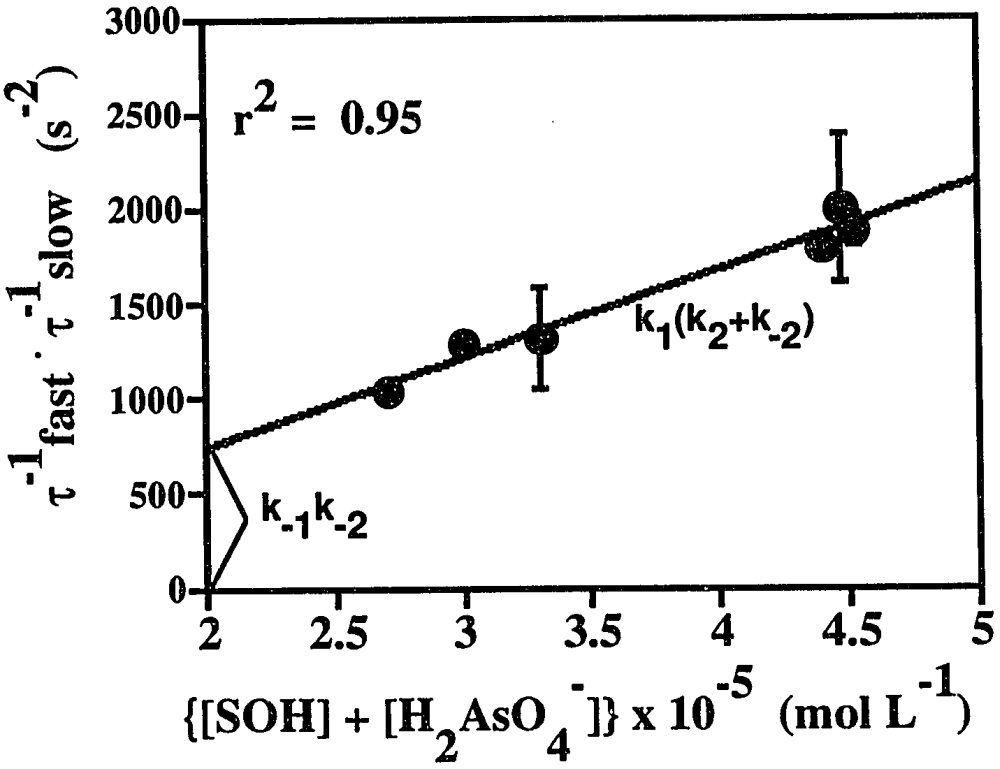

Figure 4.15 Evaluation of linearized rate equations (Eqs. 4.28 and 4.29) for the mechanism displayed in Fig. 4.11 for arsenate.

From these plots, the forward and reverse rate constants were obtained for the adsorption and desorption reactions of both the mono- and bidentate steps. Where k_1 = slope (Fig. 4.12 or 4.14), k_{-1} = intercept (Fig. 4.12 or 4.14) - slope (Fig. 4.13 or 4.15)/slope (Fig. 4.12 or 4.14), k_2 = intercept (Fig. 4.13 or 4.15) - k_{-1} - k_{-2}, and k_{-2} = intercept (Fig. 4.13 or 4.15)/k_{-1} (Bernasconi, 1976). The calculated rate constants for both chromate and arsenate adsorption/desorption on goethite are listed in Table 4.2.

Table 4.2 Calculated rate constants for chromate and arsenate adsorption/desorption on goethite.

	STEP I	STEP II
Arsenate	$k_1=10^{6.3}$ L/mol s $k_{-1}=8$ s^{-1} $K_{eq}=10^{5.35}$ L/mol s^2	$k_1=15$ s^{-1} $k_{-1}=8$ s^{-1} $K_{eq}=10^{0.26}$
Chromate	$k_1=10^{5.8}$ L/mol s $k_{-1}=129$ s^{-1} $K_{eq}=10^{3.7}$ L/mol s^2	$k_1=16$ s^{-1} $k_{-1}=38$ s^{-1} $K_{eq}=10^{-0.4}$

For both oxyanions, the rate constants for the reverse reactions (associated with the breaking of arsenate/goethite bonds) were slower than the rate constants for the forward reactions and therefore the rate limiting steps. The equilibrium constants listed in Table 4.2 were calculated using the rate constants for each reaction step in our proposed mechanism from the following relationship:

$$K_{eq}=k_{forward}/k_{reverse} \qquad (4.30)$$

The calculated equilibrium constants for steps 1 and 2 for chromate and arsenate were $10^{3.7}$,$10^{-0.4}$ and $10^{5.35}$,$10^{0.26}$, respectively. Hence, the adsorption of both oxyanions and subsequent formation of inner-sphere bidentate surface complexes are thermodynamically favorable. However, the step 2 equilibrium constant for chromate adsorption was only slightly greater than 1 which indicates that the formation of a bidentate surface complex, although thermodynamically favorable, may be less likely to form than a monodentate surface complex. This is in agreement with spectroscopic data (XAFS) which show a mixture of both mono- and bidentate surface complexes (Chapter 5).

The kinetically determined equilibrium constants for the overall formation of the bidentate oxyanion/goethite surface complexes $\{K_{eq(step\ 1)} \times K_{eq(step\ 2)}\}$ were much smaller than those calculated using the CCM (Table 4.2). Yet, the kinetically determined value for the formation of the monodentate surface complexes (step 1) were consistent with K_{int} values for the same reaction calculated with the CCM (Goldberg (1986) and Table 4.3). This suggests that the mechanism proposed for step 1 is valid. However, step 2 may involve more elementary reactions than are illustrated in Figure 4.11, which may increase the overall equilibrium constant. This is a reasonable assumption, since the p-jump apparatus can monitor only reactions that generate measurable changes in conductivity. If step 2 involves other elementary surface reactions not detected using p-jump, our proposed mechanism (Fig. 4.11) may not be complete. The development of sophisticated new spectroscopic and microscopic surface probes may resolve this issue. Nonetheless, based on our kinetic and equilibrium adsorption studies and on spectroscopic evidence (Waychunas et al., 1993; Fendorf et al., 1993), arsenate appears to form an inner-sphere bidentate surface

complex with goethite while chromate forms a combination of mono- and bidentate surface complexes with goethite.

Table 4.3 Equilibrium constants determined kinetically and using the Constant Capacitance Model (CCM)

	K_{step1}	K_{step2}	$K_{step1 \times step2}$
Chromate	$10^{3.7}$	$10^{-0.4}$	$10^{3.3}$
Chromate (CCM)	$10^{4.0}$	------	$10^{15.1}$
Arsenate	$10^{5.35}$	$10^{0.26}$	$10^{5.57}$
Arsenate (CCM)	$10^{7.2}$	------	$10^{19.2}$

4.3.3 Molecular Orbital Considerations

Molecular orbital (MO) theory has been used extensively in chemistry for predicting the nature of bonding and structures of molecules of both transition and non-transition-element compounds. Lewis octet theory and the valence-shell electron pair repulsion theory (VSEPR) have also been used for predicting bonding and structures of molecules. However, these theories have profound limitations and often fail when applied to transition metal compounds. Unlike VSEPR and Lewis octet theory, MO theory provides explanations of bonding mechanisms in transition metal complexes and has recently been used for describing redox reactions on mineral surfaces (Xyla et al., 1992; Fendorf et al., 1992). Molecular orbital theory is capable of predicting a wide range of chemical phenomena and is a powerful tool for scientists in surface and geochemistry.

The goethite surface consists of iron atoms bonded to oxygen atoms that exhibit varying degrees of protonation, depending upon the pH of the aqueous environment. In the proposed mechanism for the specific adsorption of arsenate and

chromate, a water or hydroxyl molecule is removed from the goethite surface during adsorption. The release of this molecule removes two electrons from an e_g orbital (HOMO) of the sp^3d^2 hybrid orbitals of the iron. This reaction creates an empty orbital (LUMO) available for bonding. The oxygen atoms of the oxyanions contain extra lone pairs of valence electrons which are also available for bonding. Upon specific adsorption a sigma bond is formed between a lone pair of electrons of the oxygen and the empty e_g orbital of the iron, creating a monodentate surface complex. Further bonding can take place between another oxygen of the oxyanion and an iron atom of the goethite, forming a bidentate surface complex. These simple substitution reactions are symmetry and energy allowed and are predicted to occur using MO theory. Therefore, based on molecular orbital theory chromate and arsenate would bind specifically as either mono- or bidentate surface complexes. This is in agreement with our proposed mechanism and the results from EXAFS analysis (Chapter 5).

4.4 Conclusions

Our results suggest that both chromate and arsenate are specifically adsorbed on goethite. Both oxyanions can form inner-sphere bidentate surface complexes with goethite. However, kinetically determined equilibrium constants suggested that chromate can form a mixture of mono- and bidentate surface complexes. This may depend on surface coverages and the type of mineral surface and is in agreement with spectroscopic data (XAFS) discussed in Chapter 5. In contrast, kinetic and spectroscopic data indicate that arsenate forms predominately bidentate surface complexes (Waychunas et al., 1993; Fendorf et al., 1993). The above results would suggest that chromate would be the more mobile of the two oxyanions in soil systems. This is in agreement with results of Zachara et al. (1988)

and Stollenwerk and Grove (1985) who found chromate to be fairly mobile in soil environments. The ability of these oxyanions to form mono- vs. bidentate surface complexes may be related to the charge of the anion. The arsenate anion (AsO_4^{-3}) has a net charge of -3 while the chromate anion (CrO_4^{-2}) has a net charge of -2. Therefore, based on electrostatics arsenate would have a greater affinity for the goethite surface and may more readily form bidentate surface complexes, which would make it less mobile in soil environments compared to chromate.

4.5 References

Ainsworth, C.C., D.C. Girvin, J.M. Zachara, and S.C. Smith. 1989. Chromate adsorption on geothite: effects of aluminum substitution. 53:411-419.

Amacher, M.C. 1991. Methods of obtaining and analyzing kinetic data. pp. 19-59. In D.L Sparks and D.L. Suarez (eds.) Rates of Soil Chemical Processes. SSSA Spec. Publ. 27, Soil Science Society of America, Madison, Wisconsin.

Ashida, M., M. Sasaki, H. Kan, T. Yasunaga, K. Hachiya, and T. Inoue. 1978. Kinetics of proton adsorption-desorption at TiO_2-H_2O interface by means of the pressure-jump technique. J. Colloid Interface Sci. 71:219-225.

Astumian, R. D., M. Sasaki, T. Yasunaga, and Z. A. Schelly. 1981. Proton adsorption-desorption kinetics on iron oxides in aqueous suspensions using the pressure-jump method. J. Phys. Chem. 85:3832-3835.

Baes, C.F., Jr. and R.E. Mesmer. 1976. The hydrolysis of cations. Wiley-Interscience, New York, pp. 211-220.

Bartlett, R.J. and B.R. James. 1988. Mobility and bioavailabilty of chromium in soils. pp. 267-303. In J.O. Nriagu and E. Nieboer (eds.), Chromium in the natural and human environments. John Wiley and Sons, NY.

Benjamin, M.M., and J.O. Leckie. 1981. Conceptual model for metal-ligand-surface interactions during adsorption. Environ. Sci. Tech. 15:1050-1056.

Bernasconi, C.F. 1976. Relaxation kinetics. Academic Press, New York.

Eary, L.E., and D.Rai. 1987. Kinetics of chromium(III) oxidation to chromium(VI) by reaction with manganese dioxide. Environ. Sci. Technol. 21:1187-1193.

Eigen, M., and K. Tamm. 1962. Schallabsorption in elektrolytloesungen als folge chemischer relaxation. Z. Elektrochem. 66:93-121.

Fendorf, S.E., M. Fendorf, D.L. Sparks, and R. Gronsky. 1992. Inhibitory mechanisms of Cr(III) oxidation by ß-MnO_2. J. Colloid Interface Sci. 153:37-54.

Fendorf, S.E., P. R. Grossl, D.L. Sparks, and G. M. Lamble. 1993. Oxyanion surface structures on goethite. Agronomy Abstracts. p.344. American Society of Agronomy, Madison, WI.

Goldberg, S. 1986. Chemical modeling of arsenate adsorption on aluminum and iron oxide minerals. Soil Sci. Soc. Am. J. 50:1154-1157.

Grossl, P.R., D.L. Sparks, and C.C. Ainsworth. 1994. Rapid kinetics of Cu(II) adsorption/desorption on goethite (α-FeOOH). Environ. Sci. Tech. 28:1422-1429.

Hachiya, K., M. Sasaki, T. Ikeda, N. Mikami, and T. Yasunaga. 1984. Static and kinetic studies of adsorption-desorption of metal ions on a γ-Al_2O_3 surface. 2. Kinetic study by means of pressure-jump technique. J. Phys. Chem. 88:27-31.

Hayes, K. 1987. Equilibrium, spectroscopic, and kinetic studies of ion adsorption at the oxide/aqueous interface. Ph.D. diss. Stanford Univ., Stanford, CA (Diss. Abstr. 87-23104).

Hayes, K.F., and J.O. Leckie. 1986. Mechanism of lead ion adsorption at the goethite-water interface. p.114-141. In J.A. Davis and K.F. Hayes (ed.) Geochemical processes at mineral surfaces. Proc. Am. Chem. Soc. Symp. Ser. 323, Chicago, IL., 8-13 Sept. 1985. ACS, Washington , DC.

Herbelin, A. L., and J. C. Westall. 1994. FITEQL. A computer program for the determination of chemical equilibrium constants from experimental data. Rep. 94-01, Oregon State University, Corvallis.

Hiemstra, T., J.C.M. DeWit, and W.H. Van Riemsdijk. 1989. Multisite proton adsorption modeling at the solid/solution interface of (hydr)oxides. A new approach : II. Application to various (hydr) oxides. J. Colloid. Interface Sci. 133:91-104.

Hingston, F. J., A. M. Posner, and J. P. Quirk. 1971. Competitive adsorption of negatively charged ligands on oxide surfaces. Discuss. Faraday Soc. 52:334-342.

James, B.R. and R.J. Bartlett. 1983. Behavior of chromium in soils: V. Fate of organically complexed Cr(III) added to soil. J. Environ. Qual. 12:169-172.

Jurinak, J.J., and K. K. Tanji. 1993. Geochemical factors affecting trace element mobility. J. Irrigation and Drainage Engineering. 119:848-867.

Knoche, W. 1975. Pressure-jump methods. In E. Wyn-Jones, (ed.) pp. 91-102. Chemical and biological applications of relaxation spectrometry. Reidel Publ., Dordrecht, The Netherlands.

Knoche, W. 1986. Pressure-jump methods. p. 191-218. In C. F. Bernasconi (ed.) Investigations of rates and mechanisms of reactions. Part II. Techniques of Chemistry. Vol. 5. Wiley, New York.

Mehadi, A. 1993. Reaction of Ni with soil and goethite: equilibrium and kinetic studies. Ph.D. dissertation. University of New Hampshire, Durham, New Hampshire.

Mehadi, A. 1993. Reaction of Ni with soil and goethite: equilibrium and kinetic studies. Ph.D. dissertation. University of New Hampshire, Durham, New Hampshire.

Mikami, N., M. Sasaki, K. Hachiya, and T. Yasunaga. 1983a. Kinetic study of the adsorption-desorption of the uranyl ion on a γ-Al_2O_3 surface using the pressure-jump technique. J. Phys. Chem. 87:5478-5481.

Mikami, N., M. Sasaki, K. Hachiya, R. D. Astumian, T. Ikeda, and T. Yasunaga. 1983b. Kinetics of the adsorption of PO_4 on the γ-Al_2O_3 surface using the pressure-jump technique. J. Phys. Chem. 87:1454-1458.

Mikami, N., M. Sasaki, T. Kikuchi, and T. Yasunaga. 1983c. Kinetics of adsorption-desorption of chromate on γ-Al_2O_3 surfaces using the pressure-jump technique. J. Phys. Chem. 87:5245-5248.

Rai, D., J.M. Zachara, L.E. Eary, C.C. Ainsworth, J.E. Amonette, C.E. Cowan, R.W. Szelmeczka, C.T. Resch, R.L. Schmidt, D.C. Girvin, and S.C. Smith. 1988. Chromium reactions in geologic materials. EA-5741. Electric Power Res. Inst, Palo Alto, CA.

Schwertmann, U., and R.M. Cornell. 1991. Iron oxides in the laboratory. Preparation and characterization. VCH Publishers, New York.

Schwertmann, U., and R.M. Taylor. Iron Oxides. pp. 379-438. In J.B. Dixon and S.B. Weed (eds.) Minerals in soil environments. 2nd edition. Soil Science Society of America, Madison, Wisconsin.

Sparks, D.L. 1989. Kinetics of soil chemical processes. Academic Press, New York.

Sparks, D.L., and P.C. Zhang. 1991. Relaxation methods for studying kinetics of soil chemical phenomena. pp.61-94. In D.L. Sparks and D.L. Suarez (eds.) Rates of soil chemical processes. Soil Science Society of America, Madison, Wisconsin.

Sposito, G. 1984. The surface chemistry of soils. Oxford University Press, New York.

Stollenwerk, K.G. and D.B. Grove. 1985. Adsorption and desorption of hexavalent chromium in an alluvial aquifer near Telluride, Colorado. J. Environ. Qual. 14:150-155.

Stumm., W. 1992. Chemistry of the solid-water interface. John Wiley and Sons, Inc., New York.

Waychunas, G.A., B.A. Rea, C.C. Fuller, and J.A.Davis. 1993. Surface chemistry of ferrihydrite: Part 1. EXAFS studies of the geometry of coprecipitated and adsorbed arsenate. Geochim. Cosmochim. Acta. 57:2251-2269.

Westall, J.C., 1982. FITEQL: A computer program for determination of chemical equilibrium constants from experimental data. Rep.82-01, Oregon State University, Corvallis.

Xyla A.G., B. Sulzberger, G.W Luther III, J.G. Hering, P. Van Cappellen, and W. Stumm. 1992. Reductive dissolution of manganese (III,IV) (hydr)oxides by oxalate: The effect of pH and light. *Langmuir*. 8: 95-103.

Yasunaga, T., and T. Ikeda. 1986. Adsorption-desorption kinetics of the metal-oxide-solution interface studied by relaxation methods. p. 230-253. In J.A. Davis and K.F. Hayes (ed.)Geochemical processes at mineral surfaces. Proc. Am. Chem. Soc. Symp. Ser. 323, Chicago, IL. 8-13 Sept. 1985. ACS, Washington, DC.

Zachara, J.M., C.C. Ainsworth, C.E. Cowan, and C.T. Resch. 1989. Adsorption of chromate by subsurface soil horizons. Soil Sci. Soc. Am. J. 53:418-428.

Zachara, J.M., C.E. Cowan, R.L. Schmidt, and C.C. Ainsworth. 1988. Chromate adsorption on kaolinite. Clays Clay Miner. 36:317-326.

Zachara, J.M., D.C. Girvin, R.L. Schmidt, and C.T. Resch. 1987. Chromate adsorption on amorphous iron oxyhydroxide in presence of major groundwater ions. Environ. Sci. Technol. 21:589-594.

Zhang, P.C., and D. L. Sparks. 1989. Kinetics and mechanisms of molybdate adsorption/desorption at the goethite/water interface using pressure-jump relaxation. Soil Sci. Soc. Am. J. 53:1028-1034.

Zhang, P.C., and D. L. Sparks. 1990a. Kinetics and mechanisms of sulfate adsorption/desorption on goethite using pressure-jump relaxation. Soil Sci. Soc. Am. J. 54:1266-1273.

Zhang, P.C., and D. L. Sparks. 1990b. Kinetics of selenate and selenite adsorption/desorption at the goethite/water interface. Environ. Sci. Tech. 24:1848-1856.

Brause et al., 1990). This technique has the distinct advantage over other spectroscopies in that it can be applied in-situ. Also, it can provide direct atomic level information on the structural/chemical environment of the sorbed metal. However, XAS is not without its caveats. XAS is limited to elements heavier than Sc and access to synchrotron facilities (necessary for XAS) are not readily attained. Also, although XAS provides the local chemical environment of a particular element, it provides no information on the spatial resolution of the sorbed surface species. Another problem is data analysis packages which are not user friendly and often difficult to obtain.

XAS requires the use of high intensity X-rays which are produced by electrons/positrons moving in a storage ring at high energies, in paths curved by magnetic fields (synchrotron). The synchrotron radiates a white beam of photons tangentially to its curved path (Charlet and Manceau, 1993). These high energy photons are used in the XAS experiment.

X-ray absorption spectroscopy is based on the interaction of X-rays with the core electrons of an element. It consists of recording the absorption of X-rays by a sample at different energies. The XAS experiment is conducted near the X-ray absorption edge (K,L, or M) of the particular element of interest. As the energy of the X-ray beam is increased, it can move core electrons to valence shells. As energy is increased further, the electron is ejected as an ionized photoelectron. The fate of this photoelectron is manifold. It can be absorbed, ricochet off several lattice atoms before returning to the original atom, or bounce off only one other atom. Interferences between the outgoing and incoming electronic waves caused by ejection of photoelectrons alters the ability of the atom to absorb the photon, giving rise to oscillations in the X-ray absorption spectrum (Charlet and Manceau, 1993). These oscillations are called X-ray absorption fine structure or XAFS. XAFS gives us

information on the nearest neighbors, coordination number, and bond distances of the element of interest. These characteristics make it an ideal tool for discerning the local structure of poorly crystalline or amorphous particles and the stereochemistry of surface complexes.

The use of XAS to study the sorption of metal cations and oxyanions by geochemists and surface chemists has increased in recent years (Hayes et al., 1987; Chisholm-Brause et al., 1990; Manceau and Charlet, 1992; Charlet and Manceau, 1992; Dent et al., 1992; Waychunas et al., 1993; Fendorf et al., 1994). XAS experiments conducted on the sorption of oxyanions (selenite and arsenate) on iron oxides indicate the formation of binuclear bidentate surface complexes at high surface coverages (Hayes et al., 1987; Waychunas et al., 1993). However, at low surface coverages arsenate partly forms mononuclear monodentate surface complexes (Waychunas et al., 1994). These results indicate that the type of surface complex formed by oxyanions is not only dependent on the type of surface but also on the pH and surface coverage.

The objective of this study is to examine the surface structure of arsenate and chromate sorbed on goethite using XAS. This information will be used in conjunction with kinetic data, obtained in the P-jump investigation, to obtain a thorough understanding of the sorption mechanism of chromate and arsenate on goethite.

5.2 Materials and Methods

5.2.1 Sample Preparation

A pH-stat set up was used for all batch studies (Figure 4.3). All experiments were conducted at 298 ± 0.1 K at 1 atm pressure in a N_2 environment to

eliminate CO_2 influences. Two sets of samples were prepared. The first set of samples were prepared at similar loading rates to the p-jump studies. The second set of samples were prepared at higher loading rates. Sample preparation involved adding five grams of solid to 0.480 L of 0.01 M $NaNO_3$ and allowing it to hydrate for 24 h. Following hydration the desired amount of Cr or As was added using a 0.20 M stock solution made from reagent grade sodium chromate or arsenate. The final volume was brought to 0.500 L using doubly-distilled deoinized water yielding a suspension concentration of $10gL^{-1}$. Samples were allowed to react until a stable pH was observed for about 1 hour. Approximately 55 mls of sample were removed and placed on a reciprocating shaker in a thermostated incubator at 298 ± 1 for 24 hours. This procedure was followed to insure complete reaction of the oxyanion with the goethite. After 24 hours, 5 ml of sample was filtered through a 0.20 micron Gelman filter (Gelman GA-8, Gelman Sciences, Inc., Ann Arbor, MI) and analyzed for Cr and As using an inductively coupled plasma spectrophotometer. The remaining 50 mls of sample was filtered through a 0.20 μm pore membrane in order to consolidate solids for XAFS analysis. The filtrate was than rinsed with 50 ml of high-purity water to remove the entrained electrolyte, placed in a scintillation vial and sealed with parafilm for subsequent XAFS analysis.

5.2.2 XAFS Studies

XAFS spectroscopy was performed at the National Synchrotron Light Source, Brookhaven National Laboratory, under dedicated running conditions on beam line X-11A. The electron storage ring operated at 2.528 GeV with currents ranging from ≈210 mA immediately after a fill to 110 mA before a fill.

A Si(111) water-cooled double-crystal monochromator was employed with a sagitally focused beam (Lamble and Heald, 1991) for the Cr and an unfocused beam for the As . The focused beam provided an intensity greater than three times that provided by the conventional flat monochromator arrangement over the energy range used for the Cr. A 0.50-mm pre-monochromator slit width was employed, which was readjusted as necessary to compensate for vertical motion of the stored electron beam. Higher order harmonics were rejected by detuning 30% from the maximum incident intensity (I_0).

The incident X-ray intensity was measured for Cr and As with a 15-cm-long ionization chamber. This chamber was filled with N_2(g) for Cr and a mixture of 90% N_2(g)-10% Ar(g) for As. Reference materials were run in transmission mode, and the transmitted intensity was measured with a second ionization chamber. All oxyanion-goethite systems were analyzed by fluorescence detection. The Cr K edge (5989eV) and the As K edge (11,867eV) were used for analysis.

For fluorescence detection, the samples were placed at a 45° angle to the incident beam, and a wide angle collector with an ionization chamber, a Lytle detector (EXAFS Co.), was located 45° off the sample (i.e., normal to the incident beam). The Lytle detector was filled with Ar(g) for the CrKα and Kr(g) for the AsKα fluorescence detection. A V and Ge filter along with Soller slits were placed between the sample and the detector for the Cr and As samples, respectively. This procedure was followed to reduce elastically scattered incident X-rays from entering the fluorescence detector. Samples were analyzed at N_2(l) temperatures (77 K) due to a reduction in thermal disorder. Previous studies showed no structural differences between 77 K and ambient temperatures, 298 K (Fendorf et al., 1994).

Fluorescence samples were mounted in a 4 X 6 X 25 mm slot cut in an Al block, which provided good thermal conductance necessary for temperature variation of the samples. These dimensions provided 1 mm on each side of the beam and a depth in excess of four adsorption lengths when mounted at 45° to the incident beam. The sample was sealed with 0.0013 in. thick Kapton polymide film (CHR Industries, type K-104) to prevent moisture loss while minimizing X-ray absorption. The samples were mounted on a Cu cold finger that was connected to a N_2(l) reservoir. To minimize heat transfer imposed on the cold finger, samples were precooled by immersion into N_2(l) for several minutes prior to analysis.

All samples were run at least in triplicate. Data analyses were accomplished by optimizing the fit of predicted spectra with Fourier filtered experimental spectra. Phase shifts were determined by ab initio calculations (Rehr et al., 1992) and checked using model compounds.. Amplitude parameters were defined based on α-Cr_2O_3 and sodium arsenate model compounds. Successive shells were isolated in the Fourier transformed spectra, back-transformed, and the interatomic distances (R's), coordination numbers (CN's), and Debye-Waller factors ($2\sigma^2$) varied until the best fit was obtained between the predicted and experimental curves.

5.3 Results and Discussion

EXAFS spectroscopy was employed to determine the local coordination environment of Cr(VI) and As(V) sorbed on goethite. The spectra obtained from the majority of the Cr (VI) samples proved to be too noisy for accurate data analysis. Therefore, only one loading rate of Cr(VI) from each of the two sample sets was investigated. This enabled a comparison between high and low loading rates. Surface coverages for the two Cr(VI) samples were 10.8 and 90%. Surface coverages were

based on a goethite surface area of $52 m^2/g$ and a surface site density of 10.2 sites/nm^2 (Heimstra et al., 1989). The experimental spectra were collected by fluorescence detection for Cr(VI) and As(V) over the energy range of 5789 to 7000 and 11,767 to 13,000 eV, respectively. The background absorbance of the spectra were removed and the atomic absorption was normalized to unity. To isolate the scattering contribution of the spectra, which result from the coordination environment of the absorber, a spline function was fit to the 'absorption envelope'. Such a function accounts for the atomic absorption in the absence of a coordinating field. The isolated structural function was then transformed from units of eV to $Å^{-1}$.

The experimental $\chi(k)$ spectra of Cr(VI) sorbed on goethite at two different initial loadings are shown in Figure 1 (arsenate data not shown). Fourier transformation of the $\chi(k)$ function leads to a radial structure function (RSF), in which the peak positions correspond to the interatomic distances within the material. These peak positions, however, are uncorrected for phase shifts so that the positions are slightly shifted from the true interatomic distances. By backtransforming the spectra, a theoretical model can be fit to the experimental spectra. In the theoretical model the interatomic distance R, coordination number (CN), and disorder (σ^2) are varied until the fit between the theory and experiment is optimized. This procedure results in R values within $\pm$ 0.02 Å and coordination numbers accurate to within 25% as determined from model spectra. Individual peaks of the RSF were first backtransformed and fit. After the parameters of each peak were determined the full Fourier filtered $\chi(k)$ function from 0 to 4 Å was fit to determine the local coordination environment of Cr(VI). The fit of the full spectra for each Cr(VI) loading is shown in Figure 2.

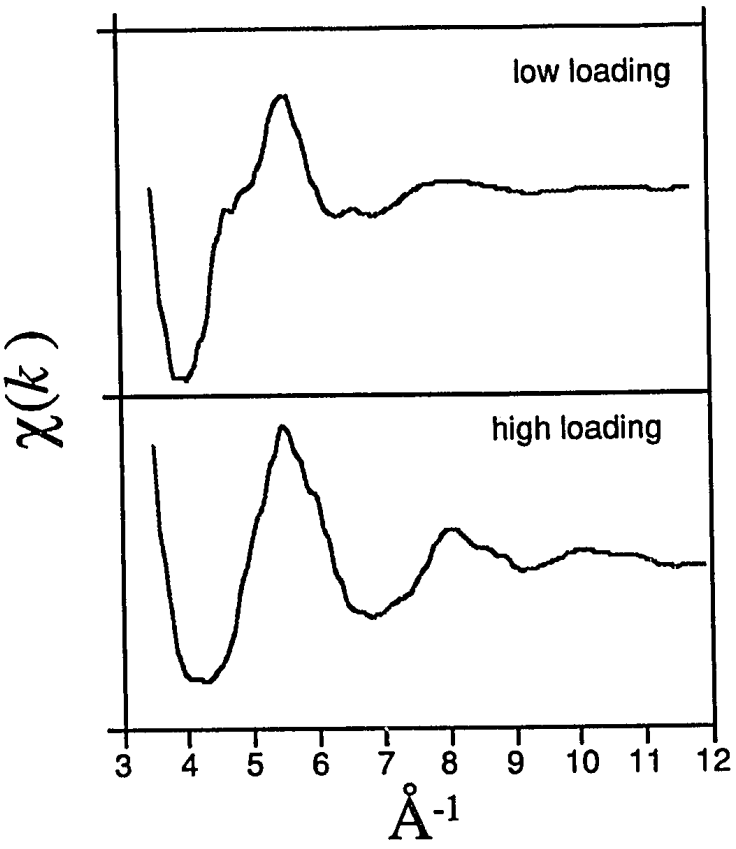

Figure 5.1 Experimental XAFS curves for Cr(VI) sorbed on goethite.

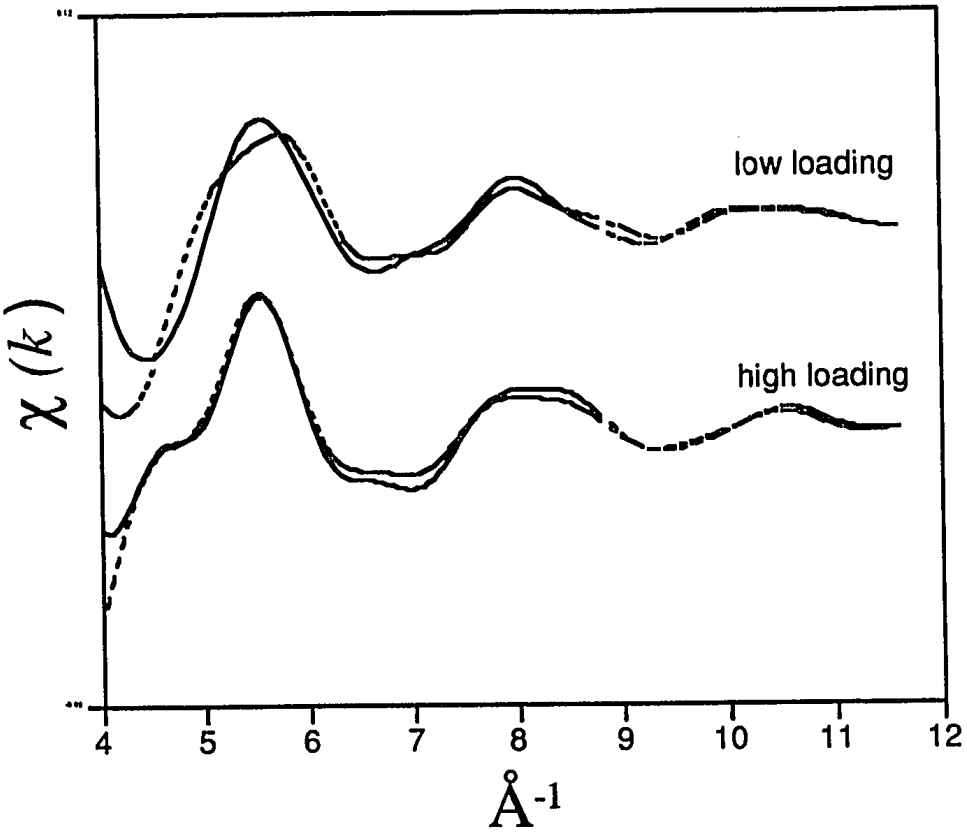

Figure 5.2 **Fourier filtered experimental XAFS spectra and theoretically based curves fit for Cr(VI) on goethite.**

The local coordination environment of Cr(VI) was deduced by using the parameters derived from the EXAFS analysis . For both samples, the central Cr atom was coordinated by 4 oxygen atoms that reside at a distance of 1.61 Å. This distance and coordination number are in agreement with values reported for the chromate ion (CrO_4^{2-}) (Wells, 1984). Beyond O, multiple Fe shells are apparent at distances of 3.32 and 3.57 Å. This was the case for both loading rates. The latter distance, 3.57 Å, corresponds to a monodentate surface complex. The shorter distance, 3.32 Å, would result from a bidentate binuclear surface complex. The surface groups active in Cr(VI) sorption as gleaned by EXAFS spectroscopy are in agreement with the expected reactivity of goethite surfaces (Hiemstra et al., 1989).

At the lower loading rate an additional Fe atom resided at a distance of 2.91 Å. This distance represents a bidentate mononuclear complex. The fits of the sample with the higher loading rate showed no indications of appreciable levels of this complex. Thus, based on the EXAFS results, 3 Cr(VI) complexes are present on the goethite surface. At low loading rates, all three complexes are appreciable. Based on the coordination number and peak intensities in the RSF, the bidentate mononuclear and monodentate complexes are in greater proportions than the bidentate binuclear complex. However, at higher loading rates the spectra are adequately described by the monodentate and binuclear complexes. Figure 5.3 dipicts chromate surface structures on goethite derived by XAFS.

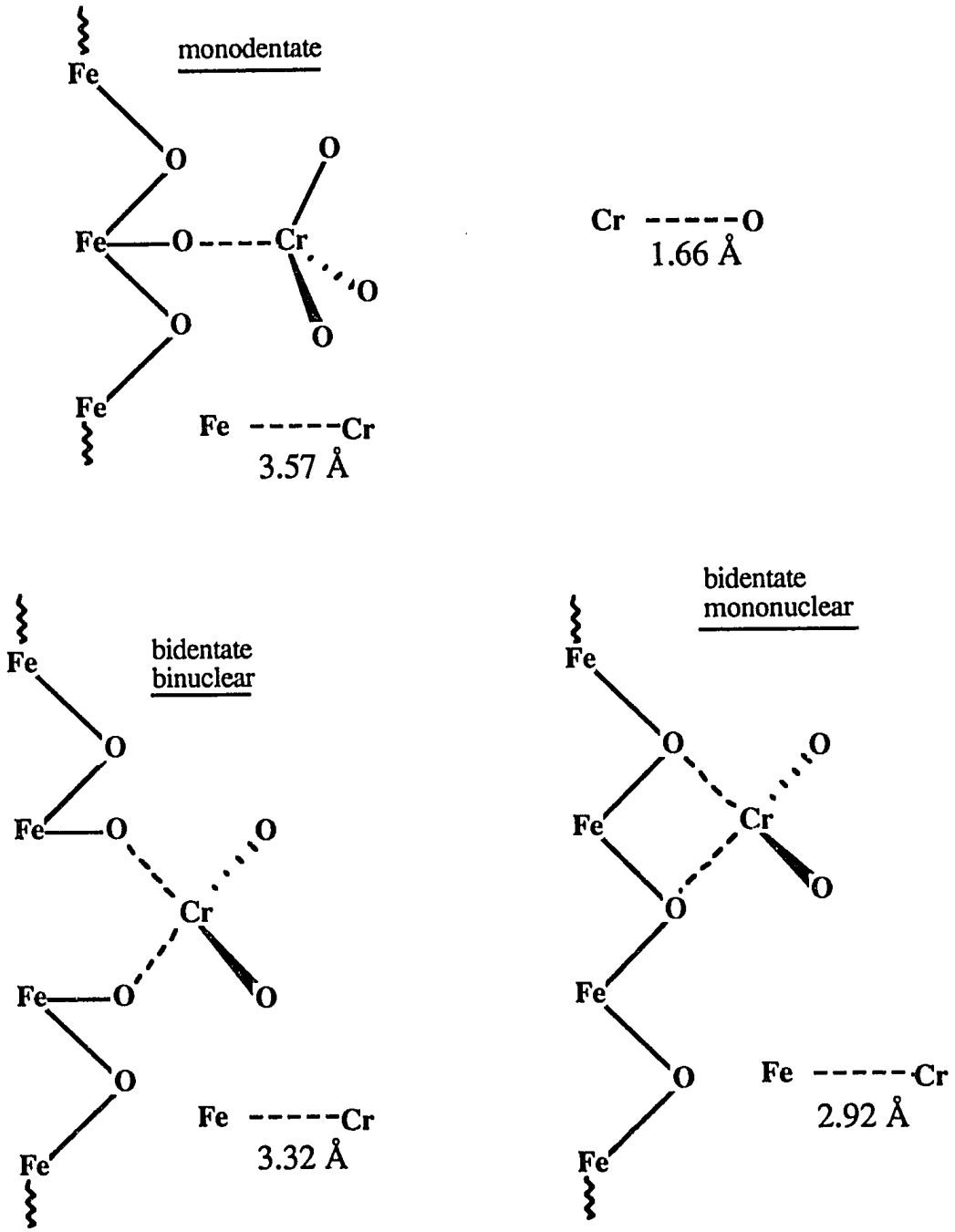

Figure 5.3 Dipiction of the chromate surface complexes derived by XAFS.

It appears that the monodentate and mononuclear bidentate complex form at low surface coverages. As coverage increases, the monodentate complex levels are enhanced. With continued increases in surface coverage, neighboring monodentate active sites become 'bridging' groups and lead to the formation of a binuclear bidentate surface complex. The monodentate and binuclear complexes thus dominate the surface species of Cr(VI) on goethite at high loading rates.

Similar results were obtained for the As(V) samples although bond distances differed slightly. At low surface coverages, all three surface complexes are discernible. However, bidentate surface complexes predominate. As surface coverages increase, binuclear bidentate complex levels increase and dominate the surface species of As(V) on goethite.

5.4 Conclusions

Based on XAFS data, the oxyanions chromate and arsenate form a combination of surface complexes on goethite. The type of surface complex depends upon the surface coverage of the oxyanions. At low surface coverages, chromate forms monodentate and bidentate mono- and binuclear complexes. All three surface complexes are appreciable at low surface coverages. In contrast, at low surface coverages, arsenate forms predominantly bidenate surface complexes. At higher surface coverages, monodentate and binuclear complexes dominate for chromate while binuclear surface complexes dominate for arsenate. These results are in agreement with rate data from the p-jump study which indicate that arsenate more favorably forms inner-sphere bidentate surface complexes on goethite than chromate.

consistent with the fact that chromate is generally considered to be the more mobile of the two oxyanions in the vadose zone.

5.5 References

Charlet, L. and A. Manceau. 1993. pp. 117-164. Structure, formation, and reactivity of hydrous oxide particles: Insights from X-ray absorption spectroscopy. In J. Buffle and H.P. van Leeuwen (ed.), Environmental Particles. Vol. 2. Lewis Publishers, Boca Raton.

Charlet. L., and A. Manceau.1992. X-ray absorption spectroscopic study of the sorption of Cr(III) at the oxide/water interface. II. Adsorption, coprecipatation and surface precipitation on ferric hydrous oxides. J.Colloid. Interface Sci. 148:443-458.

Chisholm-Brause, C.J., P.A. O'Day, G.E. Brown, Jr., and G.A. Parks. 1990. Evidence for multinuclear metal-ion complexes at the solid/water interfaces from X-ray absorption spectroscopy. Nature 349:528-530.

Dent, A.J., J.D.F. Ramsey, and S.W. Swanton. 1992. An EXAFS study of uranyl ion in solution and sorbed onto silica and montmorillonite clay colloids. J. Colloid. Interface Sci. 150: 45-60.

Fendorf, S.E., G.M. Lamble, M.G. Stapleton, M.J. Kelley, and D.L. Sparks. 1994. Mechanisms of chromium(III) sorption on silica. 1. Cr(III) surface structure derived by extended X-ray absorption fine structure spectroscopy. Environ. Sci. Technol. 28:284-289.

Hayes, K.F., A.L. Roe, G.E. Brown, K.O. Hodgson, J.O. Leckie, and G.A. Parks. 1987. X-ray absorption study of surface complexes: Selenium oxyanions on α–FeOOH. Science 238: 52-56.

Hiemstra, T., J.C.M. De Wit, and W.H. Van Reimsdijk. 1989. Multisite proton adsorption modeling at the solid/solution interface of (hydr)oxides: a new approach. II. Application to various important (hydr)oxides. J. Colloid Interface Sci. 133:105-117.

Lamble, G.M., and S.M. Heald. 1991. Operation of a dynamically bent sagittally focusing double crystal monochromator for XAFS studies. Rev. Sci. Instrum. 63: 880-884.

Manceau, A., and L.Charlet. 1992. X-ray absorption spectroscopic study of the sorption of Cr(III) at the oxide/water interface. I. Molecular mechanism of Cr(III) oxidation on the Mn oxides. J.Colloid. Interface Sci. 148:425-442.

Rehr, J. J., R. C. Albers, and S.I. Zabinsky. 1992. High-order multiple-scattering calculations of x-ray absorption fine structure. Phys. Rev. Lett. 69: 3397-3400.

Waychunas, G.A., B.A. Rea, C.C. Fuller, and J.A.Davis. 1993. Surface chemistry of ferrihydrite: Part 1. EXAFS studies of the geometry of coprecipitated and adsorbed arsenate. Geochim. Cosmochim. Acta. 57:2251-2269.

Wells, A.F. 1984. Structural Inorganic Chemistry. Oxford University Press, New York.

Chapter 6

MECHANISM OF NI(II) SORPTION ON KAOLINITE

6.1 Introduction

6.1.1 Nickel Occurrence and Mobility

Nickel is the eleventh most abundant metal found in the earth's crust. It is considered a siderophile (iron-loving element) and tends to be enriched in ultramafic rocks. Nickel often substitutes for Fe and Mg in minerals because of the similarity of their ionic radii. The concentration of nickel found in soils varies depending on the Ni content of the parent rock, pedogenic processes, and anthropogenic deposition. In trace quantities nickel plays an essential biological role in plants, animals, and microorganisms (Uren, 1992). However, at higher concentrations, Ni may become toxic. Nickel is seldom found in soils at concentrations considered to be toxic to plants and animals. By comparison, it is found in lunar soils at unusually high concentrations . The average concentration of nickel in terrestrial soils is 40 mg kg^{-1} compared to 291mg kg^{-1} found in samples returned from the Apollo missions (Hossner and Allen, 1989). This high concentration coupled with the reactive nature of the lunar soils may potentially create Ni toxicity problems. Nickel is relatively redox inactive in soils existing exclusively in the Ni^{+2} oxidation state (Uren, 1992).

Nickel is found as a trace element in most soils. Exceptions are soils formed on ultrabasic igneous rocks (serpentine soils) and polluted soils. The typical range of Ni concentrations in soils listed by Uren (1992) varied from 10-1000 ppm

with the average around 40 ppm. The typical range of Ni in plants is 0.01 to 5 ppm (Welch, 1981). Toxic concentrations in plants range from 25 to 50 ppm, but this will vary depending on plant species. For example, Slingsby and Brown (1977) found no toxicity symptoms in oats containing between 12 and 44 ppm Ni while Patterson (1971) observed Ni toxicity in wheat at 8 ppm.

The hydrated Ni $^{2+}$ ion [$Ni(H_2O)_6^{2+}$] is the most common form of Ni(II) found in the soil solution (Uren, 1992). However, its activity will decrease with an increase in pH and activities of ligands available to form complexes. The majority of Ni in soils is associated with solid phases (inorganic and organic). Nickel is often found in octahedral coordination in easily weathered primary silicate minerals, especially olivine. It is also found in hornblende, augite, biotite, ilmenite, and magnetite. Since Ni occurs in unstable primary minerals most Ni in soils is associated with secondary minerals found in the clay fraction (Uren, 1992). Nickel is often found associated with Fe and Mn hydrous oxides and the trioctahedral species of layer silicates (serpentines, saponites, vermiculite, and chlorites).

Nickel is also found in association with organic matter present in soils. However, these associations are often difficult to determine because extraction using acid or base may cause Ni to precipitate, dissociate from the organic matter, or redistribute to another phase (Uren, 1992). Therefore, Ni associated with organic matter is often labeled as exchangeable or non-exchangeable.

Literature focusing on the sorption and mobility of Ni in soils or soil constituents is limited. This lack of interest may be due to its lower toxicity and stable redox state compared to metals such as chromium. Also, there is less anthropogenic deposition of Ni compared to other heavy metals such as Pb. Nickel is used in various industrial processes such as plating and alloying industries and is one of several heavy

metals that is often found in municipal and industrial sewage sludge. Therefore, much of the research found in the literature focuses on two areas: i) the possible adverse effects of trace metal accumulation in agricultural soils amended with sewage sludges (Sposito et al., 1982a,b; Sposito et al., 1983; Sims and Kline, 1991; Emmerich et al., 1982a,b) and ii) the sorption of Ni on soil constituents in comparison with other trace metals (Schulthess and Huang, 1990; McKenzie, 1967, 1980; Bloom and McBride, 1979; Harter, 1983).

6.1.2 Spectroscopy

Mechanistic information on metal sorption reactions is often based on indirect evidence, such as macroscopic data (e.g. shape of an adsorption isotherm), without any direct atomic level evidence (Schulthess and Huang, 1990; Harter, 1983). This information is often precluded by the availability of spectroscopic and microscopic techniques. Mechanistic information obtained from spectroscopic and microscopic techniques is essential for understanding the factors affecting metal sorption/desorption processes and predicting the metal's fate and mobility in the environment. Mechanistic models based on sorption isotherm data may not be an accurate representation of reactions occuring at the mineral surface. Additionally, reaction conditions (e.g. pH, aqueous metal concentration, sorbent properties, and surface coverage) will effect the sorption mechanism and a model developed under one set of reaction conditions may not be applicable to others.

An abundance of spectroscopic and microscopic techniques are available for investigating surface reactions. However, no single technique can provide all the necessary mechanistic information for modeling these systems. A combination of spectroscopic and microscopic techniques along with laboratory data can provide a

thorough and accurate description of metal sorption reactions. For example, Fendorf and Sparks (1994) and Fendorf et al. (1994) used a combination of X-ray absorption fine structure (XAFS), high resolution transmission electron microscopy (HRTEM), and diffuse reflectance infrared Fourier transform (DRIFT) spectroscopy to examine the mechanism of Cr(III) sorption on silica. These techniques provided an accurate description of Cr(III) sorption on silica and provided an opportunity to examine the effect of an various reaction parameters on the Cr(III) sorption structure.

6.1.3 Objectives

The objective of this study was to investigate the mechanism of Ni(II) sorption on kaolinite. This information is important in determining the potential toxicity of Ni released from lunar soils. Kaolinite was chosen as the sorbent because dissolution experiments with lunar simulant indicate that this solid phase will form early during the weathering of the lunar regolith. TEM and XAFS were coupled with laboratory data to obtain a detailed description of the Ni(II)-kaolinite sorption mechanism. TEM coupled with energy dispersive spectroscopy (EDS) provided information on the spatial distribution of the sorbed Ni while XAFS was employed to ascertain the local chemical and structural environment of the sorbed Ni.

6.2 Materials and Methods

6.2.1 Solid Material

The sorbent used in this study was a well crystallized Georgia kaolinite obtained from the University of Missouri Source Clays Depository. The bulk kaolinite was ground in a corundum grinding jar and washed with doubly-distilled deionized water until a stable conductivity resulted for 24 h. The washed kaolinite

was fractionated by standard procedures (Jackson, 1969), based on a gravimetric method, to an equivalent diameter of less than 2 μm. It was than dialyzed in doubly-distilled deionized water until a stable conductivity resulted for 24 h and subsequently freeze dried. The specific surface area was 15 m^2/g as determined by a three point N_2 Brunauer-Emmett-Teller (B.E.T.) gas adsorption isotherm method.

6.2.2 Solid Characterization

The <2 μm fraction was mounted in cavities carved on glass slides and characterized by X-ray diffraction (XRD) using a Scintag XDS 2000 X ray diffractometer and Cu Kα radiation; a software routine was used for Kß stripping. Transmission electron microscopy was employed to determine particle size, presence of impurities, and semi-quantitative chemical composition after reaction with Ni. For TEM analysis a 0.50 g/L suspension was dispersed on a holey carbon film supported by a copper mesh grid. The samples were air dried and coated with carbon. Imaging was performed with a JEOL JEM 2000FX transmission electron microscope. Semi-quantitative compositions of the kaolinite surface were obtained using an energy dispersive spectrometer (EDS) and a Link ExL GEN 1089 system analyzer.

X-ray diffraction analysis yielded results diagnostic for kaolinite with no impurities present. Transmission electron microscopy (TEM) and electron diffraction revealed well crystallized and fairly uniform kaolinite particles with trace quantities of titanium (Figure 6.1).

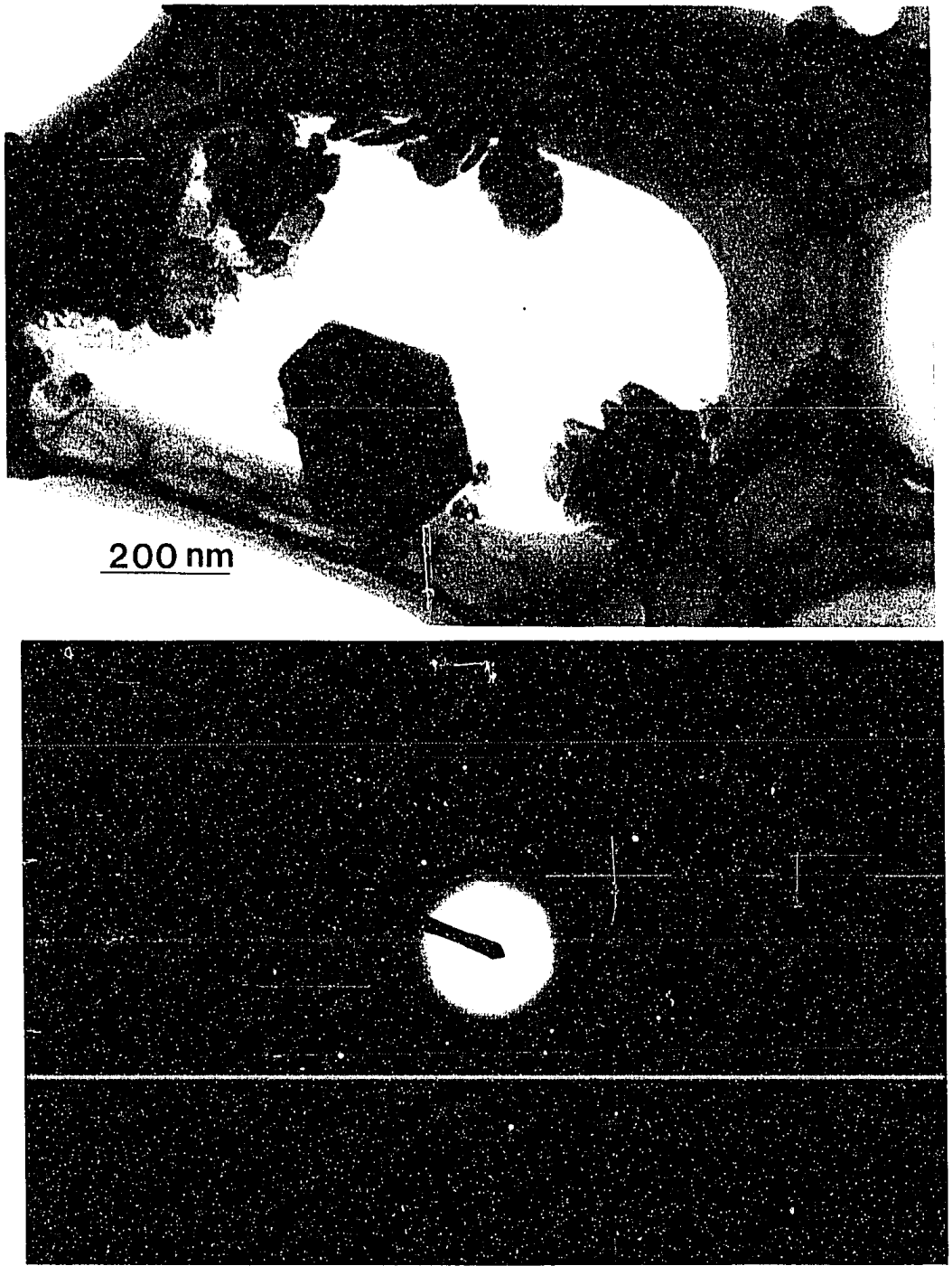

Figure 6.1 a) TEM image of a hexagonal kaolinite particle. b) Single crystal electron diffraction pattern of kaolinite.

6.2.3 Batch Studies

Batch studies were conducted to examine the amount of Ni sorbed on kaolinite as a function of pH and initial Ni concentration. Experiments were conducted at pHs 5 and 7 and initial Ni concentrations of 4.3, 8.5, 12.8, 17, and 34 mM. The pHs were chosen to represent those found in plant growth environments and were similar to those used in the lunar simulant dissolution experiments. The initial Ni concentrations were chosen to represent a range in concentrations found in lunar soils.

A pH-stat set up was used for all batch studies (Figure 4.3). All experiments were conducted at 298 ± 0.1 K at 1 atm pressure in a N_2 environment to eliminate CO_2 influences. Five grams of solid were added to 0.480 L of 0.005 M $NaNO_3$ and allowed to hydrate for 24 h. Following hydration, the desired amount of Ni was added using a 0.25 M stock solution made from reagent grade $Ni(NO_3)_2 \cdot 6H_2O$. The final volume was brought to 0.500 L using doubly-distilled deoinized water yielding a suspension concentration of 10g/L. The pH and temperature were held constant using the pH-stat system and a jacketed flask with a thermostated water pump, respectively. The system was allowed to equilibrate until the volume of base added remained constant for approximately 0.5 h. After this time, a 10 ml sample was taken and filtered through a 0.20 micron Gelman filter (Gelman GA-8, Gelman Sciences, Inc., Ann Arbor, MI). The sample was analyzed for Ni using an Inductively Coupled Plasma (ICP) spectrophotometer. The quantity of Ni sorbed was determined by difference (i.e amount added minus amount in sample). It is important to remember that the information gleaned in this study is representative of a

reaction time of approximately 4 - 5 h and may not be indicative of sorption at equilibrium (Fendorf et al., 1994).

Similar to Fendorf et al., (1994) the quantity of metal sorbed on the kaolinite is referenced to the potential surface site occupancy, ϕ

$$\phi = (\text{mol of Ni sorbed})/(\text{mol of surface sites}) \quad (6.1)$$

This term (ϕ) describes a potential site maximum if each sorbed Ni occupied a single site. However, if polymerization or nucleation should occur, then the number of surface sites occupied would be less than ϕ. At $\phi \leq 1$ a single site occupancy can account for sorption, however, at $\phi \geq 1$ nucleation or multilayer sorption is required (Fendorf et al., 1994). A surface site density of 7.9 sites/nm^2 (Carroll-Webb and Walther, 1988) was used to calculate the potential surface site occupancy.

6.2.4 XAFS Studies

Three samples, each reacted at both pH 5 and 7, were used for the XAFS studies. However, noise in the spectra at the lowest loading pH 5 sample precluded any meaningful data analysis. This may be the result of the lower loading rate, a glitch in the instrumentation during the experimental run or human error calibrating the instruments. The experimental set-up was the same as for the batch sorption studies. Upon a stable pH reading for ≈0.5 hours, 55 ml of sample was removed. A 5 ml aliquot of this sample was filtered through a 0.20 micron Gelman filter (Gelman GA-8, Gelman Sciences, Inc., Ann Arbor, MI) and analyzed for Ni using an inductively coupled plasma spectrophotometer. The remaining 50 mls of sample was filtered through a 0.20 μm pore membrane in order to consolidate solids for XAFS analysis. The filtrate was than rinsed with 50 ml of high-purity water to remove the

entrained electrolyte, placed in a scintillation vial and sealed with parafilm for subsequent XAFS analysis.

XAFS spectroscopy was performed at the National Synchrotron Light Source, Brookhaven National Laboratory, under dedicated running conditions on beam line X-11A. The electron storage ring operated at 2.528 GeV with currents ranging from ≈210 mA immediately after a fill to 110 mA before a fill.

A Si(111) water-cooled double-crystal monochromator was employed with a focused beam (Lamble and Heald, 1991). The focused beam provided an intensity greater than three times that provided by the conventional flat monochromator arrangement over the energy range used for the Ni. A 0.50-mm pre-monochromator slit width was employed, which was readjusted as necessary to compensate for vertical motion of the stored electron beam. Higher order harmonics were rejected by detuning 30% from the maximum incident intensity (I_0).

The incident X-ray intensity was measured with a 15-cm-long N_2(g) ionization chamber. Reference materials were run in transmission mode, and the transmitted intensity was measured with a second ionization chamber. All Ni-kaolinite systems were analyzed by fluorescence detection. The Ni K edge (8333eV) was used for analysis.

For fluorescence detection, the samples were placed at a 45° angle to the incident beam, and a wide angle collector with an ionization chamber, a Lytle detector (EXAFS Co.), was located 45° off the sample (i.e., normal to the incident beam). The Lytle detector was filled with Kr(g) for the NiKα fluorescence detection. A Co filter along with Soller slits were placed between the sample and the detector to reduce elastically scattered incident X-rays from entering the fluorescence detector. Samples were analyzed at N_2(l) temperatures (77 K) due to a reduction in thermal disorder.

Previous studies showed no structural differences between 77 K and ambient temperatures, 298 K (Fendorf et al., 1994).

Fluorescence samples were mounted in a 4 X 6 X 25 mm slot cut in an Al block, which provided good thermal conductance necessary for temperature variation of the samples. These dimensions provided 1 mm on each side of the beam and a depth in excess of four adsorption lengths when mounted at 45° to the incident beam. The sample was sealed with 0.00125 cm thick Kapton polymide film (CHR Industries, type K-104) to prevent moisture loss while minimizing X-ray absorption. The samples were mounted on a Cu cold finger that was connected to a $N_2(l)$ reservoir. To minimize heat transfer imposed on the cold finger, samples were precooled by immersion into $N_2(l)$ for several minutes prior to analysis.

All samples were run in triplicate. In order to determine the structural environment of Ni sorbed on Kaolinite, extensive data analysis was conducted on the average of at least three XAFS spectra. Energy calibration was accomplished by setting the inflection point in the absorption edge for a Ni (metal) foil at 8333 eV. Spurious points induced by imperfections in the crystal monochromator were removed, and the spectra were then normalized so that the total jump height was unity. Spectral contributions arising from backscattering effects were isolated by fitting a spline function to the atomic absorption and subtracting this function from the experimental curve. This results in the $\chi(k)$ (EXAFS) spectra.

The $\chi(k)$ spectra were then used to determine the type, number (CN), distance (R), and dissorder (σ) of the atoms coordinating Ni. Individual peaks comprising only 1-2 atomic shells were isolated in the Fourier transformed curves, a radial structure function (Å), and then backtransformed into $Å^{-1}$ units. Each peak was then fit with a theoretical curve to determine the local coordination environment. In

this fit, the amplitude and phase functions were derived from ab initio theory using the developments of Rehr et al. (1992). Optimization of the theoretical spectra to the experimental spectra was obtained by independently varying R for the phase, and CN and σ for the amplitude proportions of the curve. Finally, the parameters determined from individual shells were then used to model the complete Fourier filtered spectra. Based on fits to model compounds the interatomic distances are accurate to within 0.02 Å and the coordination numbers better than 30% for first shell contributions; successively further shells are of course less accurate. It should be noted that elements with similar atomic number can not be distinguished with XAFS. Thus, the theoretical fit of the EXAFS spectra can not be used to differentiate Al from Si in the surface complex. However, based on the crystallographic arrangement of kaolinite one can ascertain whether Al or Si comprises a backscattering contribution.

6.3 Results

6.3.1 Batch Studies

The results of the sorption studies are shown in Figure 6.2 and Table 6.1. At both pH 5 and 7 a nearly linear increase in the amount of Ni sorbed as a function of equilibrium concentration was observed. The quantity of Ni sorbed was greater at pH 7 than 5 and was less than 50% for all experiments. Potential surface site occupancy (ϕ) exceeded 1 for the majority of sorption experiments (Table 6.1). Therefore, in all but three experiments, monolayer coverages were exceeded, indicating nucleation or multilayer adsorption. MINTEQA2 (Allison et al., 1991) chemical speciation computer code was employed to determine Ni speciation and possible solid phases in the absence of kaolinite. At the highest initial concentration at pH 7, 99% of the Ni is present as the hydrated Ni^{+2} ion, while the solution is only slightly saturated with

respect to $Ni(OH)_2$ (IAP/SI=1.1). Hence, no multinuclear hydrolysis products are present in solution and the precipitation of solid phases in pure solutions of $Ni(NO_3)_2 \cdot 6H_2O$ are unlikely.

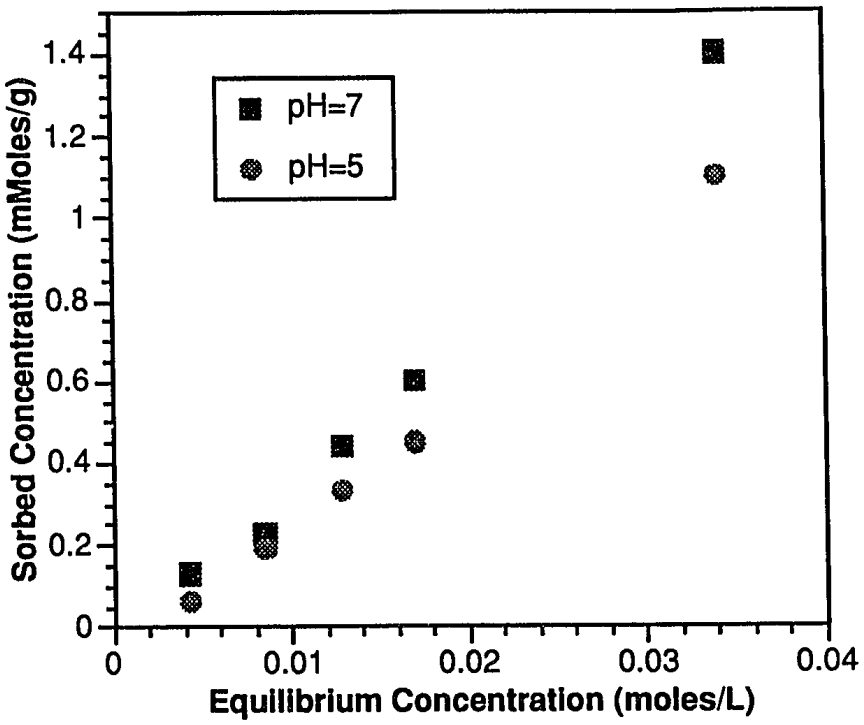

Figure 6.2 Nickel sorption on kaolinite as a function of pH and equilibrium concentration.

Table 6.1 Experimental conditions and potential site occupancy (ϕ) for the Ni/kaolinite sorption experiments.

ϕ	Init. Conc. mol L^{-1}	Sorb. Conc. mol g^{-1}	pH	% Ni sorbed
.33	0.0043	0.0000653	5.0	15.1
.97	0.0085	0.000192	5.0	22.6
1.66	0.0128	0.000327	5.0	25.6
2.27	0.0170	0.000447	5.0	26.5
5.43	0.0340	0.00107	5.0	31.5
.64	0.0043	0.000125	7.0	29.3
1.16	0.0085	0.000229	7.0	26.9
2.21	0.0128	0.000435	7.0	34.0
3.04	0.0170	0.00060	7.0	35.3
6.85	0.0340	0.00136	7.0	40.0

6.3.2 XAFS Experiments

The X-ray absorption fine structure for the Ni-kaolinite systems are shown in Fig. 6.3. The first shell for all samples consisted of approximately six oxygens coordinating the Ni at 2.01 Å. A second shell was discerned consisting of Al/Si at 2.93 Å. Futher analysis revealed a third and fourth shell consisting of Ni and Al/Si at 3.05 Å and 3.63 Å, respectively. Finally, a fifth shell was observed consisting of Ni at 4.01 Å. Coordination numbers varied with samples and are less accurate in discerning structural environments than bond distances. XAFS cannot distinguish between Al and Si due to similar atomic numbers. However, possible sites for Ni sorption can be inferred based on crystallographic parameters. Consolidating the structural parameters derived from the isolated shells resulted in a good fit of the predicted and experimental functions for all samples (Fig. 6.4).

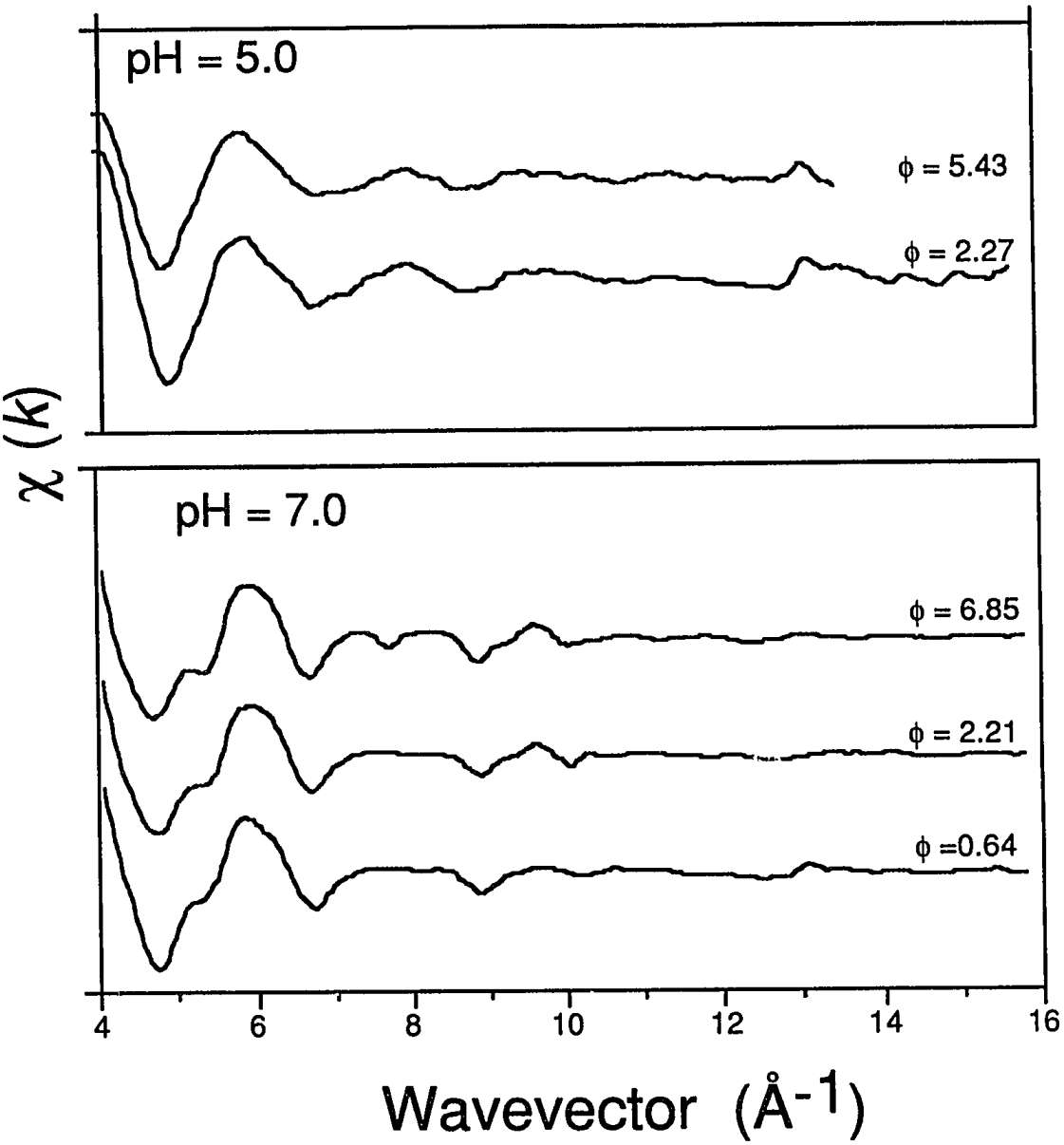

Figure 6.3 Experimental XAFS spectra of Ni(II) sorbed on kaolinite.

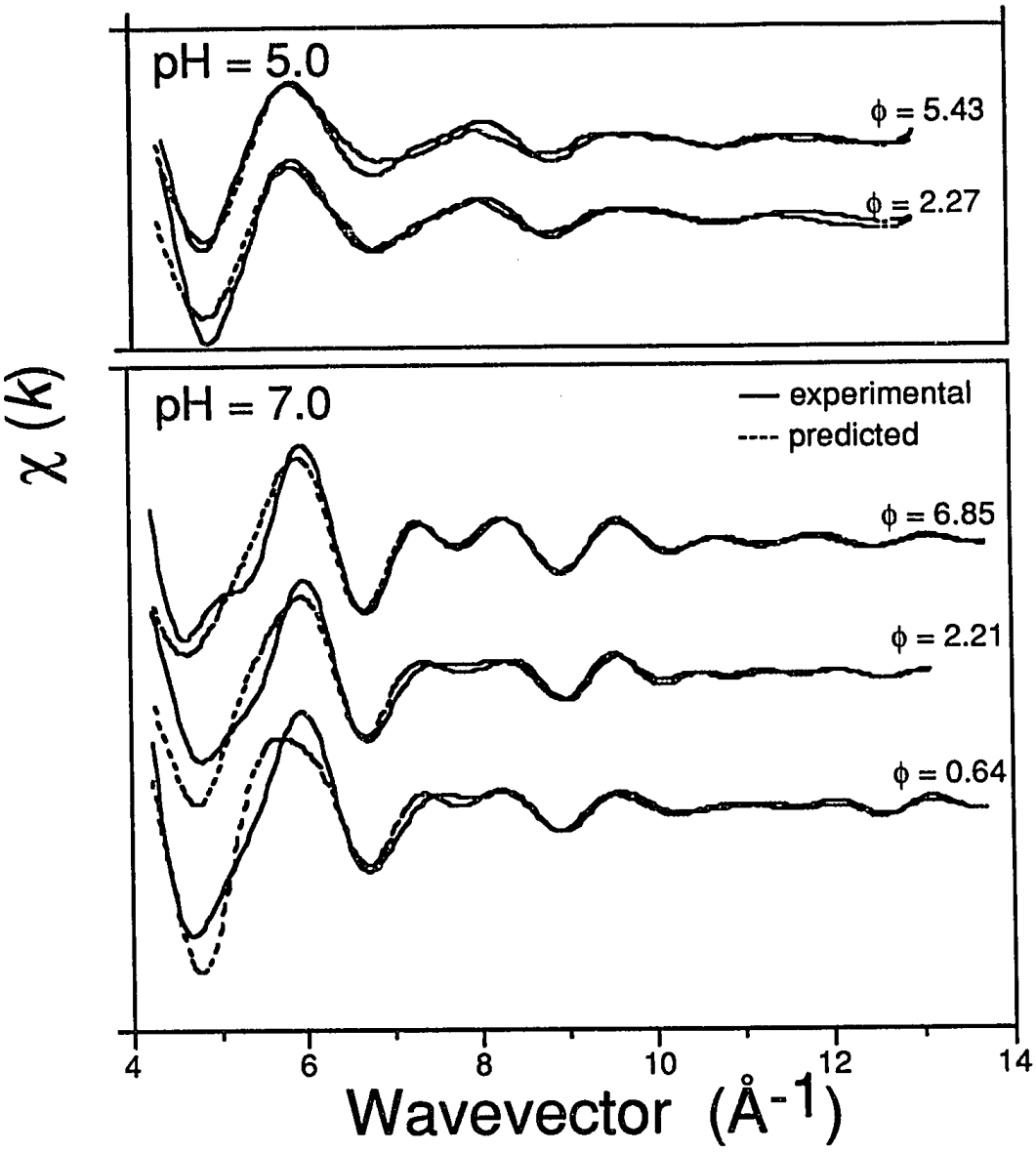

Figure 6.4 **Fit of the experimental XAFS spectra in Fig. 6.3 with parameters obtained from analysis of the isolated shells.**

Base on the bond distances obtained from XAFS and crystallographic considerations, possible modes of Ni attachment to the kaolinite surface can be inferred (Fig. 6.5). Site (i) consists of a bidentate mononuclear complex between edges of the Ni octahedra and Al octahedra. Site (ii) consists of a binuclear bidenate complex between two Al octahedra near an Al vacancy. Finally site (iii) consists of a binuclear bidentate complex between an exposed Si and Al edge. Based on bond distances it would be unlikely that site (iii) would form. The bond distances obtained from XAFS for site (i) and (ii) (2.93 Å and 3.63 Å, respectively) are in close agreement with those calculated for the kaolinite sites based on crystallographic considerations (2.90 Å and 3.64 Å, respectively). Therefore, both site (i) and (ii) may be involved with Ni sorption. However, site (ii) may be more reactive because the surface group is coordinatively less saturated due to the Al vacancy. Finally, monodenate surface complexes are possible although XAFS was unable to detect any.

Multinuclear sorption was detected for all samples indicating the presence of a precipitate. The presence of Ni at 3.05 Å (edge sharing) and 4.01 Å (corner sharing) indicated that the precipitate was similar to $Ni(OH)_2(s)$. Figure 6.5 dipicts the multinuclear complex extending away from the surface of the kaolinite.

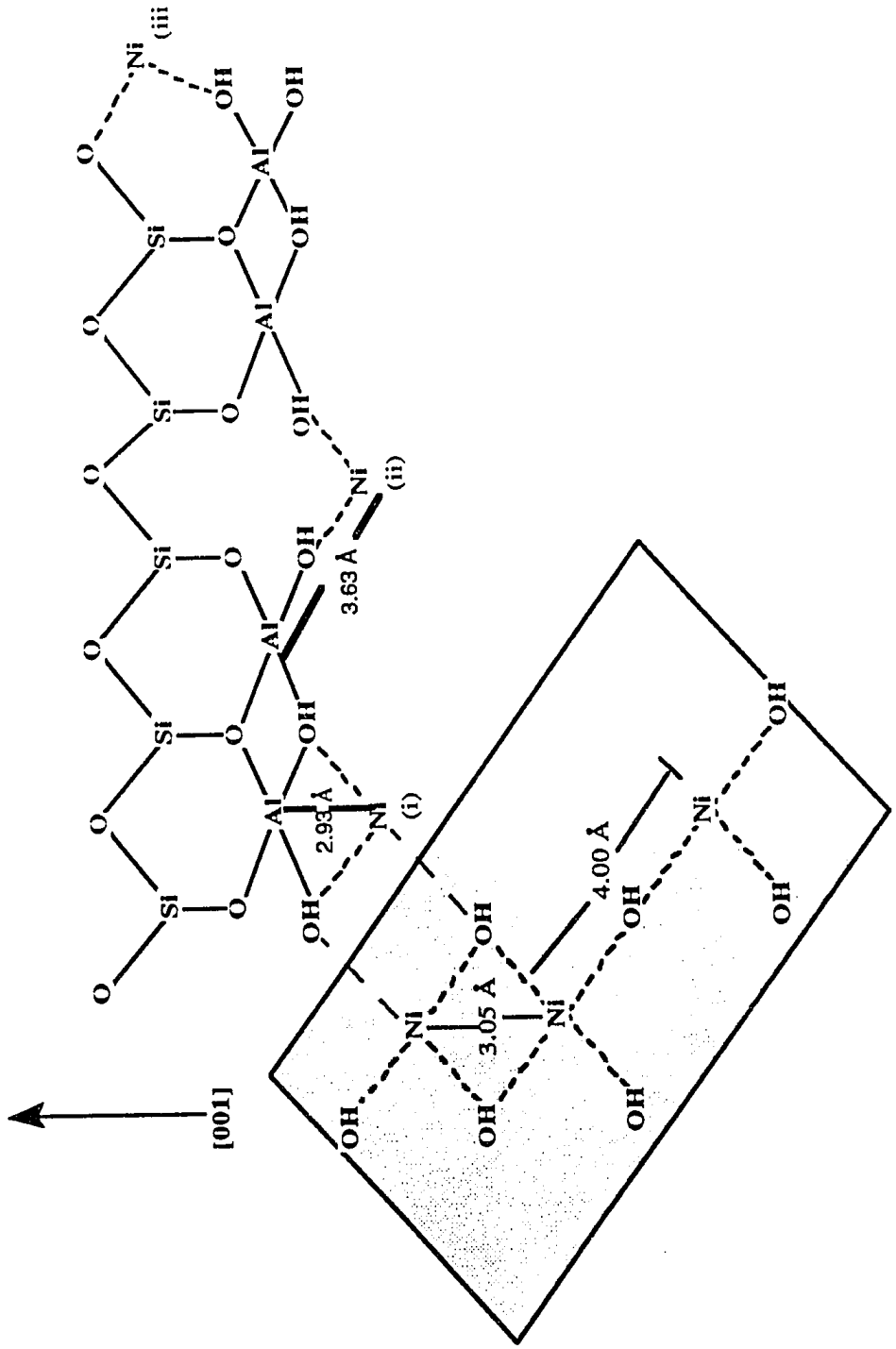

Figure 6.5 Dipiction of the surface structure derived by XAFS and possible surface sorption sites.

6.3.3 TEM Experiments

Transmission electron microscopy and EDS revealed the presence of isolated clusters of Ni rich regions (Fig. 6.5). These regions were only observed at the higher loadings for each pH and were randomly distributed on kaolinite particles. Clusters of Ni rich regions may be present at the lower loading rates, however, this may be below the detection of the TEM/EDS.

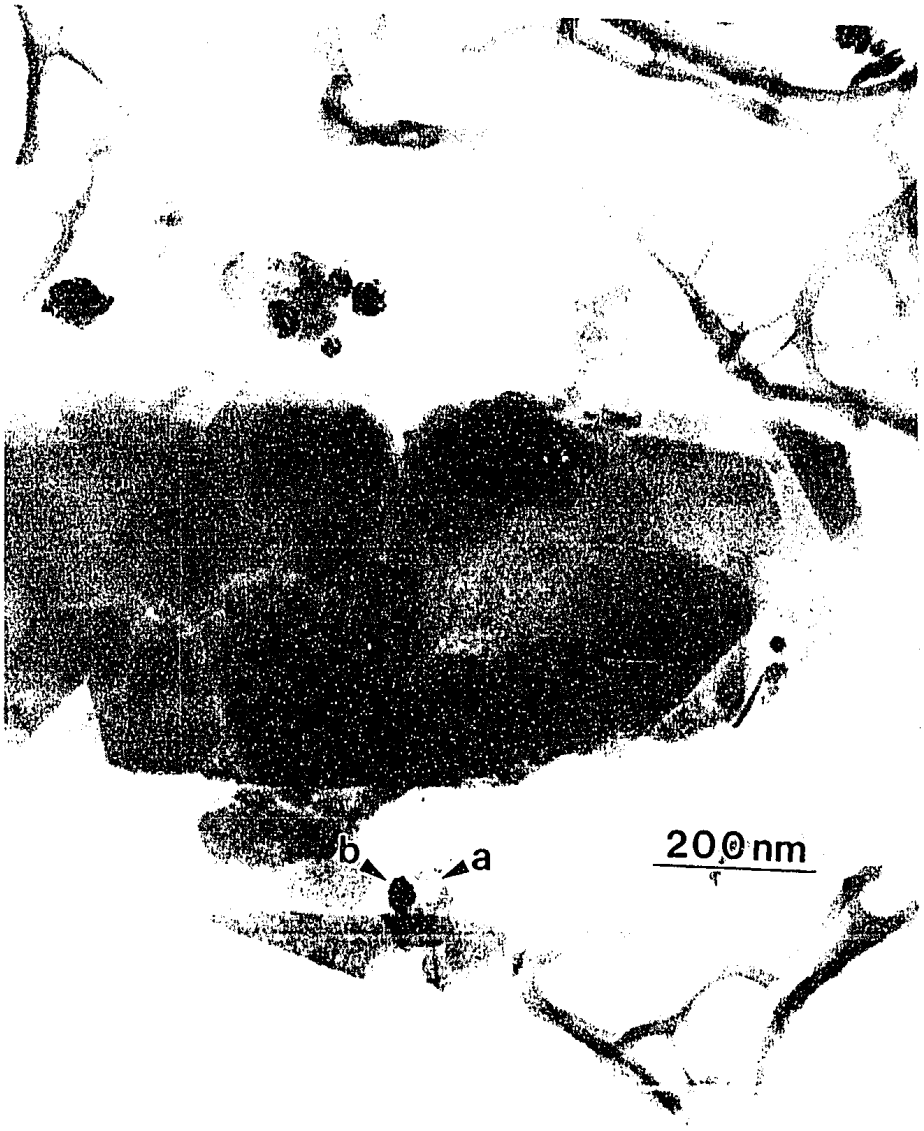

Figure 6.6 TEM image of kaolinte reacted with .034 M Ni (ϕ=6.85) showing a Ni rich cluster a) next to a Ti particle.

6.4 Discussion

XAFS results indicate that Ni(II) forms an inner sphere bidentate surface complex on kaolinite. Based on bond distances and crystallographic considerations a depiction of the surface structure was developed (Fig. 6.5). Three possible sites of sorption on the kaolinite surface were proposed (Fig. 6.5). However, based on bond distances and reactivity of the surface groups site (ii) was determined to be the dominant site for Ni sorption. At all coverages and both pHs multinuclear complexes occurred with structures similar to $Ni(OH)_2(s)$. Surface precipitation of Ni on kaolinite occurred at less than monolayer coverages and in solutions only slightly saturated with respect to $Ni(OH)_2(s)$. Similar results were obtained with the sorption of Co(II) on kaolinite (O'Day et al., 1994). Additionally, TEM results from the highest loading rates indicated that the Ni forms isolated clusters or islands that are not evenly distributed over the surface of the kaolinite. Therefore, the kaolinite surface promotes hydrolysis and the formation of multinuclear complexes.

6.5 Conclusions

Understanding metal sorption mechanisms are important for determining their fate and mobility in the environment. Atomic level investigations provide a greater description of the sorption mechanism than macroscopic techniques and therefore allow one to more accurately model a metal's fate and potentially mobility. However, an inner sphere multinuclear sorption mechanism does not preclude a metal's mobility in the subsurface. Differences in precipitate solubilities as well as sorbent surfaces will influence a metal's mobility. Additionally, the CELSS present on the lunar surface will involve small acreages of land that are intensively cropped.

Organic and inorganic ligands secreted by plants and microbes in the rhizosphere can potentially poison crystal growth or dissolve a precipitate. These factors will influence a metal's solubility and hence toxicity and mobility in a plant growth environment.

6.6 References

Bloom, P.R. and M.B. McBride. 1979. Metal ion binding and exchange with hydrogen ions in acid-washed peat. Soil Sci. Soc. Am. J. 43:687-692.

Carroll-Webb, S.A., and J.V. Walther. 1988. A surface complex reaction model for the pH-dependence of corundum and kaolinite dissolution rates. Geochim. Cosmochim. Acta 52:2609-2623.

Emmerich, W.E., L.J. Lund, A.L. Page, and A.C. Chang. 1982a. Solid phase forms of heavy metals in sewage sludge-treated soils. J. Environ. Qual. 11:178-181.

Emmerich, W.E., L.J. Lund, A.L. Page, and A.C. Chang. 1982b. Predicted solution phase forms of heavy metals in sewage sludge-treated soils. J. Environ. Qual. 11:182-186

Fendorf, S.E., and D.L. Sparks. 1994. Mechanisms of chromium(III) sorption on silica. 2. Effect of reaction conditions. Environ. Sci. Technol. 28:290-297

Fendorf, S.E., G.M. Lamble, M.G. Stapleton, M.J. Kelley, and D.L. Sparks. 1994. Mechanisms of chromium(III) sorption on silica. 1. Cr(III) surface structure derived by extended X-ray absorption fine structure spectroscopy. Environ. Sci. Technol. 28:284-289.

Harter, R.D. 1983. Effect of soil pH on adsorption of lead, copper, zinc, and nickel. Soil Sci. Soc. Am. J. 47:47-51.

Hossner, L.R., and E.R. Allen. 1989. Nutrient availability and element toxicity in lunar-derived soils pp. 85-92. *In* D.W. Ming and D.L. Henninger (eds.), Lunar base agriculture: Soils for plant growth. Soil Science Society of America, Madison, WI.

Jackson, M.L. 1969. Soil chemical alanysis. M.L. Jackson, Madison, W.I

Lamble, G.M., and S.M. Heald. 1991. Operation of a dynamically bent sagittally focusing double crystal monochromator for XAFS studies. Rev. Sci. Instrum. 63: 880-884.

McKenzie, R.M. 1967. The sorption of cobalt by Mn minerals in soils. Aust. J. Soil Res. 5:235-246.

O'Day, P.A., G.A. Parks, G.E. Brown, Jr. 1994. Molecular structure and binding sites of cobalt(II) surface complexes on kaolinite from X-ray absorption spectroscopy. Clays and Clay Minerals.42:337-355.

Patterson, J.B.E. 1971. Nickel toxicity in small grains. pp. 193-207. In D.C. Pratt (ed.), Trace elements in soils and crops. MAFF Tech. Bull. No. 21. HMSO.

Rehr, J. J., R. C. Albers, and S.I. Zabinsky. 1992. High-order multiple-scattering calculations of x-ray absorption fine structure. Phys. Rev. Lett. 69: 3397-3400.

Schulthess, C.P. and C.P. Huang. 1990. Adsorption of heavy metals by silicon and aluminum oxide surfaces on clay minerals. Soil Sci. Soc. Am. J. 54:679-688.

Sims, J.T. and J.S. Kline. 1991. Chemical fractionation and plant uptake of heavy metals in soils amended with co-composted sewage sludge. J. Environ. Qual. 20:387-395.

Slingsby, D.R. and D.H. Brown. 1977. Nickel in British serpentine soils. J. Ecol. 65:597-618.

Sposito, G., C.S. LeVesque, J.P. LeClaire, and A.C. Chang. 1983. Trace metal chemistry in arid-zone field soils amended with sewage sludge: III. Effect of time on the extraction of trace metals. Soil Sci. Soc. Am. J. 47:898-902.

Sposito, G., K.M. Holtzclaw, C.S. LeVesque, and C.T. Johnston. 1982a. Trace metal chemistry in arid-zone field soils amended with sewage sludge: II. Comparative study of the fulvic acid fraction. Soil Sci. Soc. Am. J. 46:265-270.

Sposito, G., L.J. Lund, and A.C. Chang. 1982b. Trace metal chemistry in arid-zone field soils amended with sewage sludge: I. Fractionation of Ni, Cu, Zn, Cd, and Pb in solid phases. Soil Sci. Soc. Am. J. 46:260-264.

Uren, N.C. 1992. Forms, reactions, and availability of nickel in soils. In D.L. Sparks (ed.), Advances in Agronomy, Vol 48. Academic Press, New York.

Welch, R.M. 1981. The biological significance of nickel. J. Plant Nutr. 3:345-356.

Chapter 7

SUMMARY AND CONCLUSIONS

7.1 Introduction

The overall objective of my dissertation research was to provide data to determine if Cr and Ni present in lunar soils will be released at concentrations and forms that may be toxic to plants and animals. This objective was not easily answered with only three years of research conducted with simulated lunar minerals. However, results obtained from my research will provide insight and pose challenges that will help to satisfy the above objective.

The first part of my research examined the effect of experimental conditions on the dissolution kinetics of the two lunar simulants. Reductions in pH and the presence of naturally occurring organic acids are often found in rhizosphere environments. In my research we examined the effect of these two conditions separately. Organic acids were buffered at pH 7 to separate the influence of pH on dissolution, from that of the organic molecule. The effect of pH was examined at levels that may be encountered in the rhizosphere.

Originally we had hoped to quantify the release of Cr and Ni present in the lunar simulants. However, upon receiving the two lunar simulants it became clear that the concentration of these elements was too low to be practically quantified. We decided to proceed with the dissolution studies because we felt that the information gained from them would provide important insight into the dissolution mechanism of

lunar minerals. Additionally, information on secondary weathering products is important for modeling and establishing plant growth experiments.

The two lunar simulants used in the dissolution experiments (Minnesota basalt and high Ti glass simulant) proved to be extremely different in their bulk composition and structure, which is characteristic of the various materials found in the lunar regolith. These differences were clearly shown in studies on the kinetics and mechanism of dissolution for these two materials.

7.2 Dissolution Experiments

The dissolution mechanism of the glass simulant for the pH experiments involved a coupled ion-exchange/hydrolysis reaction. Reactive solutes (H^+ or $H3O^+$) diffuse into the bulk glass and are involved in hydration, hydrolysis, and ion exchange reactions. Network modifying cations such as Ca^{2+}, Mg^{2+}, and Fe^{2+} are released via ion exchange reactions, while Al is released via hydrolysis. These reactions create a leached layer that is rich in Si and Ti. This leached layer causes the parabolic release of cations observed during the dissolution studies. Extensive leaching of the glass will cause the Si/Ti rich leached layer to repolymerize, creating a porous Si network which is no longer a diffusional barrier to the release of cations.

For the organic acids the mechanism is similar although not quite as extensive. The organic acids create a Si/Ti rich leached layer through a two step process that involves chemisorption of the organic acid and the chelating ability of the molecule. The chemisorbed organic ligand is a π-donor ligand which pushes electron density toward the framework of the glass. This increases the electron density around the metal-oxygen bond which subsequently weakens the glass framework making it more susceptible to hydrolysis. The second step involves the chelating ability of the

organic ligand. Chelation of metal ions in solution by the organic ligand will reduce their activity and subsequently increase their rate of diffusion from the bulk glass.

Both reductions in pH and the presence of organic acids accelerate the dissolution of the simulated lunar glass creating a altered or leached layer that is rich in Si and Ti. Upon drying, this leached layer will craze or crack and begin to flake off from the bulk glass. As the glass is re-wetted, new surfaces will be exposed to the solution, beginning the dissolution process again. Subsequent wetting and drying cycles may speed up the dissolution of lunar glasses.

In contrast to the glass, the mechanism of dissolution observed for the Minnesota basalt involved a surface reaction that occurred at high energy sites such as cleavage planes, fluid inclusions, and crystal dislocations. The kinetics of dissolution will depend on the crystal structure of the minerals present in the basalt. Minerals such as olivine that are single silica tetrahedra held together by ionic forces will weather much more rapidly than ilminite or feldspars. Dissolution at these sites of excess energy will exfoliate and fragment the mineral, reducing particle size and increasing surface area. This may aid in decreasing the bulk density and increasing the water retention properties of the lunar regolith.

The organic acids and reactive solutes (H^+ or $H3O^+$) dissolve the minerals present in the basalt in a similar manner to the glass. These agents are involved in surface reactions that increase electron density around the metal oxygen bond in the framework of the mineral, which makes it more susceptible to hydrolysis reactions and subsequent dissolution. Sites of high energy are perfect areas for these reactions to take place and are observed as etch pits on the surface of these minerals.

The fate of released elements resulting from mineral dissolution will be manifold including complexation with organic and inorganic ligands, precipitation and

sorption. Precipitation of solid phases will play a dominant role in a CELSS, because they will be involved in sorption reactions that will affect the availability of nutrient elements. Ferric iron present in both lunar simulants was rapidly released during dissolution and should quickly precipitate as iron oxides when it is exposed to an oxygenated environment. These materials should dominate sorption reactions during the early stages of lunar regolith weathering and will affect the fate and availability of trace metals such as Cr and Ni.

From the lunar simulant dissolution studies, it can be concluded that rhizosphere conditions will accelerate the weathering of lunar soils. Organic acids that are released in the rhizosphere by plants and microbes will play a dominant role in dissolution through a reduction in pH and organic ligand surface and complexation reactions. The lunar regolith contains a host of materials (e.g. glass, minerals, breccias, and aglutinates) and their rates and mechanism of dissolution will vary, similar to the differences observed for the basalt and glass simulants. Therefore, a lunar soil dominated by one type of material may weather more rapidly and precipitate different minerals than another. This will make quantifying the release of Cr and Ni extremely difficult and studies on one type of mineral may not be directly transferable.

Understanding the fate and mobility of these elements in a plant growth environment may be a better approach to determining their potential toxicity to plants and animals. A metal that forms an insoluble precipitate may be of little concern from a toxicity standpoint even at high concentrations. Hence, the second part of my research focused on the sorption kinetics and mechanisms of Cr and Ni on secondary weathering products.

7.3 Sorption Experiments

The first sorption experiment involved determining the kinetics and mechanism of chromate sorption on goethite. Chromate was chosen because of its toxicity and mobility in soil environments compared to Cr(III). The presence of manganese oxides in the lunar regolith create the possibility of sorption and oxidation of released Cr. Goethite was chosen as the adsorbent because dissolution experiments suggested that Fe-oxides may precipitate from solution. Pressure-jump relaxation kinetics in conjunction with X-ray absorption fine structure (XAFS) were employed to determine the kinetics and mechanism of chromate adsorption/desorption at the goethite/water interface. Additionally, arsenate adsorption was examined as a comparison to chromate. Arsenate was chosen because of the differences between the two oxyanions (diprotic vs. triprotic acid).

P-jump experiments revealed a double relaxation for both oxyanions. We proposed that oxyanion adsorption involves a two step process that results in the formation of an inner-sphere bidentate surface complex. The first step involves an initial ligand exchange reaction of the aqueous oxyanion ($HCrO4^-$ or $H2AsO4^-$) with goethite, forming an inner-sphere monodentate surface complex. This first step produces the signals associated with the fast τ values. The next step involves a second ligand exchange reaction, resulting in the formation of an inner-sphere bidentate surface complex. This step produces the signal associated with the slow τ values.

Our proposed mechanism fit our experimental data well. It was determined that desorption rate constants were slower than adsorption rate constants and therefore rate-limiting. Calculated equilibrium constants from rate constants for each step of the reaction indicated that the formation of bidentate surface complexes for both oxyanions were thermodynamically favorable. However, K_{eq} (for step II) for

chromate was only slightly greater than one suggesting that the formation of a bidentate surface complex, although thermodynamically favorable, may be less likely to form than a monodentate surface complex. Finally, equilibrium constants calculated kinetically compared well with those calculated using the CCM and the computer code FITEQL only for the formation of the monodenatate surface complex. Equilibrium constants for the overall formation of the bidentate surface complex were much smaller than those calculated using the CCM. These differences may be due to the presence of more elementary steps in going from step I to step II than can be measured with the p-jump, which would increase the overall equilibrium constant.

XAFS experiments indicated that arsenate formed predominately bidentate surface complexes while chromate formed a combination of mono- and bidenate surface complexes. These results are in agreement with our p-jump results and help to explain differences in equilibrium constants observed for Step II of the proposed mechanism for chromate. These results are also consistent with other researchers results that suggest that chromate is mobile in soil environments (Zachara et al., 1988; Stollenwerk and Grove, 1985). It would be expected that monodentate surface complexes would be more easily desorbed than bidentate surface complexes among similar species. Differences in surface complexes between chromate and arsenate may be related to the charge of the molecule. The greater charge of arsenate versus chromate (-3 vs. -2) may create a greater attraction of the arsenate molecule for the goethite surface making the formation of bidentate surface complexes more likely. However, differences in loading rates and mineral surfaces may have a dominating influence on the type of surface complex formed.

The above results suggest that although chromate is specifically adsorbed by goethite it may be more mobile in soil environments than other oxyanions such as

arsenate and phosphate. In the CELSS the addition of phosphate as a fertilizer source may desorb any chromate making it available for uptake by plants or microbes. Therefore, determining sorption mechanisms is of paramount importance in modeling the fate and mobility of trace elements. Just because a molecule is specifically adsorbed does not preclude its mobility is soil environments.

The second sorption experiment involved investigating the mechanism of Ni sorption on kaolinite. XAFS was employed to examine the local structural environment of the sorbed Ni while TEM was used to determine its spatial resolution. Results indicated that Ni sorbs via an inner sphere bidenate surface complex followed by nucleation and formation of a $Ni(OH)_2(s)$ precipitate. TEM results indicated that this precipitate forms clusters or islands on the surface of the kaolinite. These results suggest that Ni released during the weathering of the lunar regolith may be sorbed and form precipitates on the surfaces of secondary weathering products. This may reduce the quantity of Ni present in the soil solution thus limiting its toxicity. However, the presence of organic and inorganic ligands may poison crystal growth or dissolve precipitates. Additionally, more soluble polymorphs may precipatate on different solid surfaces. These factors may increase the concentration of Ni in the soil solution.

In summary, lunar materials will weather rapidly when exposed to terrestrial weathering conditions. Weathering may be even more extensive in the presence of plant root rhizospheres due to the reduction in pH and the presence of organic ligands. Release of Cr and Ni present in the simulants will occur however, the concentration released into the soil solution will depend on the type of mineral and the quantity of metal present. The fate of the released metal is manyfold including oxidation, sorption, co-precipitation, precipitation, and uptake by plants and microbes. The toxicity of Cr and Ni released into the CELSS environment will be ultimately tied

to these reactions. Therefore, in order to fully discern the toxicity of released metals in the CELSS environment, further research is necessary. Understanding the fate of Cr and Ni in the presence of rhizosphere exudates such as organic acids is especially important for modeling the fate of these metals in a plant growth environment.

7.4 References

Zachara, J.M., C.E. Cowan, R.L. Schmidt, and C.C. Ainsworth. 1988. Chromate adsorption on kaolinite. Clays Clay Miner. 36:317-326.

Stollenwerk, K.G. and D.B. Grove. 1985. Adsorption and desorption of hexavalent chromium in an alluvial aquifer near Telluride, Colorado. J. Environ. Qual. 14:150-155.

Biblography

Aagaard, P. and H.C. Helgeson. 1982. Thermodynamic and kinetic constraints on reaction rates among minerals and aqueous solutions. I. Theoretical considerations. Amer J. Sci. 282:237-285

Ainsworth, C.C., D.C. Girvin, J.M. Zachara, and S.C. Smith. 1989. Chromate adsorption on geothite: effects of aluminum substitution. Soil Sci. Soc. of Am. J. 53:411-419.

Allison, J.D., D.S. Brown , and K.J. Novo-Gradac 1991. MINTEQA2/PRODEFA2, a geochemical assesment model for environmental systems: version 3.0 user's guide. Environmental Research Laboratory Office of Research and Development. U.S. EPA, Athens, GA.

Amacher, M.C. 1991. Methods of obtaining and analyzing kinetic data. pp. 19-59. In D.L Sparks and D.L. Suarez (eds.) Rates of Soil Chemical Processes. SSSA Spec. Publ. 27, Soil Science Society of America, Madison, Wisconsin.

Amrhein, C. and D.L. Suarez. 1988. The use of a surface complexation model to describe the kinetics of ligand-promoted dissolution of anorthite. Geochim. Cosmochim. Acta. 52:2785-2793.

Antweiler, R.C. and J.I. Drever. 1982. The weathering of a late Tertiary volcanic ash: importance of organic solutes. Geochim. Cosmochim. Acta 47:623-629.

Ashida, M., M. Sasaki, H. Kan, T. Yasunaga, K. Hachiya, and T. Inoue. 1978. Kinetics of proton adsorption-desorption at TiO_2-H_2O interface by means of the pressure-jump technique. J. Colloid Interface Sci. 71:219-225.

Astumian, R. D., M. Sasaki, T. Yasunaga, and Z. A. Schelly. 1981. Proton adsorption-desorption kinetics on iron oxides in aqueous suspensions using the pressure-jump method. J. Phys. Chem. 85:3832-3835.

Averner, M.M. 1989. Controlled ecological life support system. pp. 145-153. *In* D.W. Ming and D.L. Henninger (eds.), Lunar base Agriculture: Soils for Plant Growth. Soil Science Society of America, Madison, WI.

Baes, C.F., Jr. and R.E. Mesmer. 1976. The hydrolysis of cations. Wiley-Interscience, New York, pp. 211-220.

Barman, A.K., C. Varadachari, and K. Ghosh. 1992. Weathering of silicate minerals by organic acids. I. Nature of cation solubilisation. Geoderma. 53:45-63.

Barrer, R.M. and J. Klinowski . 1975. Hydrogen mordenite and hydronium mordenite. J. Chem. Soc. Faraday Trans. 71:690-698.

Bartlett, R.J. and B.R. James. 1988. Mobility and bioavailabilty of chromium in soils. pp. 267-303. In J.O. Nriagu and E. Nieboer (eds.), Chromium in the natural and human environments. John Wiley and Sons, NY.

Benjamin, M.M., and J.O. Leckie. 1981. Conceptual model for metal-ligand-surface interactions during adsorption. Environ. Sci. Tech. 15:1050-1056.

Bennett, P.C., M.E. Melcer, D.I. Siegel, and J.P. Hassett. 1988. The dissolution of quartz in dilute aqueous solutions of organic acids at 25°C. Geochim. Cosmochim. Acta 52:1521-1530.

Berger, G.,J. Schott and M. Loubet . 1987. Fundamental processes controlling the first stage of alteration of a basalt glass by seawater: an experimental study between 200 and 320°C. Earth Planet. Sci. Lett. 84:431-445.

Bernasconi, C.F. 1976. Relaxation kinetics. Academic Press, New York.

Berner, R. A. and G.R. Holdren, Jr. 1979. Mechanism of feldspar weathering-II. Observations of feldspars from soils. Geochim Cosmochim. Acta 43:1173-1186.

Berner, R.A. 1978. Rate control of mineral dissolution under earth surface conditions. Amer. J. Sci. 278:1235-1252.

Berner, R.A. and G.R. Holdren, Jr. 1977. Mechanisms of feldspar weathering: Some observational evidence. Geology 5:369-372.

Berner, R.A. and J. Schott. 1982. Mechanism of pyroxene and amphibole weathering II. observations of soil grains. Amer. J. Sci. 282:1214-1231.

Berner, R.A., G.R. Holdren, Jr., and J. Schott. 1985. Protective surface layers on dissolving silicates. Comments on the paper "Study of the weathering of albite at room temperature and pressure with a fluidized bed reactor" by L. Chou and R. Wollast (Geochim. Cosmochim. Acta 48:2205-2217, 1984), Geochim. Cosmochim. Acta 49:1657-1658.

Bloom, P.R. and M.B. McBride. 1979. Metal ion binding and exchange with hydrogen ions in acid-washed peat. Soil Sci. Soc. Am. J. 43:687-692.

Boksay , Z. and G. Bouquet. 1975. On the reaction of water molecules with the silicate network in the glass phase.Phys. Chem. Glasses 16:81-82.

Boksay, Z., G. Bouquet, and S. Dobos. 1967. Diffusion processes in the surface layer of glass. Physics Chem. Glasses 8:140.

Boyle, J.R., G.K. Voigt, and B.L. Sawhney. 1974. Chemical weathering of biotite by organic acids. Soil Sci. 117:42-45.

Bunker, B.C., D.R. Tallant, T.J. Headley, G.L. Turner and R.J. Kirkpatrick 1988. The structure of leached sodium borosilicate glass. Phys. Chem. Glasses 29:106-120.

Bunker, B.C., G.W. Arnold, E.K. Beauchamp, and D.E. Day 1983. Mechanisms for alkali leaching in mixed-Na-K silicate glasses. J. Non-Crystalline Solids 58:295-322.

Busenberg, E. 1978. The products of the interaction of feldspars with aqueous solutions at 25°C. Geochim. Cosmochim. Acta 42:1679-1686.

Busenberg, E. and C.V. Clemency. 1976. The dissolution kinetics of feldspars at 25° C and 1 atm. CO_2 partial pressure. Geochim. Cosmochim. Acta 40:41-49.

Carroll-Webb, S.A., and J.V. Walther. 1988. A surface complex reaction model for the pH-dependence of corundum and kaolinite dissolution rates. Geochim. Cosmochim. Acta 52:2609-2623.

Casey, W.H., and B.C. Bunker.1990. Leaching of mineral and glass surfaces during dissolution. *In* M.F. Hochella, Jr. and A.F. White (eds.) Mineral-Water Interface Geochemistry. Rev. in Mineral. 23:397-426.

Casey, W.H., H.R. Westrich, and G.W. Arnold. 1988. Surface chemistry of labradorite feldspar reacted with aqueous solutions at pH= 2, 3, and 12. Geochim. Cosmochim. Acta 52:2795-2807.

Casey, W.H., H.R. Westrich, G.W. Arnold, and J.F .Banfield. 1989. The surface chemistry of dissolving labradorite feldspar. Geochim. Cosmochim. Acta 53:821-832.

Charlet, L. and A. Manceau. 1993. pp. 117-164. Structure, formation, and reactivity of hydrous oxide particles: Insights from X-ray absorption spectroscopy. In J. Buffle and H.P. van Leeuwen (ed.), Environmental Particles. Vol. 2. Lewis Publishers, Boca Raton.

Charlet. L., and A. Manceau.1992. X-ray absorption spectroscopic study of the sorption of Cr(III) at the oxide/water interface. II. Adsorption, coprecipatation and surface precipitation on ferric hydrous oxides. J.Colloid. Interface Sci. 148:443-458

Chisholm-Brause, C.J., P.A. O'Day, G.E. Brown, Jr., and G.A. Parks. 1990. Evidence for multinuclear metal-ion complexes at the solid/water interfaces from X-ray absorption spectroscopy. Nature. 349:528-530.

Chou, L. and R. Wollast. 1984. Study of the weathering of albite at room temperature and pressure with a fluidized bed reactor. Geochim. Cosmochim. Acta 48:2205-2217.

Chou, L. and R. Wollast. 1985. Study of the weathering of albite at room temperature and pressure with a fluidized bed reactor. Reply to comment by R.A. Berner, G.R. Holdren, Jr., and J. Schott. Geochim. Cosmochim. Acta 49:1659-1660.

Correns, C.W. 1940. Die chemische verwitterrung der silikate. Naturwissenschaften 28:369-376.

Correns, C.W. 1961. The experimental chemical weathering of silicates. Clay Min. Bull. 4:249-281.

Correns, C.W. 1963. Experiments on the decompositon of silicates and discussion of chemical weathering. Clays Clay Minerals 10:443-459.

Correns, C.W. and W. Von Engelhardt. 1938. Neue Untersuchungen ueber die Verwitterung des Kalifeldspates. Chemie der Erde 12:1-22.

Crovisier, J.L. , J. Honnorez, and J. P. Eberhart 1987. Dissolution of basaltic glass in seawater: Mechanisms and rate. Geochim. Cosmochim. Acta 51: 2977-2990.

Dent, A.J., J.D.F. Ramsey, and S.W. Swanton. 1992. An EXAFS study of uranyl ion in solution and sorbed onto silica and montmorillonite clay colloids. J. Colloid. Interface Sci. 150: 45-60.

Dibble, W.E., Jr. 1981. Non-equilibrium water/rock interaction. I. Model for interface-controlled reactions. Geochim Cosmochim Acta 45:79-92.

Doremus, R.H. 1975. Interdiffusion of hydrogen and alkali ions in a glass surface J. Non-Crystalline Solids 19:137.

Douglas, R.W. and T.M. El-Shamy. 1967. Reactions of glasses with aqueous solutions. J. Am. Ceram. Soc. 50:1-8.

Duff, R.B., D.M. Webley, and R.O. Scott. 1963. Solubilization of minerals by 2-ketogluconic acid-producing bacteria. Soil Sci. 95:105-114.

Duke, M.B., W.W. Mendell, and B.B. Roberts. 1985. pp. 57-68. Strategies for a permanent lunar base. In W.W. Mendell (ed.), Lunar bases and space activities of the 21st Century. Lunar and Planetary Institute, Houston

Eary, L.E., and D.Rai. 1987. Kinetics of chromium(III) oxidation to chromium(VI) by reaction with manganese dioxide. Environ. Sci. Technol. 21:1187-1193.

Eckhardt, F.E.W. 1985. Solubilization, transport, and deposition of mineral cations by microorganisms-efficient rock weathering agents. p. 161-173. *In* J.I. Drever (ed.) The Chemistry of Weathering. Reidel Publishers, Boston.

Eigen, M., and K. Tamm. 1962. Schallabsorption in elektrolytloesungen als folge chemischer relaxation. Z. Elektrochem. 66:93-121.

El-Shamy, T.M., J. Lewins and R.W.Douglas, 1972. The dependence on the pH of the decomposition of glasses by aqueous solutions. Glass. Tech. 13:81-87.

Emmerich, W.E., L.J. Lund, A.L. Page, and A.C. Chang. 1982a. Solid phase forms of heavy metals in sewage sludge-treated soils. J. Environ. Qual. 11:178-181.

Emmerich, W.E., L.J. Lund, A.L. Page, and A.C. Chang. 1982b. Predicted solution phase forms of heavy metals in sewage sludge-treated soils. J. Environ. Qual. 11:182-186

Eyring, H. 1935a. The activated complex in chemical reactions. J. Chem. Phys. 3:107-120.

Eyring, H. 1935b. The activated complex and the absolute rate of chemical reactions. Chem. Rev. 17:65-82.

Fendorf, S.E., and D.L. Sparks. 1994. Mechanisms of chromium(III) sorption on silica. 2. Effect of reaction conditions. Environ. Sci. Technol. 28:290-297

Fendorf, S.E., G.M. Lamble, M.G. Stapleton, M.J. Kelley, and D.L. Sparks. 1994. Mechanisms of chromium(III) sorption on silica. 1. Cr(III) surface structure derived by extended X-ray absorption fine structure spectroscopy. Environ. Sci. Technol. 28:284-289.

Fendorf, S.E., M. Fendorf, D.L. Sparks, and R. Gronsky. 1992. Inhibitory mechanisms of Cr(III) oxidation by ß-MnO_2. J. Colloid Interface Sci. 153:37-54.

Fendorf, S.E., P. R. Grossl, D.L. Sparks, and G. M. Lamble. 1993. Oxyanion surface structures on goethite. Agronomy Abstracts. p.344. American Society of Agronomy, Madison, WI.

Furrer, G. and W. Stumm. 1986. The coordination chemistry of weathering: I. Dissolution kinetics of Al_2O_3 and BeO. Geochim. Cosmochim. Acta 50:1847-1860.

Glasstone, S., K. Laidler, and H. Eyring. 1941. The theory of rate processes. McGraw-Hill, New York.

Goldberg, S. 1986. Chemical modeling of arsenate adsorption on aluminum and iron oxide minerals. Soil Sci. Soc. Am. J. 50:1154-1157.

Gossens, D.A., J.G. Philippaerts, R. Gijbels, A.P. Pijpers, S. Van Tendeloo, and E. Althaus. 1989. A SIMS, XPS, SEM, TEM, FTIR study of feldspar surfaces after reacting with acid solutions. p. 271-274. *In* D.L. Miles (ed.) Water-Rock Interaction WRI-6. A.A. Balkema, New York.

Grandstaff, D.E. 1977 Some kinetics of bronzite orthopyroxene dissolution. Geochim. Cosmochim. Acta 41:1097-1103.

Grandstaff, D.E. 1978. Changes in surface area and morphology and the mechanism of forsterite dissolution. Geochim. Cosmochim. Acta 42:1899-1901.

Graustein, W.C. 1975. On chemical weathering and forests. Geol. Soc. Amer. Abst. 7:1090-1091.

Grossl, P.R. and W.P. Inskeep 1992. Kinetics of octacalcium phophate crystal growth in the presence of organic acids. Geochim. Cosmochim. Acta 56:1955-1961.

Grossl, P.R., D.L. Sparks, and C.C. Ainsworth. 1994. Rapid kinetics of Cu(II) adsorption/desorption on goethite (α-FeOOH). Environ. Sci. Tech. 28:1422-1429.

Hachiya, K., M. Sasaki, T. Ikeda, N. Mikami, and T. Yasunaga. 1984. Static and kinetic studies of adsorption-desorption of metal ions on a γ-Al_2O_3 surface. 2. Kinetic study by means of pressure-jump technique. J. Phys. Chem. 88:27-31.

Harter, R.D. 1983. Effect of soil pH on adsorption of lead, copper, zinc, and nickel. Soil Sci. Soc. Am. J. 47:47-51.

Hayes, K. 1987. Equilibrium, spectroscopic, and kinetic studies of ion adsorption at the oxide/aqueous interface. Ph.D. diss. Stanford Univ., Stanford, CA (Diss. Abstr. 87-23104).

Hayes, K.F., A.L. Roe, G.E. Brown, K.O. Hodgson, J.O. Leckie, and G.A. Parks. 1987. X-ray absorption study of surface complexes: Selenium oxyanions on αFeOOH. Science 238: 52-56.

Hayes, K.F., and J.O. Leckie. 1986. Mechanism of lead ion adsorption at the goethite-water interface. p.114-141. In J.A. Davis and K.F. Hayes (ed.) Geochemical processes at mineral surfaces. Proc. Am. Chem. Soc. Symp. Ser. 323, Chicago, IL., 8-13 Sept. 1985. ACS, Washington , DC.

Helgeson, H.C., W.M. Murphy, and P. Aagaard. 1984. Thermodynamic and kinetic constraints on reaction rates among minerals and aqueous solutions. II. rate constants, effective surface area, and the hydrolysis of feldspar. Geochim. Cosmochim. Acta 48:2405-2432.

Helgeson, H.C.,1971. Kinetics of mass transfer among silicates and aqueous solutions. Geochim. Cosmochim. Acta 35:421-469.

Hellmann, R., C.M. Eggleston, M.F. Hochella, Jr., and D.A. Crerar. 1990. The formation of leached layers on albite surfaces during dissolution under hydrothermal conditions. Geochim. Cosmochim. Acta 54:1267-1281.

Hench, L.L. and D.E. Clark. 1979. Physical chemistry of glass surfaces. J. Non-Crystalline Solids 28:83-105.

Herbelin, A. L., and J. C. Westall. 1994. FITEQL. A computer program for the determination of chemical equilibrium constants from experimental data. Rep. 94-01, Oregon State University, Corvallis.

Hiemstra, T., J.C.M. DeWit, and W.H. Van Riemsdijk. 1989. Multisite proton adsorption modeling at the solid/solution interface of (hydr)oxides. A new approach : II. Application to various (hydr) oxides. J. Colloid. Interface Sci. 133:91-104.

Hingston, F. J., A. M. Posner, and J. P. Quirk. 1971. Competitive adsorption of negatively charged ligands on oxide surfaces. Discuss. Faraday Soc. 52:334-342.

Holdren, G.R. Jr., and J.E. Adams. 1982. Parabolic dissolution kinetics of silicate minerals: An artifact of nonequilibrium precipitation processes? Geology 10:186-190.

Holdren, G.R., Jr. and P.M. Speyer. 1985. pH dependent changes in the rates and stoichiometry of dissolution of an alkali feldspar at room temperature, Amer. J. Sci. 285:994-1026.

Holdren, G.R., Jr. and P.M. Speyer. 1987. Reaction rate-surface area relationships during the early stages of weathering. II. Data on eight additional feldspars. Geochim. Cosmochim. Acta 51:2311-2318.

Holdren, G.R., Jr. and R.A.Berner. 1979. Mechanism of feldspar weathering. I. Experimental studies. Geochim Cosmochim Acta 43:1161-1171.

Hossner, L.R., and E.R. Allen. 1989. Nutrient availability and element toxicity in lunar-derived soils. pp. 85-92. *In* D.W. Ming and D.L. Henninger (eds.), Lunar base agriculture: Soils for plant growth. Soil Science Society of America, Madison, WI.

Huang, W.H. and W.C. Kiang. 1972. Laboratory dissolution of plagioclase feldspars in water and organic acids at room temperature. Amer. Mineral. 57:1849-1859.

Huang, W.H. and W.D. Keller. 1970. Dissolution of rock-forming silicate minerals in organic acids: simulated first-stage weathering of fresh mineral surfaces. Amer. Mineral. 57:2076-2094.

Inskeep, W.P., and P.R. Bloom. 1985. An evaluation of rate equations for calcite precipitation kinetics at pCO_2 less than 0.01 atm and pH greater than 8. Geochim. Cosmochim. Acta 49: 2165-2180.

Isard, J.O. 1967. The dependence of glass-electrode properties on composition. In G. Eisenman (ed.) Glass Electrodes for Hydrogen and Other Cations. Marcel Dekker, New York.

Jackson, M.L. 1969. Soil chemical analysis. M.L. Jackson, Madison, W.I

James, B.R. and R.J. Bartlett. 1983. Behavior of chromium in soils: V. Fate of organically complexed Cr(III) added to soil. J. Environ. Qual. 12:169-172.

Jorgensen, S.S. 1967. Dissolution kinetics of silicate minerals in aqueous catechol solutions. J. Soil Sci. 27:183-195.

Jurinak, J.J., and K. K. Tanji. 1993. Geochemical factors affecting trace element mobility. J. Irrigation and Drainage Engineering. 119:848-867.

Keller, W.D. and W.H. Huang. 1971. Response of Apollo 12 lunar dust to reagents simulative of those in the weathering environment of Earth. p. 973-981. Proceedings of the Second Lunar Science Conference, Vol. I, The M.I.T. Press, Cambridge.

Klein, C. and C.S. Hurlburt, Jr. 1985. Manual of mineralogy. John Wiley and Sons, New York.

Knoche, W. 1975. Pressure-jump methods. In E. Wyn-Jones, (ed.) pp. 91-102. Chemical and biological applications of relaxation spectrometry. Reidel Publ., Dordrecht, The Netherlands.

Knoche, W. 1986. Pressure-jump methods. p. 191-218. In C. F. Bernasconi (ed.) Investigations of rates and mechanisms of reactions. Part II. Techniques of Chemistry. Vol. 5. Wiley, New York.

Krumbein, W.E. and B.D. Dyer. 1985. The plant is alive-weathering and biology, a multi-faceted problem. p. 143-160. *In* J.I. Drever (ed.). The chemistry of weathering. Reidel Publishers, Boston.

Lagache, M. 1965. Contribution a l'etude de l'alterstion des feldspaths dans l'eau, entre 100 et 200°C, sous diverses pressions de CO_2 et application a la synthese des mineraux argileaux. Soc. Francaise Mineral. Cristallogr. Bull 88:223-253.

Lagache, M. 1976. New data on the dissolution of alkali feldspars at 200°C in CO_2 charged water. Geochim Cosmochim. Acta 40:157-161.

Lagache, M., J Wyart, and G. Sabatier. 1961. Mecanisme de la dissolution des feldspaths alcalins dans l'eau pure ou chargee de CO_2 a 200°C. C.R. Acad. Sci. Paris 253:2296-2299.

Lamble, G.M., and S.M. Heald. 1991. Operation of a dynamically bent sagittally focusing double crystal monochromator for XAFS studies. Rev. Sci. Instrum. 63: 880-884.

Lanford, W. A., K. Davis , P. Lamarche , T. Laursen, and R. Groleau 1979. Hydration of soda-lime glass. J. Non-Crystalline Solids 33:249-266.

Lasaga, A.C. 1981. Transition state theory. p 135-169. *In* A.C. Lasaga and R. J. Kirkpatrick (ed). Kinetics of Geochemical Processes. Reviews in Mineralogy 8, Mineral. Soc. Amer., Washington, DC.

Luce, R.W., R.W Bartlett, and G.A.Parks. 1972. Dissolution kinetics of magnesium silicates. Geochim. Cosmochim. Acta 36:35-50.

Manceau, A., and L.Charlet. 1992. X-ray absorption spectroscopic study of the sorption of Cr(III) at the oxide/water interface. I. Molecular mechanism of Cr(III) oxidation on the Mn oxides. J.Colloid. Interface Sci. 148:425-442.

Manley, E.P. and L.J. Evans. 1986. Dissolution of feldspars by low-molecular-weight aliphatic and aromatic acids. Soil Science 141:106-112.

Mast, M.A., and J.I. Drever. 1987. The effect of oxalate on the dissolution rates of oligoclase and tremolite. Geochim.Cosmochim. Acta 51:2559-2568.

McKay, D.S., and D.W. Ming. 1989. Mineralogical and chemical properties of the lunar regolith. pp. 45-69. *In* D.W. Ming and D.L. Henninger (eds.), Lunar base Agriculture: Soils for Plant Growth. Soil Science Society of America, Madison, WI.

McKenzie, R.M. 1967. The sorption of cobalt by Mn minerals in soils. Aust. J. Soil Res. 5:235-246.

Mehadi, A. 1993. Reaction of Ni with soil and goethite: equilibrium and kinetic studies. Ph.D. dissertation. University of New Hampshire, Durham, New Hampshire.

Mikami, N., M. Sasaki, K. Hachiya, and T. Yasunaga. 1983a. Kinetic study of the adsorption-desorption of the uranyl ion on a γ-Al_2O_3 surface using the pressure-jump technique. J. Phys. Chem. 87:5478-5481.

Mikami, N., M. Sasaki, K. Hachiya, R. D. Astumian, T. Ikeda, and T. Yasunaga. 1983b. Kinetics of the adsorption of PO_4 on the γ-Al_2O_3 surface using the pressure-jump technique. J. Phys. Chem. 87:1454-1458.

Mikami, N., M. Sasaki, T. Kikuchi, and T. Yasunaga. 1983c. Kinetics of adsorption-desorption of chromate on γ-Al_2O_3 surfaces using the pressure-jump technique. J. Phys. Chem. 87:5245-5248.

Ming, D.W., and G.E. Lofgren. 1990. Crystal morphologies of minerals formed by hydrothermal alteration of synthetic lunar basaltic glass. *In* L.A. Douglas (ed.), Soil micromorphology: A basic and applied science. Developments in soil science 19, Elsevier Science Publishers B.V. Amsterdam.

Mogk, D.W. and W.W. Locke. 1988. Application of auger electron spectroscopy (AES) to naturally weathered hornblende. Geochim. Cosmochim. Acta 52:2537-2542.

Motschi, W. 1983 Cu(II) boung to hydrous surfaces, EPR measurements characterize surface coordination. Naturwissenschaften. 70:519-520.

Mularie, W.M., W.F. Furth and A.R.C. Westwood.1979. Influence of surface potential on the kinetics of glass reactions with aqueous solutions. J. Mater. Sci. 14:2659-2664.

Murphy, W.M. and H.C. Helgeson. 1987. Thermodynamic and kinetic constraints on reaction rates among minerals and aqueous solutions. III. Activated complexes and the pH-dependence of the rates of feldspar, pyroxene, wollastonite, and olivine hydrolysis. Geochim. Cosmochim. Acta 51:3137-3153.

Nesbitt, H.W. and I.J. Muir. 1988. SIMS depth profiles of weathered plagioclase, and processes affecting dissolved Al and Si in some acidic soil solutions. Nature 334:336-338.

O'Day, P.A., G.A. Parks, G.E. Brown, Jr. 1994. Molecular structure and binding sites of cobalt(II) surface complexes on kaolinite from X-ray absorption spectroscopy. Clays and Clay Minerals.42:337-355.

Paces, T. 1973. Steady-state kinetics and equilibrium between groundwater and granitic rock. Geochim. Cosmochim. Acta 37:2641-2643.

Parker, D.R., W.A. Norvell , and R.L. Chaney. 1993. GEOCHEM-PC: A chemical speciation program for IBM and compatible computers. *In* R.H. Loeppert et al. (ed.) Soil Chemical Equilbrium and Reaction Models. SSSA, Madison, WI.

Patterson, J.B.E. 1971. Nickel toxicity in small grains. pp. 193-207. In D.C. Pratt (ed.), Trace elements in soils and crops. MAFF Tech. Bull. No. 21. HMSO.

Petit, J.C., G. Della Mea. J.C. Dran, J. Schott, and R.A. Berner, 1987a. Mechanism of diopside dissolution from hydrogen depth profiling. Nature 325:705-707.

Petit, J.C., J.C. Dran, and G. Della Mea. 1987b. Effects of ion plantation on the dissolution of minerals. Part II: Selective dissolution, Bull. Mineral. 110:25-42.

Petrovic R., R.A. Berner, and M.B. Goldhaber. 1976. Rate control in dissolution of alkali feldspars-I. Study of residual feldspar grains by X-Ray photoelectron spectroscopy. Geochim Cosmochim. Acta 40:537-548.

Petrovich, R. 1981a. Kinetics of dissolution of mechanically comminuted rock-forming oxides and silicates I. Deformation and dissolution of quartz under laboratory conditions. Geochim. Cosmochim. Acta 45:1665-1674.

Petrovich, R. 1981b. Kinetics of dissolution of mechanically comminuted rock-forming oxides and silicates I. Deformation and dissolution of oxides and silicates in the laboratory and at the earth's surface. Geochim. Cosmochim. Acta 45:1675-1686.

Rai, D., J.M. Zachara, L.E. Eary, C.C. Ainsworth, J.E. Amonette, C.E. Cowan, R.W. Szelmeczka, C.T. Resch, R.L. Schmidt, D.C. Girvin, and S.C. Smith. 1988. Chromium reactions in geologic materials. EA-5741. Electric Power Res. Inst, Palo Alto, CA.

Rana, A.R. and R.W. Douglas. 1961. The reaction between glass and water, Part 2. Discussion of the results.Phys. Chem. Glasses 2:196-205.

Rehr, J. J., R. C. Albers, and S.I. Zabinsky. 1992. High-order multiple-scattering calculations of x-ray absorption fine structure. Phys. Rev. Lett. 69: 3397-3400.

Rimstidt, J.R. and H.L. Barnes. 1980. The kinetics of silica-water reactions. Geochim. Cosmochim. Acta 44:1683-1699.

Rimstidt, J.R., and P.M. Dove. 1986. Mineral/solution reaction rates in a mixed flow reactor: Wollastonite hydrolysis. Geochim. Cosmochim. Acta 50:2509-2516.

Schalscha, E.B., H. Appelt, and A. Schatz. 1967. Chelation as a weathering mechanism-I. Effect of complexing agents on the solubilization of iron from minerals and granodorite. Geochim. Cosmochim. Acta 31:587-596.

Schott, J. and J.C. Petit. 1987. New evidence for the mechanisms of dissolution of silicate minerals. p. 293-315. *In* W. Stumm (ed.). Aquatic surface chemistry. Wiley Interscience, New York.

Schott, J. and R.A. Berner. 1983. X-ray photoelectron studies of the mechanism of iron silicate dissolution during weathering. Geochim. Cosmochim. Acta 47:2233-2240.

Schott, J., R.A. Berner, and E.L. Sjoberg. 1981. Mechanisms of pyroxene and amphibole weathering. I: Experimental studies of iron-free minerals. Geochim Cosmochim. Acta 45:2133-2135.

Schulthess, C.P. and C.P. Huang. 1990. Adsorption of heavy metals by silicon and aluminum oxide surfaces on clay minerals. Soil Sci. Soc. Am. J. 54:679-688.

Schwertmann, U., and R.M. Cornell. 1991. Iron oxides in the laboratory. Preparation and characterization. VCH Publishers, New York.

Schwertmann, U., and R.M. Taylor. Iron Oxides. pp. 379-438. In J.B. Dixon and S.B. Weed (eds.) Minerals in soil environments. 2nd edition. Soil Science Society of America, Madison, Wisconsin.

Shotyk, W. and H.W. Nesbitt. 1992. Incongruent and congruent dissolution of plagioclase feldspar: effect of feldspar composition and ligand complexation. Geoderma 55:55-78.

Siever, R. and N.Woodford. 1979. Dissolution kinetics and the weathering of mafic minerals. Geochim. Cosmochim. Acta 43:17-24.

Sims, J.T. and J.S. Kline. 1991. Chemical fractionation and plant uptake of heavy metals in soils amended with co-composted sewage sludge. J. Environ. Qual. 20:387-395.

Slingsby, D.R. and D.H. Brown. 1977. Nickel in British serpentine soils. J. Ecol. 65:597-618.

Song, S.K. and P.M. Huang. 1988. Dynamics of potassium release from potassium-bearing minerals as influenced by oxalic and citric acids. Soil Sci. Soc. Am. J. 52:383-390.

Sparks, D.L. 1989. Kinetics of soil chemical processes. Academic Press, New York.

Sparks, D.L., and P.C. Zhang. 1991. Relaxation methods for studying kinetics of soil chemical phenomena. pp.61-94. In D.L. Sparks and D.L. Suarez (eds.) Rates of soil chemical processes. Soil Science Society of America, Madison, Wisconsin.

Sposito, G. 1984. The surface chemistry of soils. Oxford University Press, New York.

Sposito, G., C.S. LeVesque, J.P. LeClaire, and A.C. Chang. 1983. Trace metal chemistry in arid-zone field soils amended with sewage sludge: III. Effect of time on the extraction of trace metals. Soil Sci. Soc. Am. J. 47:898-902.

Sposito, G., K.M. Holtzclaw, C.S. LeVesque, and C.T. Johnston. 1982a. Trace metal chemistry in arid-zone field soils amended with sewage sludge: II. Comparative study of the fulvic acid fraction. Soil Sci. Soc. Am. J. 46:265-270.

Sposito, G., L.J. Lund, and A.C. Chang. 1982b. Trace metal chemistry in arid-zone field soils amended with sewage sludge: I. Fractionation of Ni, Cu, Zn, Cd, and Pb in solid phases. Soil Sci. Soc. Am. J. 46:260-264.

Stevenson, F.J. 1967 Organic acids in soil. p. 119-146.*In* A.D. McLaren and G.H. Peterson (eds.) Soil Biochemistry Marcel Dekker Inc., New York.

Stevenson, F.J. and M.S. Ardakani. 1972. Organic matter reactions involving micronutrients in soils. p. 79-114. *In* J.J. Mortvedt et al. (ed.) Micronutrients in Agriculture. SSSA, Madison, WI.

Stollenwerk, K.G. and D.B. Grove. 1985. Adsorption and desorption of hexavalent chromium in an alluvial aquifer near Telluride, Colorado. J. Environ. Qual. 14:150-155.

Stumm, W. and E. Wieland. 1987. Dissolution of oxide and silicate minerals: rates depend on surface speciation. p 367-400. *In* W. Stumm (ed.). Aquatic surface chemistry. Wiley Interscience, New York.

Stumm, W., G. Furrer , E. Wieland, and B.Zinder. 1985. The effects of complex-forming ligands on the dissolution of oxides and alumino-silicates. p. 55-74.*In* J.I. Drever (ed.) The Chemistry of Weathering. Reidel Publishing Co., New York.

Stumm., W. 1992. Chemistry of the solid-water interface. John Wiley and Sons, Inc., New York.

Tan, K.H. 1980. The release of silicon, aluminum, and potassium during decomposition of soil minerals by humic acid. Soil Sci. 129:5-11.

Thorseth, I.H., H. Furnes, and O. Tumyr. 1991. A textural and chemical study of Icelandic palagonite of varied composition and its bearing on the mechanism of the glass-palagonite transformation. Geochim. Cosmochim. Acta 55:731-749.

Thorseth, I.H., H.Furnes, and M. Heldal.1992. The importance of microbiological activity in the alteration of natural basaltic glass. Geochim. Cosmochim. Acta 56:845-850.

Uren, N.C. 1992. Forms, reactions, and availability of nickel in soils. *In* D.L. Sparks (ed.), Advances in Agronomy, Vol 48. Academic Press, New York.

Waychunas, G.A., B.A. Rea, C.C. Fuller, and J.A.Davis. 1993. Surface chemistry of ferrihydrite: Part 1. EXAFS studies of the geometry of coprecipitated and adsorbed arsenate. Geochim. Cosmochim. Acta. 57:2251-2269.

Wehrli, B., S. Ibric, and W. Stumm. 1990. Adsorption kinetics of vanadyl (IV) and chromium (III) to aluminum oxide: evidence for a two-step mechanism. Colloids and Surfaces. 51:77-88.

Weiblen, P.W., M.J Murawa, and K.J. Reid. 1990. Preparation of simulants for lunar surface materials. Proceedings of Space '90. Aerospace/ASCE/Albuquerque, NM.

Weiland, E., B. Wehrli, and W. Stumm. 1988. The coordination chemistry of weathering: III: a generalization on the dissolution rates of minerals. Geochim. Cosmochim. Acta 52:1969-1981.

Welch, R.M. 1981. The biological significance of nickel. J. Plant Nutr. 3:345-356.

Westall, J.C., 1982. FITEQL: A computer program for determination of chemical equilibrium constants from experimental data. Rep.82-01, Oregon State University, Corvallis.

White, A. F. 1983. Surface chemistry and dissolution kinetics of glassy rocks at 25° C. Geochim. Cosmochim. Acta 47:805-815.

White, A.F., and H.C. Claassen. 1980. Kinetic model for the short-term dissolution of a rhyolitic glass. Chem. Geol. 28:91-109.

Wollast, R. 1967. Kinetics of the alteration of K-feldspar in buffered solutions at low temperature. Geochim. Cosmochim. Acta 31:635-648.

Wollast, R., and L. Chou. 1985. Kinetic study of the dissolution of albite with continuous flow-through fluidized bed reactor. p. 75-96. *In* J.L. Drever (ed.) The chemistry of weathering. Reidel Publishing Company, Boston.

Wyart, J., A. Oberlin, and C. Tchoubar. 1963. Etude en microscopeet mircodiffraction electroniques de la boehmite formee lors de l'alteration de l'albite. C.R. Seances Acad. Sci., Ser. 2. 256:554-555.

Xyla, A.G., B. Sulzberger, G.W Luther III, J.G. Hering, P. Van Cappellen, and W. Stumm. 1992. Reductive dissolution of manganese (III,IV) (hydr)oxides by oxalate: The effect of pH and light. *Langmuir.* 8: 95-103.

Yasunaga, T., and T. Ikeda. 1986. Adsorption-desorption kinetics of the metal-oxide-solution interface studied by relaxation methods. p. 230-253. In J.A. Davis and K.F. Hayes (ed.)Geochemical processes at mineral surfaces. Proc. Am. Chem. Soc. Symp. Ser. 323, Chicago, IL. 8-13 Sept. 1985. ACS, Washington, DC.

Zachara, J.M., C.C. Ainsworth, C.E. Cowan, and C.T. Resch. 1989. Adsorption of chromate by subsurface soil horizons. Soil Sci. Soc. Am. J. 53:418-428.

Zachara, J.M., C.E. Cowan, R.L. Schmidt, and C.C. Ainsworth. 1988. Chromate adsorption on kaolinite. Clays Clay Miner. 36:317-326.

Zachara, J.M., D.C. Girvin, R.L. Schmidt, and C.T. Resch. 1987. Chromate adsorption on amorphous iron oxyhydroxide in presence of major groundwater ions. Environ. Sci. Technol. 21:589-594.

Zhang, P.C., and D. L. Sparks. 1989. Kinetics and mechanisms of molybdate adsorption/desorption at the goethite/water interface using pressure-jump relaxation. Soil Sci. Soc. Am. J. 53:1028-1034.

Zhang, P.C., and D. L. Sparks. 1990a. Kinetics and mechanisms of sulfate adsorption/desorption on goethite using pressure-jump relaxation. Soil Sci. Soc. Am. J. 54:1266-1273.

Zhang, P.C., and D. L. Sparks. 1990b. Kinetics of selenate and selenite adsorption/desorption at the goethite/water interface. Environ. Sci. Tech. 24:1848-1856.